University of Windsor
Scholarship at UWindsor

Electronic Theses and Dissertations | Theses, Dissertations, and Major Papers

2010

Liquid water removal process in the PEMFC cathode side

Xiaojing Liu
University of Windsor

Follow this and additional works at: https://scholar.uwindsor.ca/etd

Recommended Citation

Liu, Xiaojing, "Liquid water removal process in the PEMFC cathode side" (2010). *Electronic Theses and Dissertations*. 196.
https://scholar.uwindsor.ca/etd/196

This online database contains the full-text of PhD dissertations and Masters' theses of University of Windsor students from 1954 forward. These documents are made available for personal study and research purposes only, in accordance with the Canadian Copyright Act and the Creative Commons license—CC BY-NC-ND (Attribution, Non-Commercial, No Derivative Works). Under this license, works must always be attributed to the copyright holder (original author), cannot be used for any commercial purposes, and may not be altered. Any other use would require the permission of the copyright holder. Students may inquire about withdrawing their dissertation and/or thesis from this database. For additional inquiries, please contact the repository administrator via email (scholarship@uwindsor.ca) or by telephone at 519-253-3000ext. 3208.

LIQUID WATER REMOVAL PROCESS IN THE PEMFC CATHODE SIDE

by
Xiaojing Liu

A Thesis
Submitted to the Faculty of Graduate Studies
through Mechanical Engineering
in Partial Fulfillment of the Requirements for
the Degree of Master of Applied Science at the
University of Windsor

Windsor, Ontario, Canada

2010

© 2010 Xiaojing Liu

Liquid Water Removal Process in the PEMFC Cathode Side

by

Xiaojing Liu

APPROVED BY:

Dr. Chunhong Chen
Department of Electrical and Computer Engineering

Dr. Gary Rankin
Department of Mechanical, Automotive & Materials Engineering

Dr. Biao Zhou, Advisor
Department of Mechanical, Automotive & Materials Engineering

Dr. Andrzej Sobiesiak, Chair of Defense
Department of Mechanical, Automotive & Materials Engineering

January 14, 2010

AUTHOR'S DECLARATION OF ORIGINALITY

I hereby certify that I am the sole author of this thesis and that no part of this thesis has been published or submitted for publication.

I certify that, to the best of my knowledge, my thesis does not infringe upon anyone's copyright nor violate any proprietary rights and that any ideas, techniques, quotations, or any other material from the work of other people included in my thesis, published or otherwise, are fully acknowledged in accordance with the standard referencing practices. Furthermore, to the extent that I have included copyrighted material that surpasses the bounds of fair dealing within the meaning of the Canada Copyright Act, I certify that I have obtained a written permission from the copyright owner(s) to include such material(s) in my thesis and have included copies of such copyright clearances to my appendix.

I declare that this is a true copy of my thesis, including any final revisions, as approved by my thesis committee and the Graduate Studies office, and that this thesis has not been submitted for a higher degree to any other University or Institution.

ABSTRACT

The liquid water removal process in the Proton Exchange Membrane Fuel Cell (PEMFC) has a large influence on the fuel cell performance since the PEMFC works under a relatively low temperature. In this project, the water behavior in both the gas flow channels and porous layer at the cathode side of a PEMFC with different channel geometry are studied numerically. Commercial Computational Fluid Dynamics (CFD) software package FLUENT 6.3.26 is used to conduct the simulation. The methodology applied in the numerical investigation using the Volume of Fluid (VOF) model in this software package and the numerical fuel cell model constructed in this project is validated with an experiment.

DEDICATION

To my parents Huanfa Liu and Zhen Wang also my aunt Ying Wang.

ACKNOWLEDGEMENTS

I would like to thank my professor, Dr. Biao Zhou, for his guidance, encouragement and allowing me the opportunity to join the high quality research team I have come to know. Sincere thanks to Dr. Gary Rankin, Dr. Chunhong Chen and Dr. Andrzej Sobiesiak for their time and help in the development of this thesis.

Additional thanks to Le Dinh Anh for his contributions.

I am also grateful for the support given by the AUTO21^{TM}, Network of Centers of Excellence (Grant D07-303), the Natural Sciences and Engineering Research Council of Canada (NSERC), and the University of Windsor.

Finally, special thanks to my parents Huanfa Liu and Zhen Wang. Thank you for putting up with my difficult times and for supporting me while I complete one of my dreams.

Table of Contents

AUTHOR'S DECLARATION OF ORIGINALITY iii
ABSTRACT iv
DEDICATION v
ACKNOWLEDGEMENTS vi
LIST OF TABLES x
LIST OF FIGURES xi
LIST OF ABBREVIATIONS xiii
CHAPTER 1. INTRODUCTION 1
1.1 Fuel cell technology 1
1.2 Classification of fuel cells 2
1.3 Proton exchange membrane fuel cell (PEMFC) 2
1.4 Liquid water effect in PEMFC 3
CHAPTER 2. LITERATURE REVIEW 5
2.1 Numerical studies review 5
2.2 Experimental studies review 9
2.3 Objective 12
CHAPTER 3. NUMERICAL MODEL SETUP 13
3.1 Numerical simulation domain setup 13
3.2 Mathematical model setup 17
3.3 Grid setup 19
3.4 Initial settings of water 20
CHAPTER 4. NUMERICAL MODEL VALIDATION 22
4.1 Purpose of the experiment 22
4.2 Experimental methodology 22
4.3 Experiment setup 23
4.3.1 Construction of the test bench 23
4.3.2 Transparent fuel cell 24
4.3.3 Camera 25

4.4 Initial setting of the fluids 25
4.4.1 Air inlet mass flow rate 25
4.4.2 Liquid water inlet mass flow rate 26
4.4.3 Contact angle 26
4.5 Experiment results and analysis 28
4.6 Comparison of the numerical simulation results and experiment results 31
4.7 Summary 38
CHAPTER 5. LIQUID WATER REMOVAL PROCESS IN SERPENTINE CHANNEL WITH POROUS LAYER 39
5.1 General process of liquid water removal 39
5.2 Liquid water emerging into the channel from porous layer 41
5.3 Liquid water moving inside the porous layer 48
5.4 Summary 55
CHAPTER 6. LIQUID WATER REMOVAL PROCESS IN STIRRED TANK REACTOR CHAMBER WITH POROUS LAYER 56
6.1 General process of liquid water removal 56
6.2 Liquid water moving inside the porous layer 58
6.3 Liquid water emerging into the chamber from porous layer 67
6.4 Summary 70
CHAPTER 7. LIQUID WATER REMOVAL PROCESS IN PARALLEL BAFFLE BLOCKED CHANNEL WITH POROUS LAYER 72
7.1 General process of liquid water removal 72
7.1.1 Identification of the names for different segments in the geometry 72
7.1.2 General process of liquid water removal 73
7.2 Liquid water behavior at the inlet manifold area 75
7.3 Liquid water behavior at the outlet manifold area 78
7.4 Liquid water accumulation in the cavities 81
7.4.1 Liquid water accumulation process 82
7.4.2 Liquid water driven away from the cavity 85

7.5 Liquid water moving inside the porous layer 87
7.6 Summary..... 90
CHAPTER 8. CONCLUSION..... 92
REFERENCE..... 93
VITA AUCTORIS 95

LIST OF TABLES

Table. 1. Droplet deformation from the same domain with different grid size 19

LIST OF FIGURES

Fig. 1. A schematic of fuel cell technology concept..... 1
Fig. 2. Basic concept of a PEMFC..... 2
Fig. 3. 3D domain for the validation model..... 14
Fig. 4. 3D domain for the serpentine channel with porous layer case 14
Fig. 5. 3D domain for STR chamber with porous layer case 16
Fig. 6. 3D domain for PBB channel with porous layer case..... 16
Fig. 7. Liquid water film initial state illustrated with the serpentine with porous layer case 21
Fig. 8. Schematic of the test bench for the validation experiment..... 23
Fig. 9. A picture of the transparent fuel cell used in the experiment..... 24
Fig. 10. A picture of the commercial camera used in the experiment..... 25
Fig. 11. Contact angle measured with one liquid water droplet on the MEA 27
Fig. 12. Contact angle measured with one liquid water droplet on the stainless steel flow field plate 27
Fig. 13. Contact angle measured with one liquid water droplet on the transparent end plate 27
Fig. 14. Liquid water removal process in the transparent fuel cell..... 30
Fig. 15. Liquid water removal process comparison from both the validation model and the experiment..... 35
Fig. 16. Pressure drop data get from both the validation model and the experiment.. 37
Fig. 17. General process of liquid water removal in serpentine channel with porous layer domain..... 40
Fig. 18. The droplet held near the bending area of the channel due to the back flow 44
Fig. 19. The droplet collides with the wall at the bend area of the channel 46
Fig. 20. One droplet catches up with another when moving along the channel 47
Fig. 21. Pressure field caused by gas flow before the liquid water film is set..... 49
Fig. 22. Liquid water movement inside the porous layer at the beginning period of the simulation 52

Fig. 23. Liquid water movement inside the porous layer along with time 54
Fig. 24. General liquid water removal process in STR chamber and the porous layer domain 57
Fig. 25. Liquid water removal process in the porous layer at the beginning period ... 61
Fig. 26. Liquid water removal process in the porous layer along with time 63
Fig. 27. Liquid water film broken into liquid water ligaments 66
Fig. 28. Liquid water emerging into the chamber area from the porous layer 70
Fig. 29. PBB channel with porous layer geometry with the name of different sections 72
Fig. 30. General process of liquid water removal in PBB channel with porous layer domain 75
Fig. 31. Liquid water behavior at the inlet manifold area 77
Fig. 32. Liquid water brought into the outlet manifold by the gas flow at the beginning period 79
Fig. 33. Liquid water behavior in the outlet manifold along with time 81
Fig. 34. Liquid water accumulated in the cavities attached with the porous layer 82
Fig. 35. Liquid water accumulation process in the cavities 84
Fig. 36. Liquid water droplet driven from one cavity to the next cavity 87
Fig. 37. Liquid water removal process inside the porous layer 90

LIST OF ABBREVIATIONS

Re	Reynolds number
d	hydraulic diameter
P	wetted perimeter
S	momentum Source term
g	acceleration of gravity ($m \cdot s^{-2}$)
u	velocity vector ($m \cdot s^{-1}$)
K	surface curvature
s	phase volume fraction
υ	kinematic viscosity ($m^2 \cdot s^{-1}$)
ρ	density
ε	porosity
μ	dynamic viscosity ($Pa \cdot s$)
χ	surface tension coefficient
$\dot{m}$	mass flow rate (kg / s)
$\dot{V}$	volume flow rate
f	Darcy friction factor

Subscripts

g	gas
l	liquid
c	continuity equation
m	momentum equation
ch	channel
p	porous layer

CHAPTER 1

INTRODUCTION

1.1 Fuel cell technology

A fuel cell is a kind of power supply system which converts the energy generated by the electrochemical reaction to electrical energy directly. The general concept of a fuel cell includes the electrolyte in the middle and two electrodes on each side of the electrolyte, one electrode is called cathode, and the other is called anode. The electrolyte allows the protons generated by the electrochemical reaction in the anode side to transfer through it to the other side, but prevents the electrons generated at the same time to go across. In this case, the electrons are forced to go through the external circuit to reach the cathode side and complete the electrochemical reaction. Consequently, electricity is formed within the circuit. A schematic of this fuel cell technology concept with Hydrogen and Oxygen as reactants for example is shown in Figure 1.

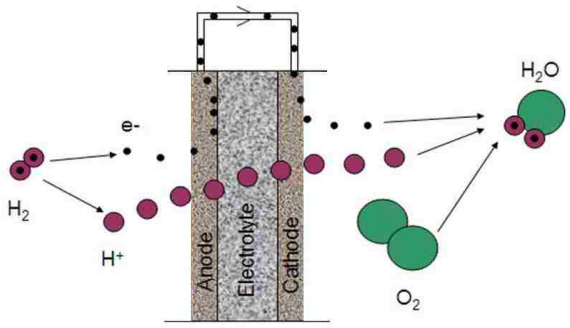

Fig. 1. A schematic of fuel cell technology concept

This technology has been recognized as one of the most promising power generation systems which have the potential to substitute the traditional power sources used in a variety of applications nowadays, because it has the advantage of high efficiency, low contamination and low noise. However it is still in the research stage not commercialized yet, because some criteria like durability, reliability, and power density are still waiting to be improved. Thus the methods to optimize these properties have become the center of the research concentration recently.

1.2 Classification of fuel cells

Along the history of the fuel cell development, generally five categories of fuel cell classified by their main electrolyte solution are proved to be applicable. They are Alkaline Fuel Cell (AFC), Molten Carbonate Fuel Cell (MCFC), Phosphoric Acid Fuel Cell (PAFC), Solid Oxide Fuel Cell (SOFC) and Proton Exchange Membrane Fuel Cell (PEMFC). Among all these types of fuel cells, the PEMFC attracted the highest research interest for aerospace and vehicle applications due to its low operation temperature and relatively high power density.

1.3 Proton exchange membrane fuel cell (PEMFC)

A typical single PEM fuel cell is normally constructed with several key components: Membrane Electrolyte Assembly (MEA) including proton exchange membrane, catalyst layers and gas diffusion layers on both sides of the membrane; flow field plates with flow channels embedded on each side of the MEA; and end plates on each side of the fuel cell with clamping solutions to hold the whole fuel cell together. The basic concept of a single PEMFC is shown in Figure 2.

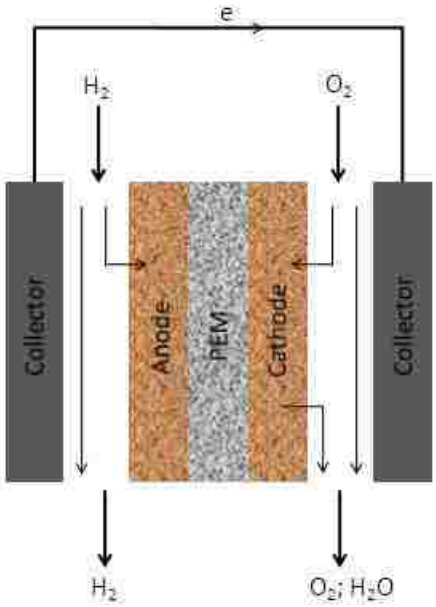

Fig. 2. Basic concept of a PEMFC

The electrochemical reaction in the PEMFC is divided into two steps, the two half reactions occur in the anode side and the cathode side of the fuel cell separately. The anode electrode is where the oxidation reaction shown in equation 1.1 takes place.

$$H_2 \rightleftharpoons 2H^+ + 2e^- \tag{1.1}$$

While the reduction reaction as in equation 1.2 takes place at the cathode electrode.

$$\frac{1}{2}O_2 + 2H^+ + 2e^- \rightleftharpoons H_2O \tag{1.2}$$

As shown in above equations, PEMFC consumes Hydrogen and Oxygen, and generates water at the cathode side while the PEMFC system is running.

1.4 Liquid water effect in PEMFC

Since PEMFC operates under a low temperature (30 to 100℃), condensation of the water generated in the electrochemical reaction in PEMFC is inevitable. Condensed liquid water appears mainly at the cathode side of the PEMFC where water is generated from the reduction reaction. Some liquid water may transfer to the anode side across the MEA due to water concentration difference and the permeability of the MEA, but the amount of the liquid water in the anode side would be very small compared to that in the cathode side.

The reduction reaction occurs at the interface of the membrane and the cathode side catalyst layer in the PEMFC. The condensed water will move through the porous layers and the gas flow channel, while the amount of water increases by continuous reaction. The liquid water behavior in these areas has a large influence on the fuel cell performance. On one hand, a certain amount of water in the PEMFC is necessary to help enhance the ion conductivity of the membrane. On the other hand, too much liquid water can corrupt the fuel cell performance causing instability and low efficiency. The reason for saying liquid water will corrupt the fuel cell performance is that the porous layers and channel where liquid water will move through are also the essential path ways for the reactant gas to reach the membrane and join the reaction. The liquid water in these areas will influence or even block the gas flow, thus

reducing the electrochemical reaction rate and reduce the fuel cell performance. As a matter of fact, to improve the PEMFC performance, a detailed investigation of the liquid water removal process is unavoidable.

CHAPTER 2

LITERATURE REVIEW

Fluid flow inside the fuel cell is deemed to be one of the most important factors influencing fuel cell performance. In recent research, gas and liquid water transportation behavior inside the PEMFC has become the center of the research concentration. To investigate physical phenomena, experimentation is always firstly considered, however in a PEMFC system, electrochemical reaction and multi-component mass transport are involved together, so the detailed investigation cannot be achieved by experiments. Therefore, numerical modeling and simulation are mostly applied to investigate the PEMFC in detail. In recent years, along with the continuous improvement of numerical models, different experimental setups are also constructed to observe some of the phenomena in the PEMFC and validate the numerical models. For example, the end plate of a single fuel cell are made transparent to see the water movement in the gas flow channel, and neutron imaging technology used to take pictures of the water movement inside the porous layer.

2.1 Numerical studies review

To investigate the fluid flow inside a fuel cell, numerical models are developed to simulate the fuel cell system. One-dimensional models are developed at the beginning period of the fuel cell related research. A one-dimensional mathematical model of PEMFC cathode was presented by Bernardi and Vebrugge [1]. The mechanism of fluid transport in the fuel cell system including both reactants and water was investigated. However since it is only a one dimensional model, the difference of the mass concentration along the gas flow channel and the decrease and increase of the mass concentration with time are not considered. Nguyen and Yi [2] developed a two-dimensional, steady-state, mass and energy transport model simulating the fluid flow phenomena in a plane along the flow direction and perpendicular to the membrane. The distribution of pressure and temperature along the channel, the convection of water across the membrane as well as the current density along the

channel were obtained, but the variations of velocity and concentration across the channel were not considered. H.-C. Liu et al. [3] proposed a two-dimensional fuel cell model to examine the effect of baffles on the gas distribution. Setting baffles in the channel is an important channel pattern idea that is later applied in the intedigitated channels. However the variations across the channel were not considered either.

Following one- and two-dimensional models, three-dimensional models with different channel shapes were constructed for further study. A three-dimensional numerical model of a straight gas flow channel in a PEMFC was proposed by Dutta et al. [4] using a commercial CFD software FLUENT. Applying the same software, a 3D model of a PEM fuel cell with serpentine flow channels, which is one of the most popular shapes of the channel used in fuel cell, is later proposed by Nguyen et al. [5]. In this serpentine channel, the effective consumption of reactants for the reaction is increased as compared to the straight channels. A study investigating the steady-state gas transport phenomena in a parallel flow channel was conducted by Cha et al. [6] in which oxygen concentration along the gas flow channel, which may affect fuel cell performance, were discussed. A three-dimensional, transient numerical PEMFC model was developed by Kumar and Reddy. [7]. The effect of different gas flow fields on the PEMFC is studied with serpentine, parallel, multi-parallel and discontinuous flow-fields individually in this paper.

The basic shapes for channel such as parallel or serpentine are commonly accepted currently, however these kinds of channel still have their own defects making them not perfect. Thus, different kinds of improvements have been made on these shapes to achieve better cell performance. A general review of different shapes of channel is performed by Li and Sabir. [8]. The channel design is classified into six main types in this paper, they are pin-type flow field, series-parallel flow field, serpentine flow field, integrated flow fields, interdigitated flow field and flow-field designs made from metal sheets. A three-dimensional dual serpentine shape gas flow channel is proposed

by R. Boddu et al. [9]. Fluid flow and heat transfer inside this improved serpentine flow channel are considered in this study. With this dual serpentine channel, the effective reactant area on the MEA can be increased. Comparing the single serpentine and dual serpentine model applied in this paper, the effective area on the MEA is increased by 0.56%. Two bio-inspired designs combining the advantages of the existing serpentine and interdigitated patterns are proposed by J.P. Kloess et al. [10]. Both numerical simulation and experiment have been conducted to investigate the effects of these two kinds of new flow channel patterns on fuel cell performance. A lower pressure drop from the inlet to outlet is achieved in the leaf or lung design than the existing interdigitated flow patterns. Also, more uniform flow diffusion to the gas diffusion layer was found in these two bio-inspired flow channel patterns. Kuo et al. [11] investigated the performance of a PEMFC with a novel wave like gas flow channel by numerical simulation. Compared with the conventional straight gas flow channel, the wavelike channel increases the reactant flow velocity, enhances the fluid transport through the porous layer, and improves the temperature distribution. As a result, reactant utilization efficiency and superior heat-transfer characteristics are achieved in this kind of channel design.

The research mentioned above made very important contributions to fuel cell technology. They explained the fluid transportation process in PEM fuel cells with different channel design, and discussed the advantages and disadvantages of these flow fields in detail. However the liquid water effect is neglected in their simulation. Yi et al. [12] found that water vapor condensation is unavoidable on both sides of the fuel cell and proposed a method using water transport plate to remove excess liquid water to the coolant flow channels by a pressure difference. Since then, the liquid water effect in a fuel cell system has been recognized as a very important factor for fuel cell improvement. Different CFD models with the consideration of liquid water transportation in the fuel cell were developed to analyze this important effect. Berning et al. [13] presented a three-dimensional model and studied the distribution of the gas

flow velocity, species concentration, mass transfer rate, electric current and temperature by the simulations, and also provided detailed insight into water transport mechanisms and mass transport limitations in this paper. Hontanon et al. [14] applied a 3D gas flow model using the commercial software FLUENT and found that the membrane thickness, cell voltage and current density will affect water transportation across the membrane. You and Liu [15] simulated the liquid water concentration in the cathode side of a PEM fuel cell and concluded that a multi-phase model must be used to obtain more practical simulation results. Wang et al. [16] constructed a two-phase flow model to simulate the liquid water formation and the effects of the liquid water on the performance of a PEMFC cathode. A 3D model of a U shape channel was constructed by Quan et al. [17] to investigate the liquid water effect inside a fuel cell channel. The simulation results in this paper indicate that the bending area of the fuel cell channel gives an important influence on the gas flow as well as the liquid water distribution in a PEMFC. Jiao et al. [18-21] conducted 3D multi-phase model simulations for different shapes of fuel cell gas flow channel. Several kinds of initial liquid water settings are studied to simulate different water condensation phenomena. The simulations were conducted using the VOF (volume of fluid) model in FLUENT. And the liquid water removal process in the channel models is discussed in detail. Le et al. [22, 23] introduced general 3D models using the software package FLUENT simulating a whole fuel cell constructed with serpentine channel and serpentine parallel integrated channel respectively. Liquid water effect is considered in these models. The detail of the physics regarding mass concentration, heat transfer, species transport and electrochemical reaction in these model are also presented. Zhan et al. [24] studied 3D numerical models, one with a straight channel and the other with a U shape channel considering the hydrophilicity of graphite plate (GP) and the hydrophobicity of the gas diffusion layer (GDL) for the walls of the gas channel, using the volume-of-fluid (VOF) model of FLUENT software. The simulation results show that the hydrophilicity and the hydrophobicity of the channel wall play an important role in the liquid water motion. The more hydrophobic the

surfaces of the channel are the easier the water is discharged. Quan and Lai [25] investigated the water behavior in the gas flow channel of a PEMFC cathode as well. It is proposed in this paper, as it is a very important fluid flow path way inside a fuel cell, the porous gas diffusion layer must be considered in the numerical model. Therefore the calculation domain in this paper includes a U shape channel as well as a layer of porous media attached. The software package FLUENT with VOF model is applied in this two-phase flow simulation, and the effects of the channel surface hydrophilicity, gas flow channel geometry, and air inlet velocity on the liquid water behavior, and the liquid water content as well as the pressure drop inside the channel are discussed in detail. However the liquid water behavior inside the porous layer is not discussed. In the authors' knowledge, there is no literature available to address the phenomena that occur when the water goes through the porous layer and enters the channel area which is a very important factor influencing the PEMFC performance.

2.2 Experimental studies review

Other than numerical simulation, experiment is a very important method used to study PEMFC and validate the numerical models. A transparent fuel cell with a straight channel is made by Hussaini et al. [26]. The visualization of cathode channel flooding in a fuel cell is achieved through this setup. Xu and Zhao [27] did an experiment with a conventional serpentine flow field and an enhanced serpentine flow field to a single polymer electrolyte-based fuel cell. It is shown from this study that the new flow field resulted in substantial improvements in both cell performance and operating stability compared to the conventional serpentine flow field design. The conventional pin flow channel has been proven to be applicable in PEMFC as well. However the stability and efficiency of the fuel cell with this kind of channel are still waiting to be improved. An experiment with an improved pin channel called a cascade-type channel is performed by A.M. López et al. [28]. In this new design, the conventional square shape pins are changed to thin bar shape pins perpendicular to the inlet to outlet direction. This design helped to yield a smooth pressure field and a more uniform gas

flow distribution over the catalyst layers, thus making the fuel cell performance more stable and efficient compared to the conventional pin flow channel. An auto-humidified operation of the channel-less, self-draining fuel cell, based on a stirred tank reactor is demonstrated by Hogarth and Benziger [29]. This is also a kind of improved pin flow channel. Experiment has been performed to compare the performance of the stirred tank reactor fuel cell with a fully humidified serpentine flow channel fuel cell. The results show that the stirred tank reactor fuel cell gives a better performance at high current densities. The new design also has the advantage of simplifying the fuel cell control by making the humidifiers unnecessary in the system. However, though it is been proved by experiment that this new design offers many benefits, the water removal process inside this channel which influences the cell performance is still unknown since the experiment has its limitation on observing the detail of the water behavior inside the fuel cell. Yan et al. [30] experimentally investigated the effects of interdigitated flow channel design on the cell performance of PEMFC. The effectiveness of the interdigitated flow channel design and the conventional parallel flow channel design are compared. Different baffle blocked positions of the interdigitated flow channel are studied. However, the effect of the baffles to the fluid flow inside the channel and porous layers was not investigated as well, since it is hard to observe the flow detail through an experiment. As a matter of fact, a validated numerical model is needed to study these phenomena in detail.

Due to the porosity and the hydrophilicity of the gas diffusion layer and catalyst layer, the water transportation inside the porous layers is quite different with the water behavior in the gas flow channel, but also gives a significant influence on the fuel cell performance. Bazylak et al. [31] conducted an experiment to study the influence of the material properties on the water droplet movement on GDL. The water transportation behavior in a straight channel with GDL attached is studied experimentally by Djilali's group [32] as well. Sinha et al. [33] did both simulation and experiment to investigate the material influence to the water behavior inside a

PEMFC. Kumbur et al. [34] investigated the liquid droplet deformation at the interface of the diffusion media (DM) and the gas flow channel theoretically and experimentally. In Kumbur's study, the results presented indicate that the operational conditions, droplet height, chord length, channel size and level of surface hydrophobicity of the DM directly affect the instability. However the droplet deformation is studied only with a straight channel, the effects from different channel shapes and the liquid transportation inside the porous layers were not mentioned. Hartnig et al. [35] did an experiment to visualize the liquid water inside the porous layers of the PEMFC using high-resolution synchrotron X-ray radiography technology. The results of this study clearly show the initial spots of liquid water formation beneath the ribs of the flow field channel. However it is in-plane visualization, the method to achieve three-dimensional view is still under research.

All of the research mentioned above gave significant contributions to the fuel cell technology improvement. At the current time, it is possible to give further attempts in this area and create a model that can help to obtain results considering all the necessary domains for the liquid water removal process but not be so complicated that it consumes too much time for calculation.

According to the commonly accepted theory, a large portion of water in the fuel cell cathode side is generated from the chemical reaction at the common plane between the membrane and the cathode side catalyst layer as mentioned at the beginning of this project. This means that it is inevitable that the water has to move across the porous layer before it enters the channel area. As a result, water transport in the porous layer is very important as well. To investigate this process and also give a more realistic simulation result for the water removal process in the fuel cell channel, a PEM fuel cell cathode side model is proposed with three different kinds of channels and one porous layer attached to each of them using the commercial CFD software FLUENT 6.3.26 in this project. To simplify the complex process of real PEM fuel cell

operating conditions, the detail of phase-change and heat transfer is not considered in this project. The chemical reactions were not considered either since the effect of the electro-chemical reactions inside the PEMFC on the liquid water behavior is mainly to continuously produce water.

In the following chapters, the water removal process in all the possible paths at the cathode side of a PEMFC is studied. The computational domain, mathematical model, grid independency and initial settings are introduced. The results from the simulation in different aspects are presented and concluded which may help the further study of PEMFC technology.

2.3 Objective

The focus of this project is on the liquid water effect in both the gas flow channel and the porous layers in the cathode side of a single PEMFC. The investigation is conducted using the commercial Computational Fluid Dynamics (CFD) software package FLUENT 6.3.26. The methodology applied in the numerical investigation with the Volume of Fluid (VOF) model in this software package and the numerical fuel cell model constructed in this project is validated with an experiment in this study. The liquid water removal process in serpentine channel, stirred tank reactor (STR) chamber and parallel baffle blocked (PBB) channel with a porous layer attached on each one are studied individually using the validated model.

CHAPTER 3

NUMERICAL MODEL SETUP

3.1 Numerical simulation domain setup

The numerical simulation domain concerned in this project is a full scale single PEM fuel cell cathode side including gas flow channel as well as porous layers. These are the only two areas in the cathode side of a fuel cell that allow gas and liquid water to pass through. A simulation with exactly the same flow field in the experiment setup is conducted to validate the numerical model. The liquid water removal process of the serpentine channel, Stirred Tank Reactor (STR) chamber and Parallel baffle-blocked (PBB) channel with porous layer configuration are studied in this project.

To prove that the numerical model constructed in this project is applicable and meaningful, a validation model is proposed with the same domain and same initial fluid flow condition with the experiment as shown in Figure 3. The width of the channel is 2mm and the height of the channel is 1.7 mm according to the experiment setup. The inlet and outlet straight channel has a length of 20 mm and the area of the serpentine channel is 20mm by 20mm. The distance between each channel segment in the serpentine area is 1mm. And the porous layer area is 2mm larger than the serpentine area from each edge.

The serpentine channel is currently one of the most widely used channel configurations in fuel cell research. This type of channel has no branches, but is bent into several segments. In this project, we studied a calculation domain with nine segments as indicated in Figure 4. The channel width of each segment and the distance between adjacent segments are 2mm. The height of the channel which is indicated by the Z direction dimension is 2mm as well. The straight segment of the channel is 40mm in length. The porous layer attached to the channel has a thickness of 0.3mm which is the common dimension of a real fuel cell component.

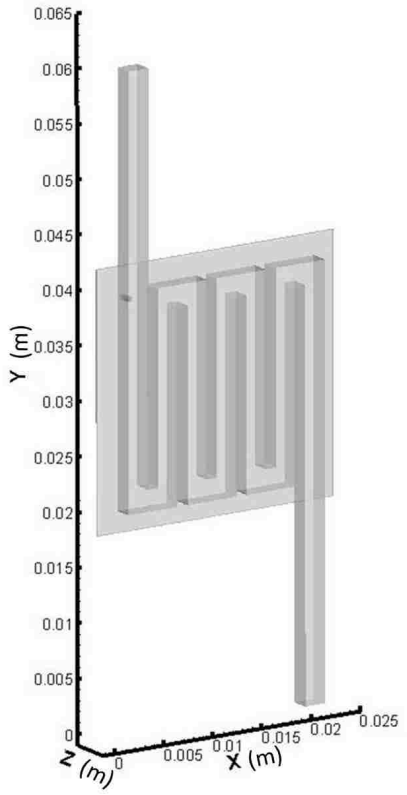

Fig. 3. 3D domain for the validation model

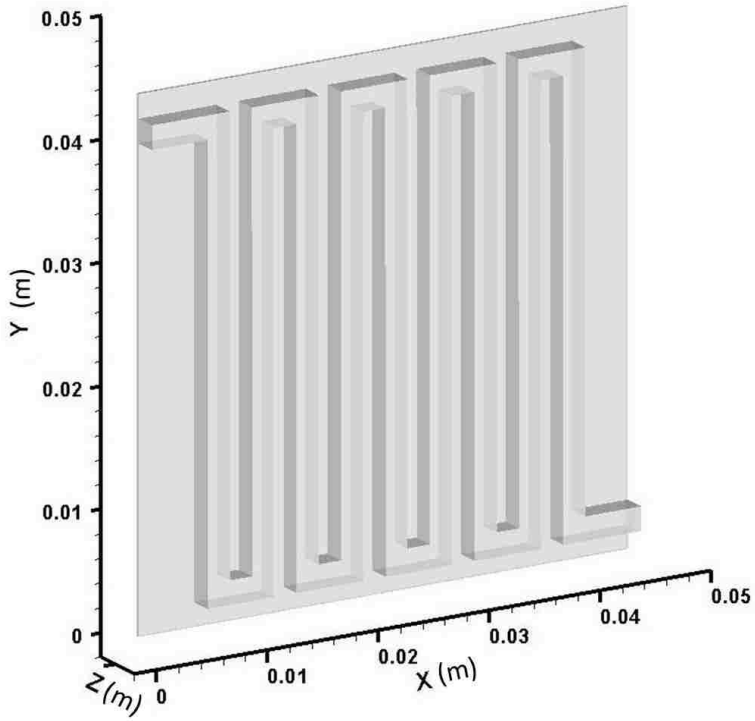

Fig. 4. 3D domain for the serpentine channel with porous layer case

The STR channel is a kind of self-draining channel studied experimentally by previous researchers. They made a fuel cell with a STR channel to examine its self-draining and auto-humidifying property and its influence on the fuel cell performance. In our project, we applied a model domain with exactly the same STR channel in the experimental research by the other researchers as shown in Figure 5 and examine the liquid water removal process within both channel and porous layers using numerical simulation. The channel cross section is 3mm by 3mm, the length of the square channel area is 15mm, and the length of the square porous layer area is 19mm. For the serpentine with porous layer case, the thickness of the porous layer is also 0.3mm.

The PBB channel is a novel channel geometry proposed in this project as shown in Figure 6. The baffles block the channel into several sections and force the fluid to go through the porous layers attached to the channel. This enhances the gas usage efficiency and helps the liquid water removal process from the porous layers. The PBB channel applied in this project contains four baffle-blocked channel branches in parallel, and each branch is blocked by three baffles with a baffle thickness of 1mm. The channel cross section is 2mm by 2mm, the length of each channel is 11mm and the distance between each channel is 2mm. The length of the square porous layer area is 19mm and the thickness of the porous layer is 0.3mm as well.

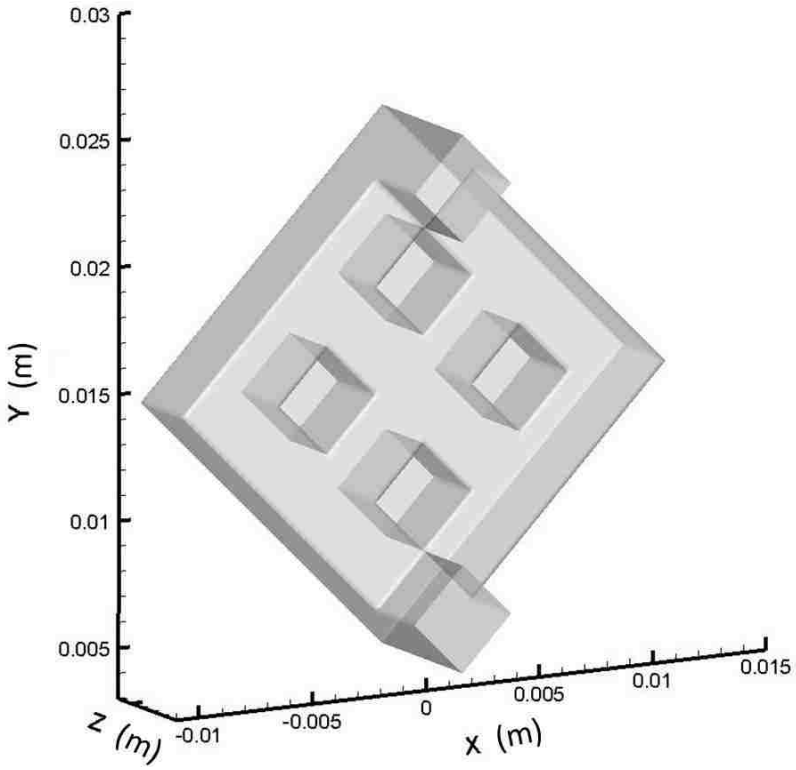

Fig. 5. 3D domain for STR chamber with porous layer case

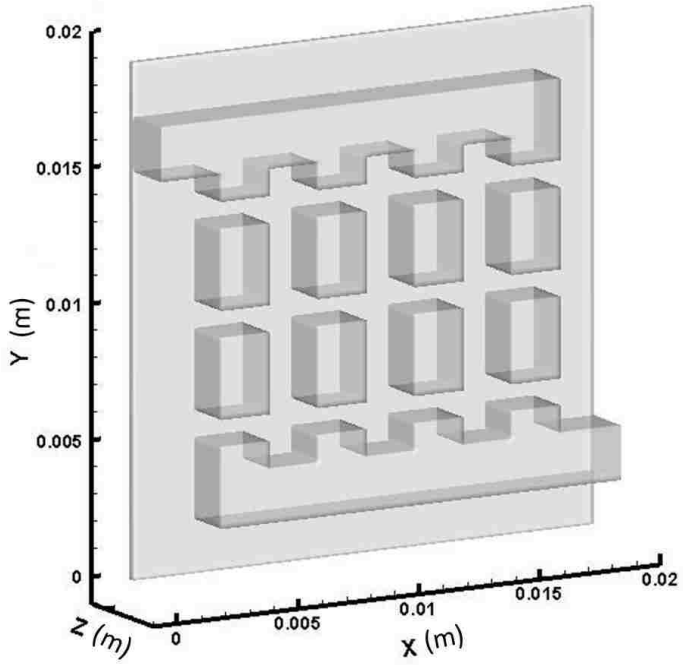

Fig. 6. 3D domain for PBB channel with porous layer case

3.2 Mathematical model setup

The numerical simulation in this project was applied in conjunction with the commercial software package FLUENT 6.3.26 with a 3D unsteady VOF (volume of fluid) model, which is suitable for locating the interface between different fluid phases. A UDF (user defined function) is applied to export the data from the calculation domain.

The Reynolds number in this model can be calculated by

$$\mathrm{Re} = \frac{ud}{\upsilon} \tag{3.1}$$

here $$d = \frac{4A}{P} \tag{3.2}$$

where P is the wetted perimeter, and A is the cross sectional area.

The fluid flow applied in this project is laminar since the Reynolds number calculated through the whole process of simulation is less than 1400. Also in this project, the flow is considered as isothermal and without phase change as this project mainly is concentrating on the liquid water removal process modeling.

The governing equations of mass and momentum is applied in both the channel and the porous layer area. The conservation of mass in the channel area can be written as

$$\frac{\partial \varepsilon\rho}{\partial t} + \nabla(\varepsilon\rho\mathbf{u}) = S_c \tag{3.3}$$

where, in our case, $S_c = 0$

and the conservation of momentum can be expressed as

$$\frac{\partial(\varepsilon\rho\mathbf{u})}{\partial t} + \nabla(\varepsilon\rho\mathbf{u}\mathbf{u}) = -\varepsilon\nabla p + \nabla[\varepsilon\mu\nabla\mathbf{u}] + \rho g + S_m \tag{3.4}$$

Here, the surface tension is accounted for by using the continuum surface force (CSF) model [36], and is expressed in terms of the pressure jump across the interface. This depends on the surface tension coefficient and is implemented in the momentum equation as the source term.

$$S_m = \chi K_{ch} \frac{\rho\nabla s_l}{(\rho_l + \rho_g)/2} \tag{3.5}$$

where χ represents the surface tension coefficient, K represents the surface

curvature. ρ and μ in above source terms represent the density and dynamic viscosity in a volume fraction weighted average manner respectively. They can be calculated using

$$\rho = \rho_g + s_l(\rho_l - \rho_g) \tag{3.6}$$

$$\mu = \mu_g + s_l(\mu_l - \mu_g) \tag{3.7}$$

In the porous layer area, the governing equations of mass and momentum are also applied. The conservation of mass is the same as in the channel area, and the conservation of momentum has the same equation, but a different source term as shown below:

$$S_m = \chi K_p \frac{\rho \nabla s_l}{(\rho_l + \rho_g)/2} - \frac{\mu}{\tau_g}\varepsilon^2 \mathbf{u} \tag{3.8}$$

The second term of this equation expresses the gas permeability in the porous layer domain.

In the VOF model, different phases share the same momentum equation, and the interface between phases is tracked throughout the domain by computing the volume fraction for all types of fluids in each computational cell. For the two phase flow concerned in this project, the volume fraction equation is shown below

$$\frac{\partial(\varepsilon s_l \rho_l)}{\partial t} + \nabla \cdot (\varepsilon s_l \rho_l \mathbf{u}) = 0 \tag{3.9}$$

and $s_l + s_g = 1$ (3.10)

Where s_l is the volume fraction of liquid and s_g is the volume fraction of gas. The sum of these two volume fraction functions is equal to 1, since we have only two phases in this project.

A non-slip boundary condition is applied to the walls of the channel and porous layer. Velocity inlet and pressure outlet are applied for the inlet and outlet of the domain.

3.3 Grid setup

In order to use FLUENT to simulate the water removal process in both channel and porous layers, the calculation domain is meshed with a grid of reasonable size. To prove that the grid quantity applied in the model used in this project is reasonable for the cases studied in later chapters, a grid check is performed with a simplified domain including a straight channel and a porous layer attached. Three different grid sizes are applied in this domain for comparison. The left column shows the case meshed with 0.0004 m cells, the middle column shows the results from the case meshed with 0.0002 m cells, and the right column shows the results from the case meshed with 0.0001 m cells. One droplet is set near the inlet area at the beginning for all three cases, and the droplet deformation at different time steps are shown in Table 1.

Table. 1. Droplet deformation from the same domain with different grid size

Grid size	0.0004m	0.0002m	0.0001m
T=0s	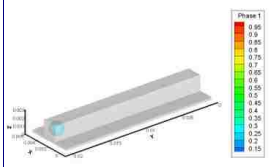	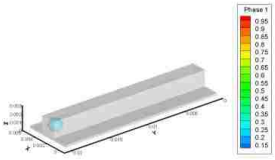	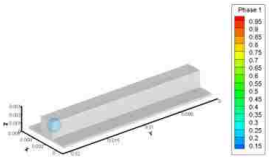
T=0.0008s	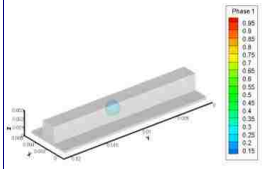	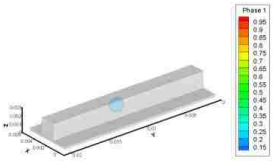	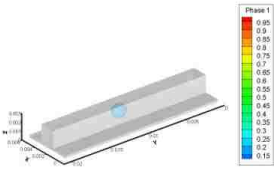
T=0.0016s	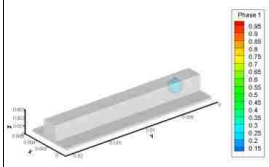	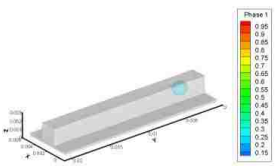	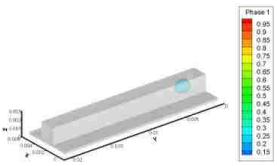

From the pictures in table 1, we can see that the case in the left column with a coarse grid does not show a visible water droplet deformation along with time, while the middle column case and the right column case show a clear shape change of the droplet from the original sphere droplet to an egg shape with time. Theoretically for CFD simulation, one can always achieve better results with finer mesh. However, considering current computation capability and the time needed for simulation, the case in the right column will consume too much resource while giving a similar result with a 0.0002 mm mesh as in the middle column case. So in this project, the 0.0002 mm grid is applied to simulate the cases in later chapters.

In the cases we are going to discuss in later chapters, we have the grid size of 0.0002 m for each edge for the channel domain, 0.0002 m in X and Y directions, and 0.00005 m in Z direction in the porous layer domain. The time step applied in the simulations is 10^{-4} s.

3.4 Initial settings of water

After the domain has been determined and the governing equations are applied to the model, a thin water film with thickness of 0.1 mm is set in the porous layer domain between the two planes z = 0.0001 m and z = 0.0002 m. This is seen as the red color area indicated in Figure 7, and simulates the water generated from the common plane between the membrane and the cathode side catalyst layer.

As shown in Figure 7 (b), the water film is placed in the middle of the porous layer, but not adjacent to the plane z = 0 m in the porous layer, where water is generated in the real fuel cell system. The reason for this is because the main point for this project is to examine the water removal process, how water comes out of the porous layer and emerges into the channel area. Varying the location of the water film at initial conditions only changes the computational time required to witness the full effects of water removal from the porous layer. Therefore in this project, we applied the middle

water film case as our model.

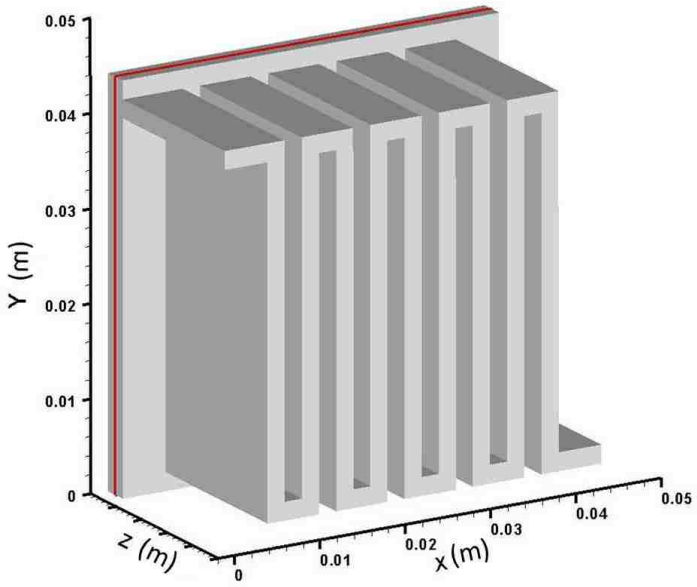

(a) Liquid water film indicated by the red color (X:Y:Z=1:1:10)

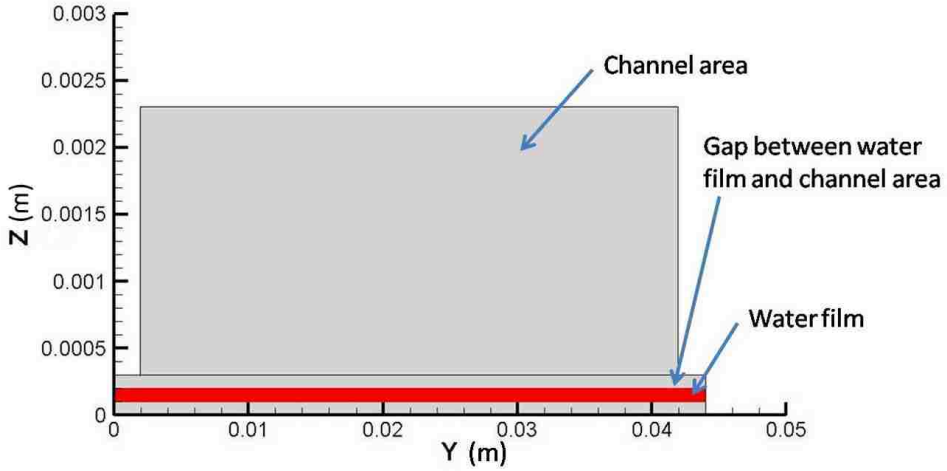

(b) Liquid water film initial state sketch (–X direction view) (Y:Z = 1:10)

Fig. 7. Liquid water film initial state illustrated with the serpentine with porous layer case

CHAPTER 4

NUMERICAL MODEL VALIDATION

4.1 Purpose of the experiment

To validate the numerical model and examine the liquid water removal process in a single transparent PEMFC, a validation experiment is conducted. The simulation is conducted using a numerical validation model with the same domain and same initial settings as the experiment. Results from both experiment and simulation are compared.

4.2 Experimental methodology

The liquid water behavior in the fluid flow paths of the PEMFC is a very important factor influencing the fuel cell performance and the fuel cell stability. However, visualization of the liquid water movement inside a regular PEMFC is not possible since the channel is not exposed to human's eyes. A single transparent PEMFC is constructed in this experiment with the end plates fabricated from transparent plexiglass instead of graphite. With this material change, the fluid flow inside the flow channel can be visualized while the fuel cell system is running.

To validate the numerical model used in following chapters, the same initial conditions are applied to both the experiment and the validation model. In order to make sure that the initial liquid water goes into the channel at the same position of the channel with same flow rate in both experiment and numerical model, a syringe is inserted into the cathode side flow channel of the transparent PEMFC in the experiment. The needle outlet is fixed at the same position as the liquid water inlet in the numerical validation model. And the flow rate of the liquid water injection is recorded from the experiment and set in the validation model.

After these settings, the transparent fuel cell is placed horizontally with the cathode side facing up. The inlet of the fuel cell is connected to a test bench which supplies

the desired air flow to the fuel cell. A camera is fixed above the transparent fuel cell to record the liquid water removal process inside the flow channel.

These methods to do the experiments are discussed and optimized by the author and Le [37] together.

4.3 Experiment setup

4.3.1 Construction of the test bench

To do a fuel cell experiment, a test bench is needed to run the fuel cell system. For validating the numerical model used in later chapters, the test bench in the group lab [38] is modified by the author and Le [37] to a structure as shown in the schematic in Figure 8.

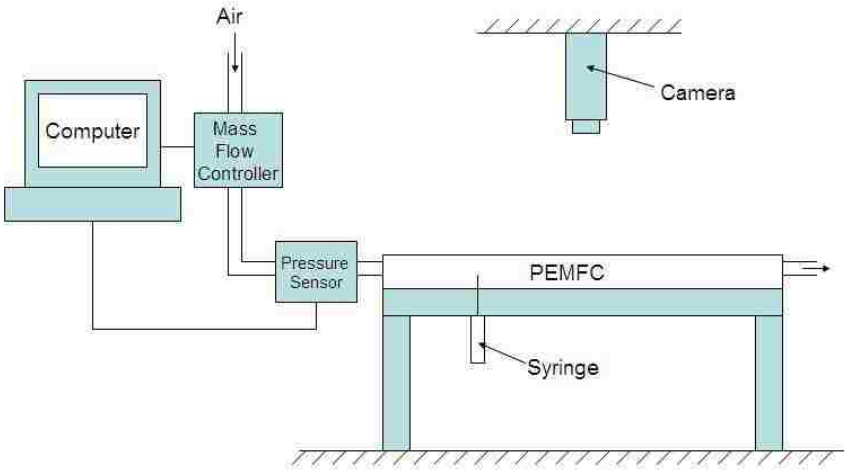

Fig. 8. Schematic of the test bench for the validation experiment

The fuel cell is horizontally fixed on a stable frame, and the syringe for injecting liquid water droplet to the cathode channel enters from the bottom through the anode side and MEA. Air flow supplied from an air cylinder passes a mass flow controller and a pressure sensor and goes into the inlet of the transparent fuel cell. The flow rate and the inlet air pressure are recorded using the Labview control panel installed in the computer connected to the system. A camera placed vertically above the transparent

fuel cell records the liquid water removal process inside the cathode side channel when the fuel cell system is running.

4.3.2 Transparent fuel cell

The transparent fuel cell is a single PEMFC with flow channel in a serpentine shape as the left channel shown in Figure 9. This fuel cell is designed by the author using the software package CATIA. The end plate of this fuel cell is made from plexiglass to make it transparent, so that the liquid water motion inside the serpentine channel can be recorded by the camera positioned directly above the horizontally placed fuel cell.

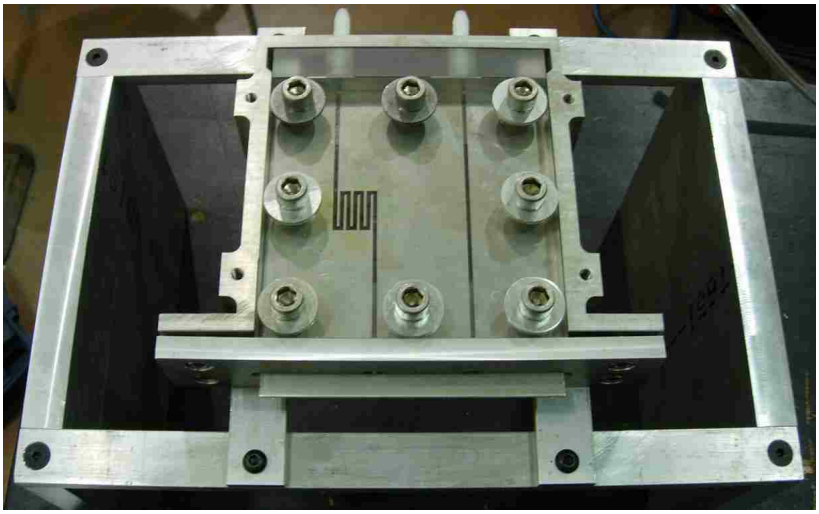

Fig. 9. A picture of the transparent fuel cell used in the experiment

A supporting frame is designed to support and fix the fuel cell horizontally with the cathode side facing up, so that the fluid flow in the channel will be influenced by the gravity only from the direction perpendicular to the MEA, and the cathode side where water is produced in the real fuel cell system can be recorded using the camera.

In this experiment, since the research concentrates on the liquid water removal process inside the cathode side of a PEMFC, the anode side flow channel and the isolation between the cathode side and the Anode side in the experiment setup is neglected. A syringe is used to pierce the MEA from the anode side into the cathode

side channel to inject the liquid water droplet. In this way, the initial liquid water droplet in the desired position can be achieved. In the mean time the vision of the camera will not be blocked.

4.3.3 Camera

A commercial camera is used in this experiment to capture the liquid water movement inside the fuel cell channel. The model number of this camera is JVC GZ-MG37. The pixel is 800.0 x, and the frame rate is 30 pictures per second.

Fig. 10. A picture of the commercial camera used in the experiment

4.4 Initial setting of the fluids

4.4.1 Air inlet mass flow rate

In the experiment done by the author, the air flow rate at the air inlet area of the transparent fuel cell is 1.07 L/min during the whole process according to the mass flow controller connected in the system. To set the same condition in the validation model, the air inlet mass flow rate is calculated as below.

$$\dot{m}_{air,in} = \rho_{air}\dot{V}_{air} = 1.225kg/m^3 \times 1.07L/\min = 2.18\times10^{-5}kg/s \quad (4.1)$$

4.4.2 Liquid water inlet mass flow rate

To control and record the liquid water inlet flow rate, a syringe is used to inject the liquid water with approximately uniform velocity into the flow channel in the experiment. The initial volume of the liquid water inside the syringe is recorded at the beginning before the experiment is conducted, and the time of the liquid water injection during the experiment is recorded. Finally the volume of the liquid water left inside the syringe after the experiment is recorded as well. By subtracting the volume of the liquid water left inside the syringe after the experiment from the initial volume of the liquid water inside the syringe, the total volume of liquid water which is injected into the channel during the experiment can be determined. Dividing this volume by the time of the liquid water injection, the average volume flow rate of the liquid water injection in the author's experiment is calculated as indicated in the equation below.

$$\dot{V}_{liquid} = \frac{V_{initial} - V_{left}}{t} = \frac{0.9mL - 0.6mL}{10s} = 3 \times 10^{-8} m^3 / s \tag{4.2}$$

To set the same condition in the validation model, the liquid water inlet mass flow rate is calculated as below.

$$\dot{m}_{liquid,in} = \rho_{liquid} \dot{V}_{liquid} = 999kg / m^3 \times 3 \times 10^{-8} m^3 / s = 3 \times 10^{-5} kg / s \tag{4.3}$$

4.4.3 Contact angle

To measure the contact angle of the droplet contacting different channel walls, one droplet is put on each piece of material used to build up the channel of the PEMFC, and pictures are taken from the horizontal direction. The contact angles are measured from these pictures using a protractor. The results show that the air-liquid water contact angle contacting the MEA is 130° as shown in Figure 11, the air-liquid water contact angle contacting the stainless steel flow field plate is 53° as shown in Figure 12, and the air-liquid water contact angle contacting the transparent end plate is 43° as shown in Figure 13.

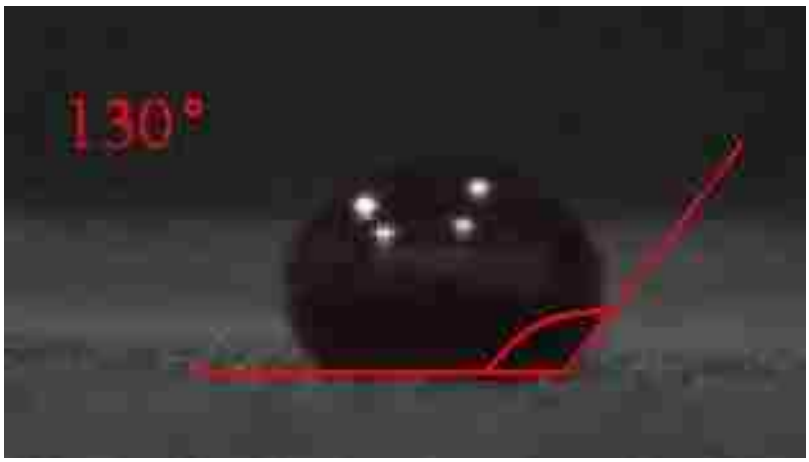

Fig. 11. Contact angle measured with one liquid water droplet on the MEA

Fig. 12. Contact angle measured with one liquid water droplet on the stainless steel flow field plate

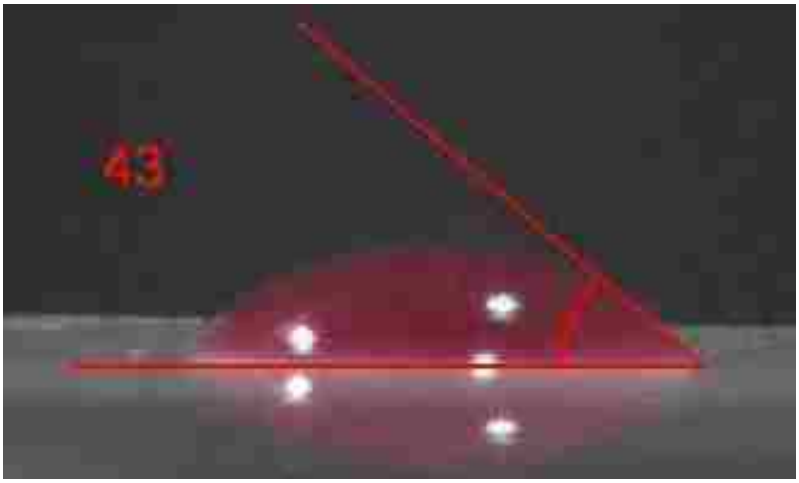

Fig. 13. Contact angle measured with one liquid water droplet on the transparent end plate

4.5 Experiment results and analysis

The results from the author's experiment are shown in Figure 14. To better visualize the liquid water inside the channel, the liquid water is dyed with red color. Droplets are injected at the inlet area of the serpentine channel in sequence. Once the droplet left the head of the syringe and passes into the channel, it goes quickly along the flow direction and hits the wall at the bending area. The liquid water tends to accumulated at this area for a short time. Then it becomes a slot moving along the flow direction attached with the side wall of the channel. Mostly this liquid water slot sticks to one wall of the channel during the whole removal process in the fuel cell channel. A thicker area at the head of the liquid water slot can be observed sometimes when the slot reaches a bend in the channel. This is due to the centrifugal effect when the fluid meets a turn. Finally the liquid water will gradually be drained out of the channel through the outlet.

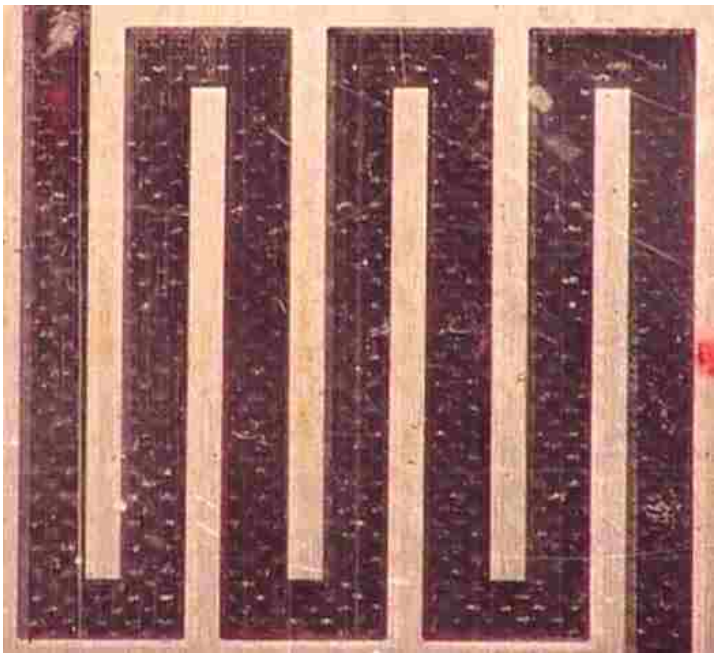

(a) t = 0 s; First droplet injected

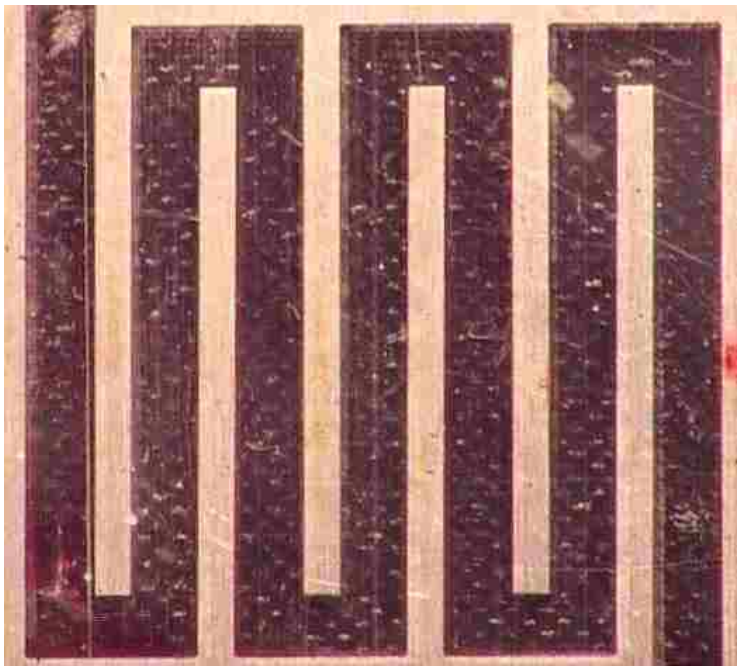

(b) t = 0.13 s; Liquid water accumulated at the bending area of the first segment in the channel

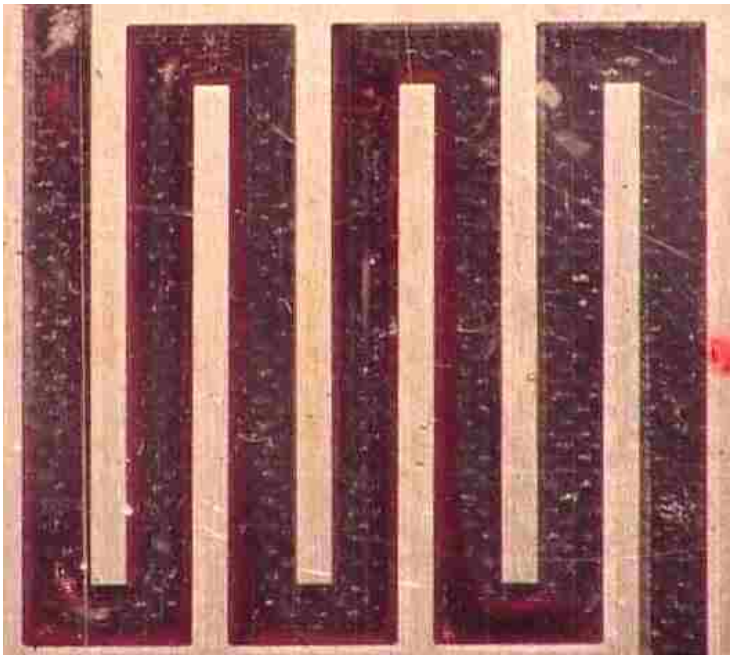

(c) t = 0.77 s; Liquid water slot stick to the channel wall and move along the flow direction

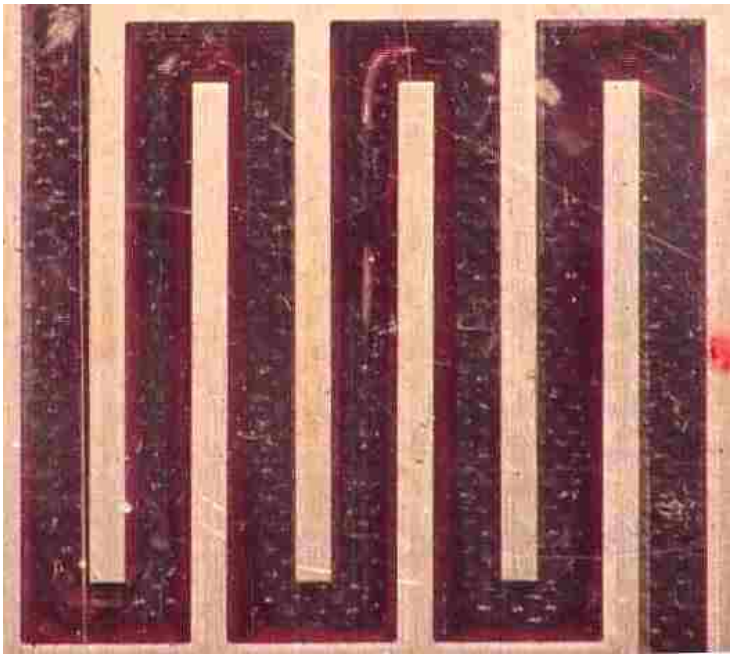

(d) A thicker area at the head of the liquid water slot observed when the slot reaches the bending area of the channel

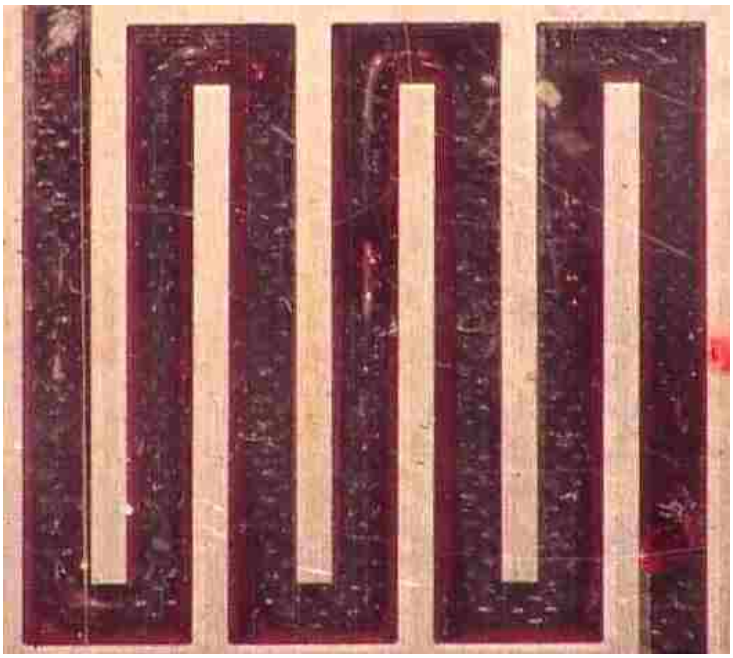

(e) t = 1 s; The liquid water slot approaching the outlet of the channel

Fig. 14. Liquid water removal process in the transparent fuel cell

4.6 Comparison of the numerical simulation results and experiment results

4.6.1 Image comparison

A numerical model with the same domain from the experiment setup is designed and created by the author and Le [37] together. The liquid water removal process from the numerical model with the initial conditions same as in the author's experiment is studied by the author, and the results from this model are compared with the experiment results as in Figure 15. To compare these two results, t = 0 s is artificially set to the instant when the first liquid water droplet is injected into the channel but has not yet fully departed the syringe as indicated in Figure 15 (a). As Figure 15 (b) shows, the droplets that are injected into the channel move with the gas flow to the first bend area of the serpentine channel, and hit the wall in front of it. A part of the liquid water from this droplet become tiny droplets and are drained with the flow, while another part of the liquid water accumulate at the bend area for a short period of time. After that, the liquid water forms a slot and moves along with the gas flow attaching to the wall of the channel as shown in Figure 15 (c) to (j). Finally at t = 1 s, the liquid water slot approaches the outlet of the channel. It can be seen from this comparison that the liquid water position in the channel in both simulation and experiment are qualitatively the same.

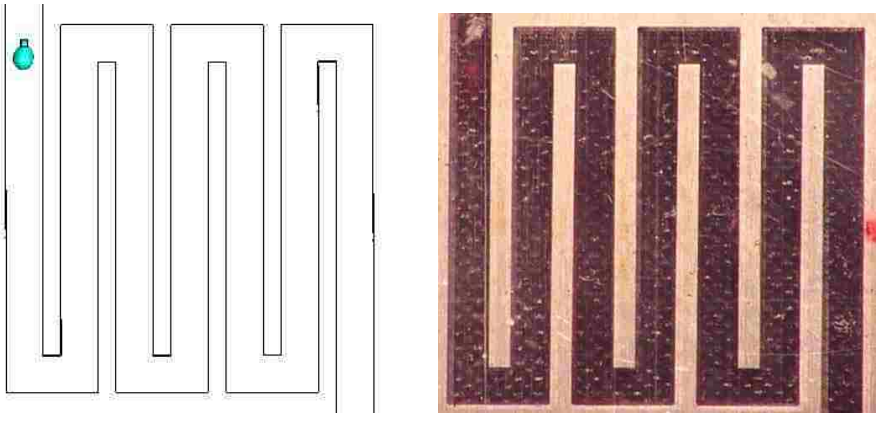

(a) t = 0 s; First droplet injected

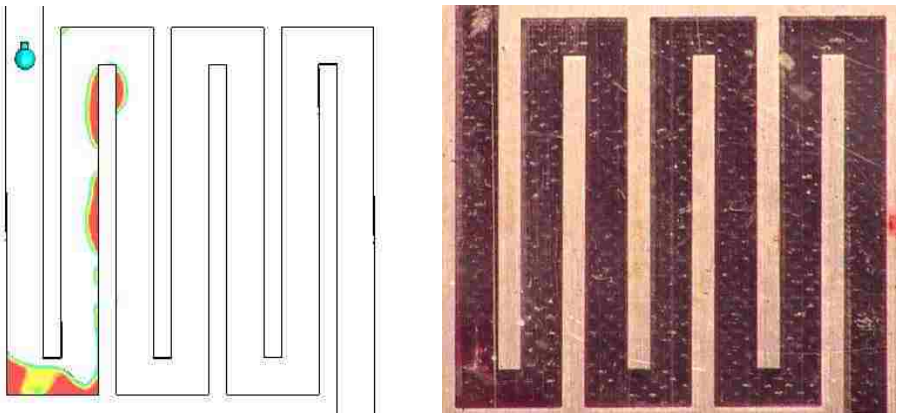

(b) Liquid water accumulated at the bending area of the first segment in the channel; figure captured at t = 0.145 s from numerical model and figure captured at 0.13 s from experiment

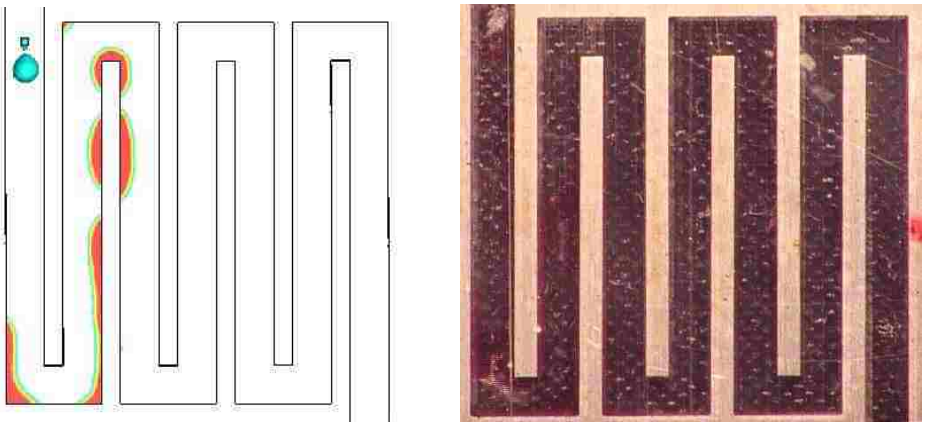

(c) t = 0.2 s; Liquid water move along the second segment of the channel

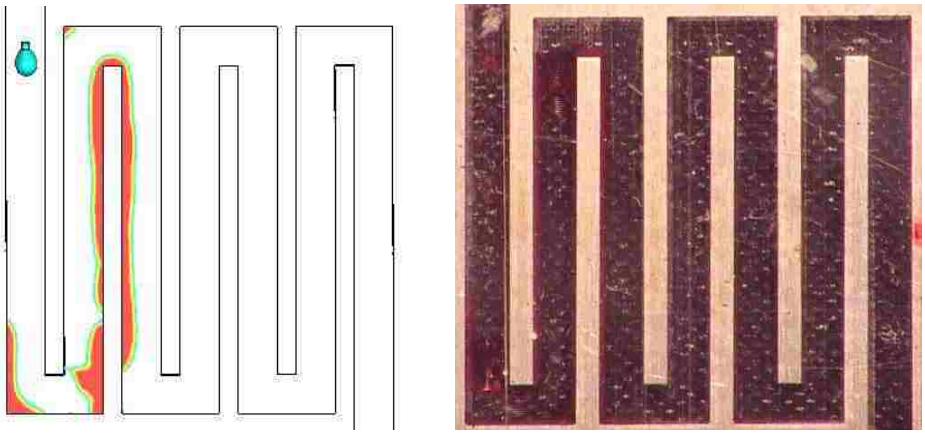

(d) t = 0.3 s; Liquid water become a slot moving along the channel

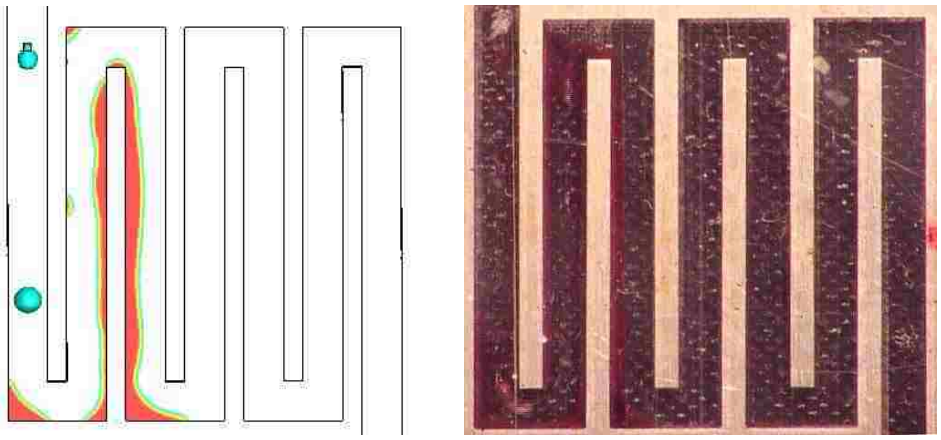

(e) t = 0.4 s; Liquid water reaches a bending area of the channel

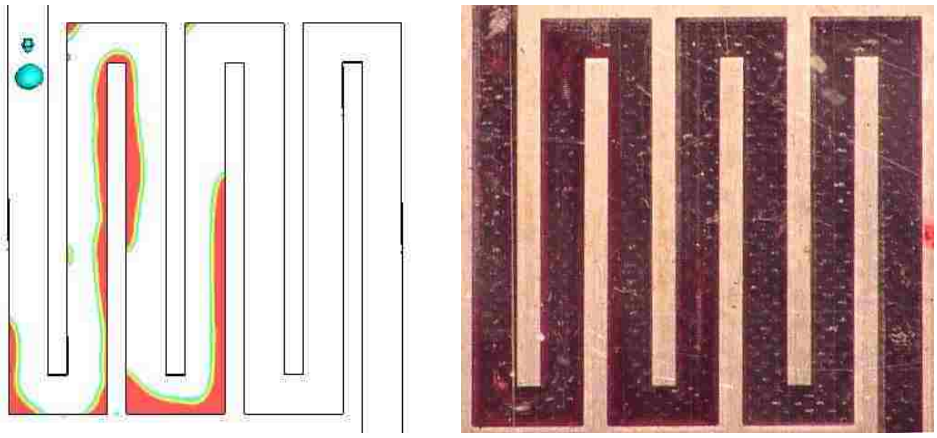

(f) t = 0.5 s; Liquid water slot moves along with the gas flow to the forth segment of the channel

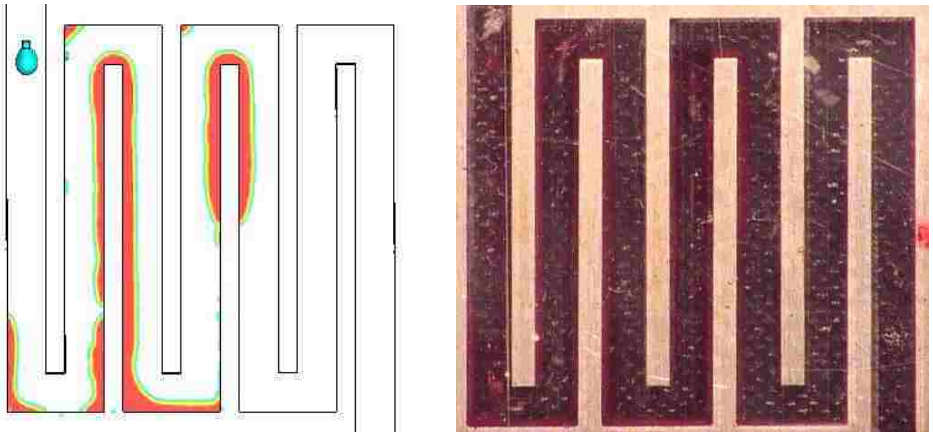

(g) t = 0.6 s; Liquid water slot reaches the fifth segment of the channel

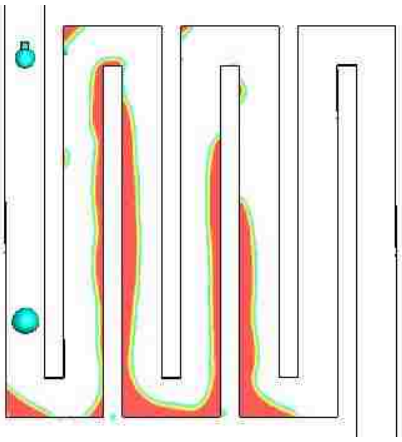
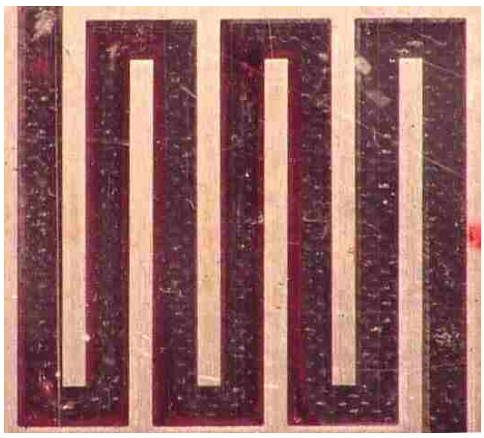

(h) t = 0.7 s; Liquid water slot reaches a bending area again

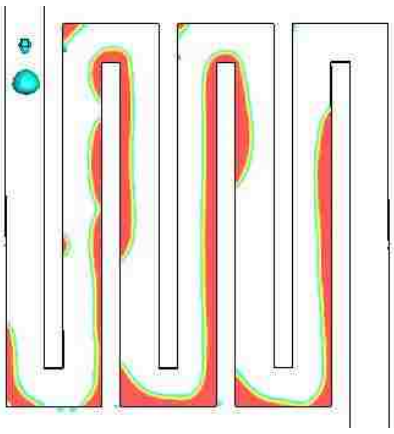
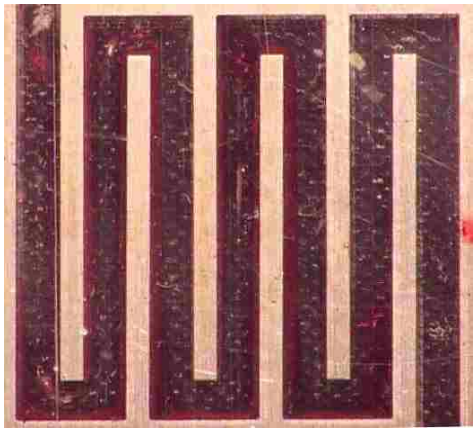

(i) t = 0.8 s; Liquid water slot stick to the channel wall and move to the sixth segment of the channel

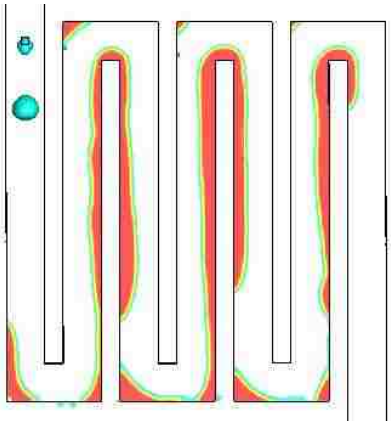
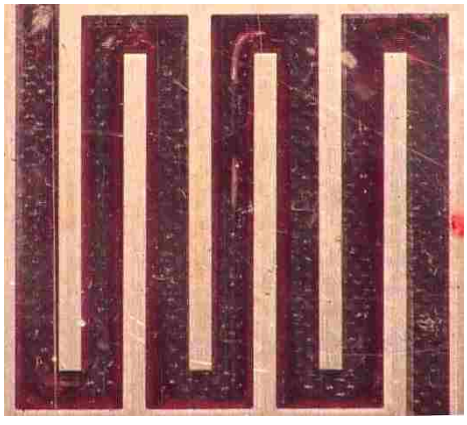

(j) t = 0.9 s; Liquid water slot moves to the last segment of the channel

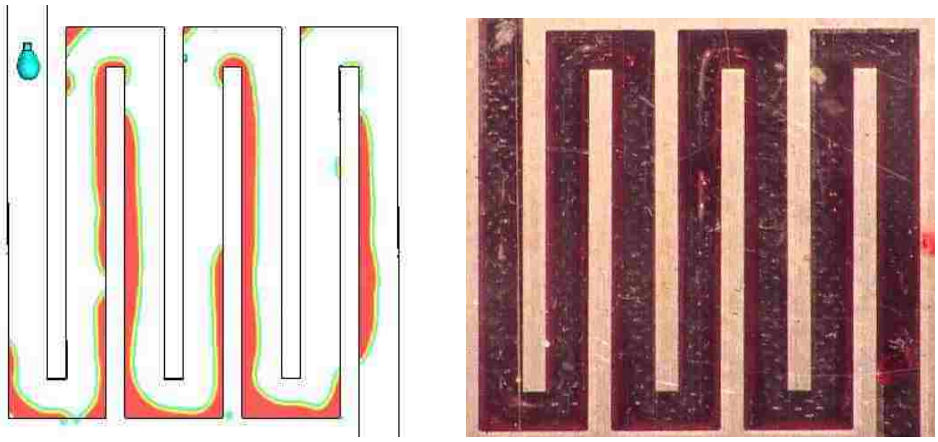

(k) Liquid water approach the outlet of the channel; figure captured at t = 0.97 s from the numerical model and figure captured at t = 1 s from the experiment

Fig. 15. Liquid water removal process comparison from both the validation model and the experiment

4.6.2 Pressure drop comparison

To further validate the numerical model applied in this project, the pressure drop data from both the experiment and the validation model are compared. The pressure drop data from the validation model is collected using the UDF function in Fluent [37], and the result is shown in Figure 16 (a), the pressure drop in the calculation domain starts to increase when the liquid water is injected into the channel. It continues to go higher along with time as more liquid water is injected. Fluctuations are observed, the peaks of these fluctuations correspond each liquid water droplet injected into the channel. Notice that though there are fluctuations observed, the overall trend of the pressure data is increasing from approximately 430 Pa to 480 Pa gradually. The pressure drop data from the experiment is shown in Figure 16 (b), the trend of the pressure drop along with time measured from the transparent fuel cell is quite similar with the data from the numerical validation model. A similar growth rate is indicated by the slope of the linear trend line from both numerical and experimental data. However most of the fluctuations captured from the validation model are not captured by the pressure transducer in the experiment system. This is mainly due to the relatively low

sensitivity and the flexibility of the hose used to connect the inlet of the transparent fuel cell to the test bench. Also the equipment used in the experiment usually responds to the data somewhat late causing the subtle change of the data not well detected. The hose in the experiment system as well as the part of the fuel cell channel that is longer than the calculation domain in the experiment setup and the manifold in the experiment system also induce a higher pressure drop. This can be observed by comparing the pressure drop data at each time instant from Figure 16 (a) and (b). The pressure drop in the connected hose is measured to be 20 Pa from the experimental setup. The extra pressure drop caused by the experiment setup can be calculated by using Darcy formulation [37] for the laminar flow.

$$\Delta P_L = f \frac{L}{D} \frac{\rho V_{avg}^2}{2} \tag{4.4}$$

Here $\rho V_{avg}^2 / 2$ is the dynamic pressure and f is the Darcy friction factor.

The pressure drop in the manifold is

$$\Delta P_1 = \frac{64}{\mathrm{Re}} \frac{L}{D} \frac{\rho V_{avg}^2}{2} = \frac{64}{612.5} \frac{0.1}{0.002} \frac{1.225 \times 5.25^2}{2} = 88 \text{ Pa} \tag{4.5}$$

And the pressure drop in the extra channel is

$$\Delta P_2 = \frac{57}{\mathrm{Re}} \frac{L}{D} \frac{\rho V_{avg}^2}{2} = \frac{57}{612.5} \frac{0.07}{0.0018} \frac{1.225 \times 5.25^2}{2} = 61 \text{ Pa} \tag{4.6}$$

Thus, the total pressure drop due to connection is approximate 169 Pa. By deducting this number, the pressure drop data from the validation model and the experiment are approximately the same.

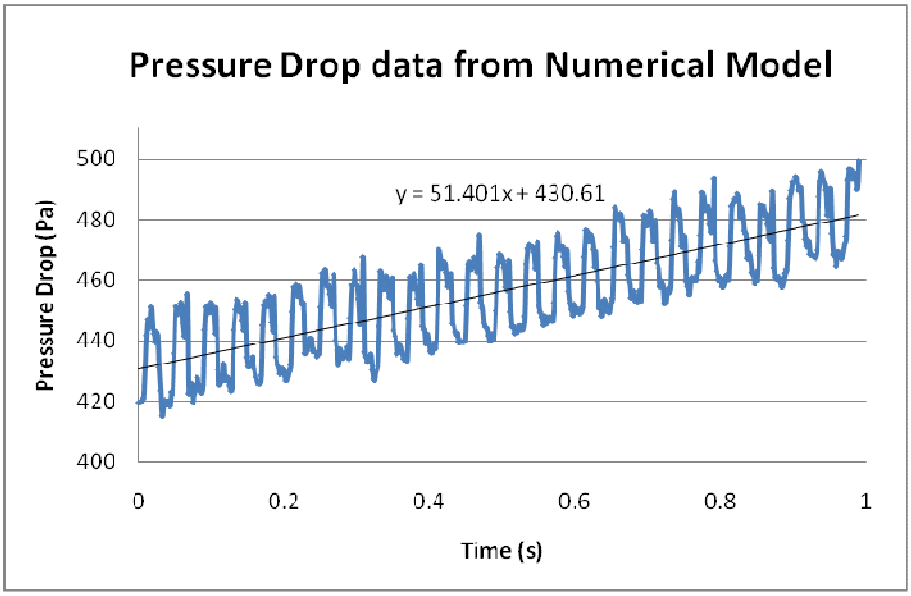

(a) Pressure drop data from the validation model

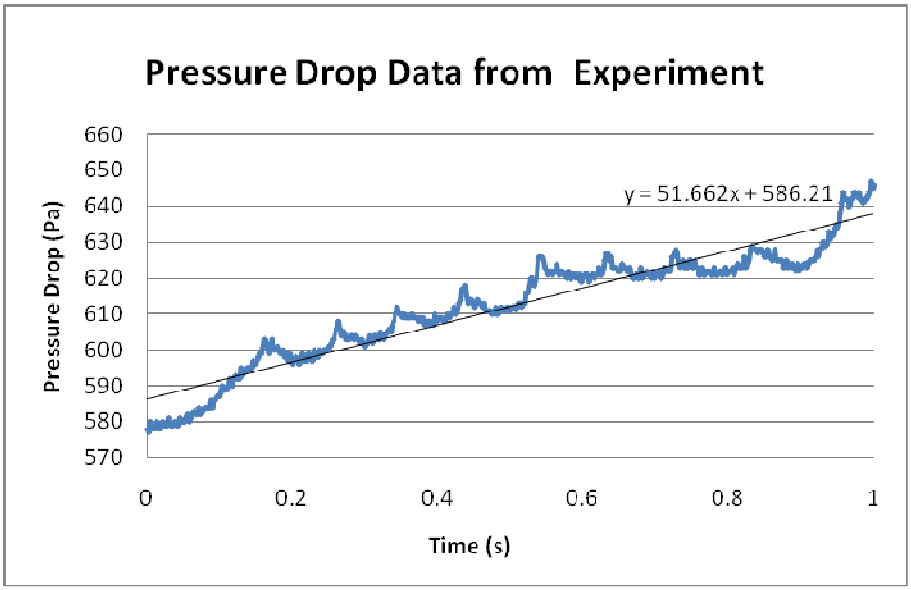

(b) Pressure drop data from the experiment

Fig. 16. Pressure drop data get from both the validation model and the experiment

4.7 Summary

1. The feature of the liquid water movement in the channel is approximately the same in the experiment result and the numerical result.
2. The time for each stage of the liquid water movement in the channel is similar from the experiment result and the numerical result.
3. The pressure drop during the whole process of liquid water removal is similar from the experiment result and the numerical result. Some fluctuations are not captured in the experiment result due to the relatively low sensitivity and the flexibility of the hose used to connect the inlet of the transparent fuel cell to the test bench. Also the equipment used in the experiment usually responds to the data somewhat late causing the subtle change of the data not well detected.

CHAPTER 5

LIQUID WATER REMOVAL PROCESS IN SERPENTINE CHANNEL WITH POROUS LAYER

5.1 General process of liquid water removal

To show the water removal process, global water movement in this case is studied step by step. As can be seen in Figure 17, liquid water begins to emerge into the channel from the corner area a short period after the simulation begins. Most of the droplets emerged into the channel move along with the gas flow attached to the wall of the channel and are finally purged through the outlet. However some of them will be trapped at the corner area. While a portion of the liquid water comes into the channel area from the porous layer, another part of the liquid water remains inside the porous layer becoming oscillating droplets and will be removed more slowly than the other part.

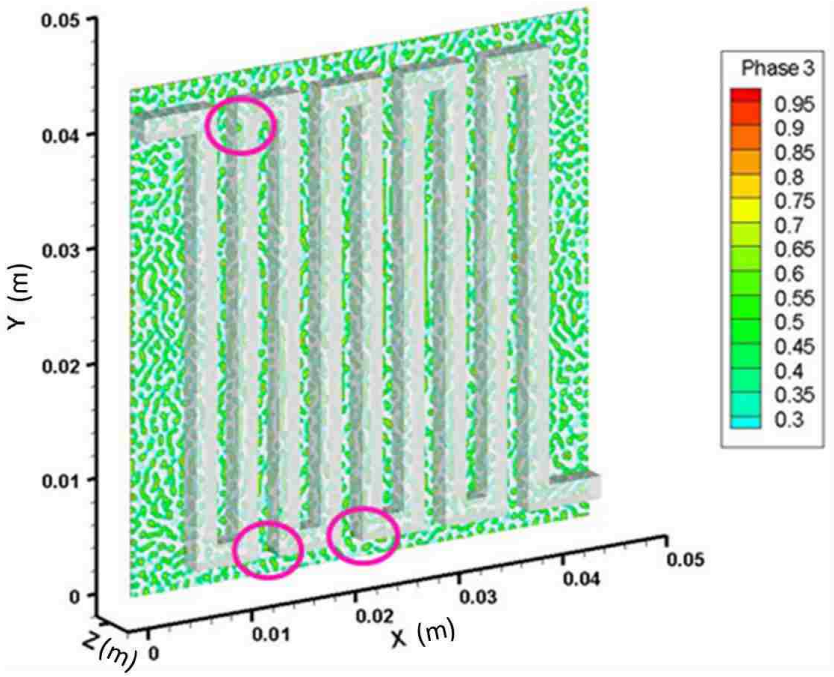

(a) t = 0.16 s

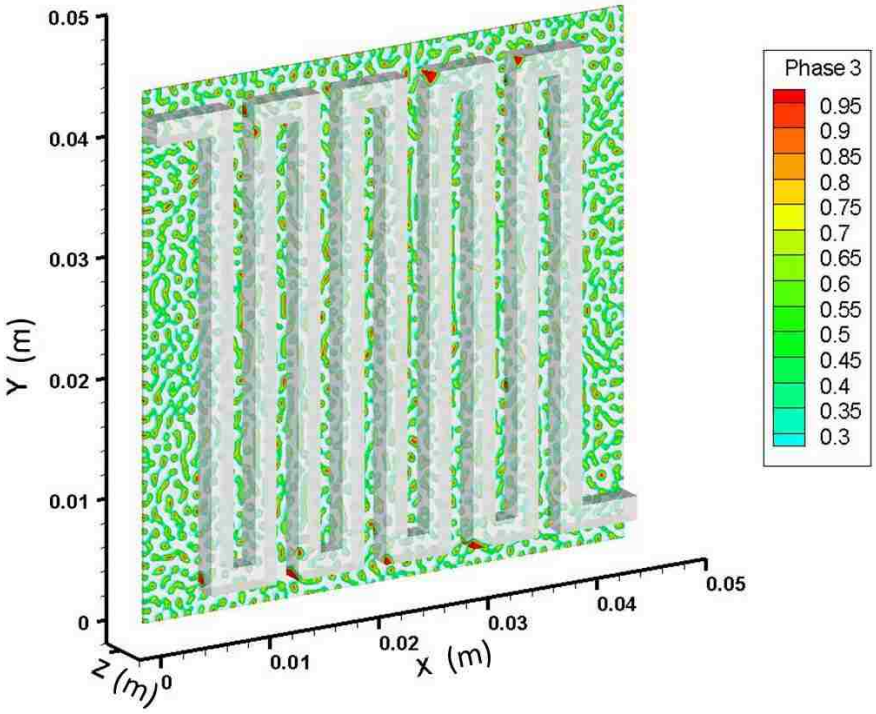

(b) t = 0.36 s

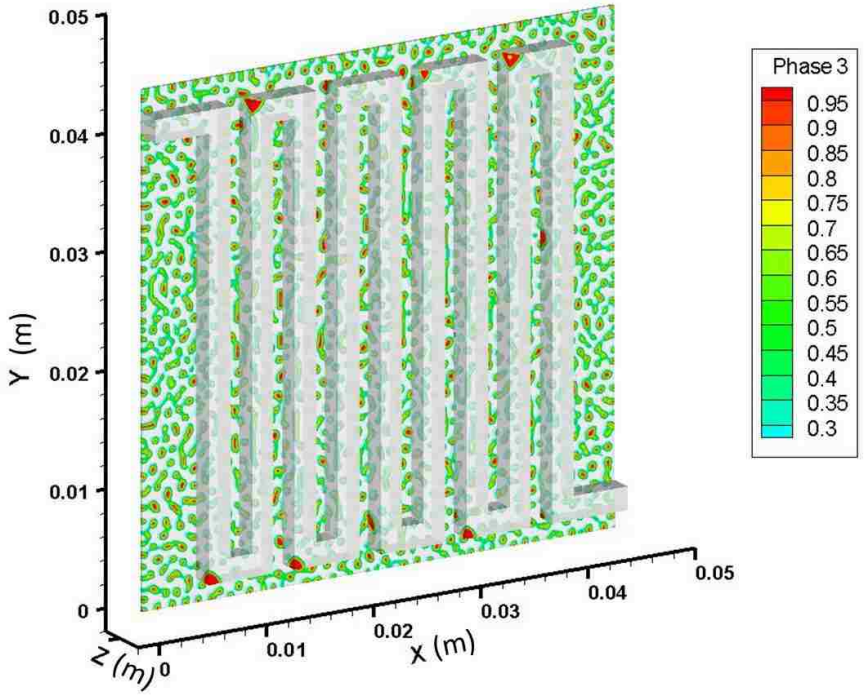

(c) t = 0.56 s

Fig. 17. General process of liquid water removal in serpentine channel with porous layer domain

5.2 Liquid water emerging into the channel from porous layer

From Figure 17 (a) we can see that water starts to emerge into the channel area a short time after the simulation begins. It was observed that most of the water which emerged into the channel domain will stay attached to at least one wall of the channel, and move along the general gas flow direction. When the droplets get to the bend area of the channel, most of them will be held in a certain position near the corner and oscillate for a period of time as shown in Figure 18. This is due to the back flow region that appears at the bend areas when the gas meets the wall. The water droplet which is held there by the back flow will grow larger and larger along with time as more droplets come to the same position and join the previous droplet. When this droplet reaches a certain volume, it will move forward along the general flow direction and collide with the wall in front of it. A part of this volume of liquid water will become small free droplets move along with the flow to the next segment of the channel, while another part of it will be trapped in the corner area or suspended near the corner area as shown in Figure 19. This trapped or suspended water at the corner area phenomenon is very similar to the phenomenon observed by Spernjak et al. [40] from their experimental results. The pictures shown in Figure 18 and Figure 19 are the section of the calculation domain at x = 0.02105 m, which shows the phenomena mentioned above clearly.

Some of the small droplets that emerged into the channel from the porous layer will stay in a certain position inside the channel attached to the porous layer until a larger droplet meets it as shown in Figure 20, and sometimes two moving droplets will meet each other in the channel as well. Subsequently, the combined larger droplets will reach the position near the bend area where the droplets are held and oscillate for a while until a certain volume of liquid water is reached, then collide at the corner. Within all these processes, the droplets are attached to at least one wall of the channel, while only a few of the smallest droplets become free droplets that move with the flow and are drained out directly. Figure 20 indicates the section of the calculation domain at x = 0.03305 m.

In Figures 18 to 20, it can be seen that the droplets in these pictures are not as round as one would expect. Instead, they are in a shape of sharp triangles. This is because the ratio of Y and Z axis has been adjusted to 1:10 in these pictures so that the liquid water can be seen clearly. If shown in regular ratio, the water droplets which emerged into the channel domain are in fact round. Also, as mentioned in the previous paragraph, the sections in Figures 18 to 20 are all near one wall of the channel. This is because the droplets observed in these pictures are attached not only to one wall of the channel. They attach to the common plane of the channel and porous layer, and are also attached to a wall of the channel which is perpendicular to the porous layer.

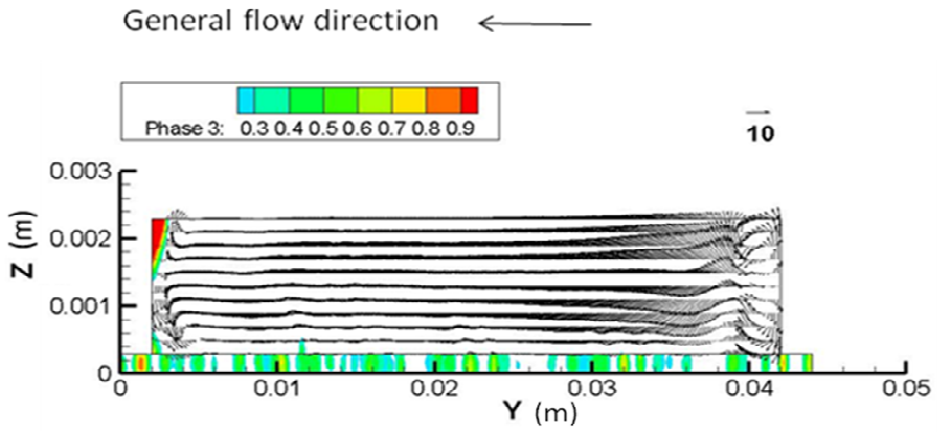

(a) t = 0.28 s

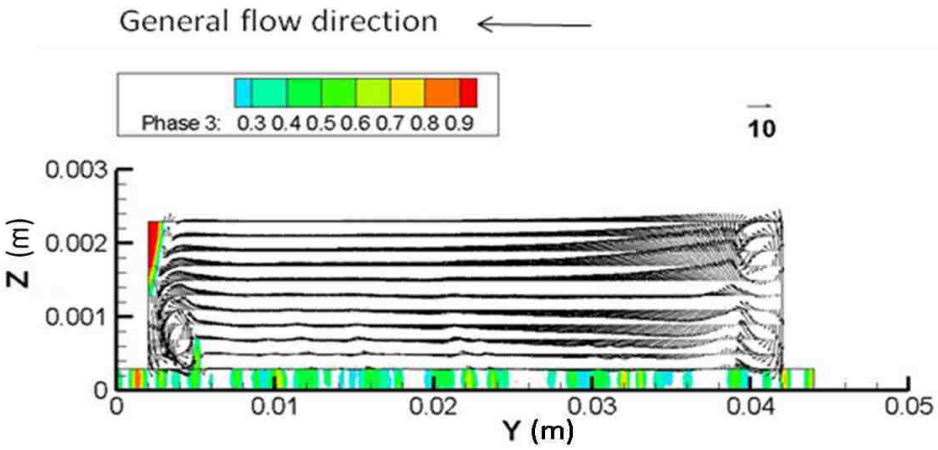

(b) t = 0.3 s

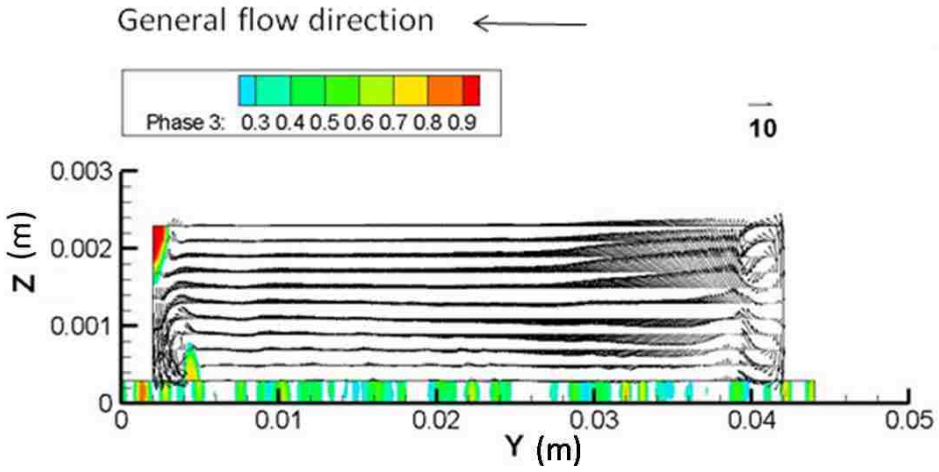

(c) t = 0.32 s

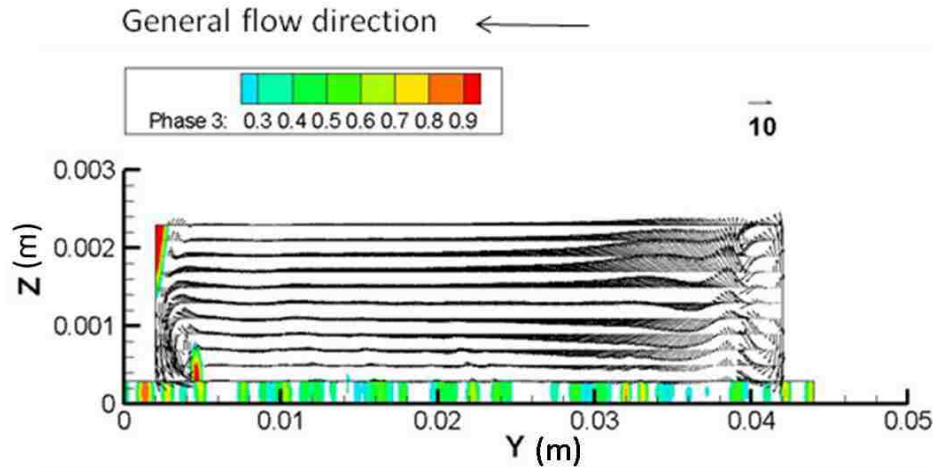

(d) t = 0.34 s

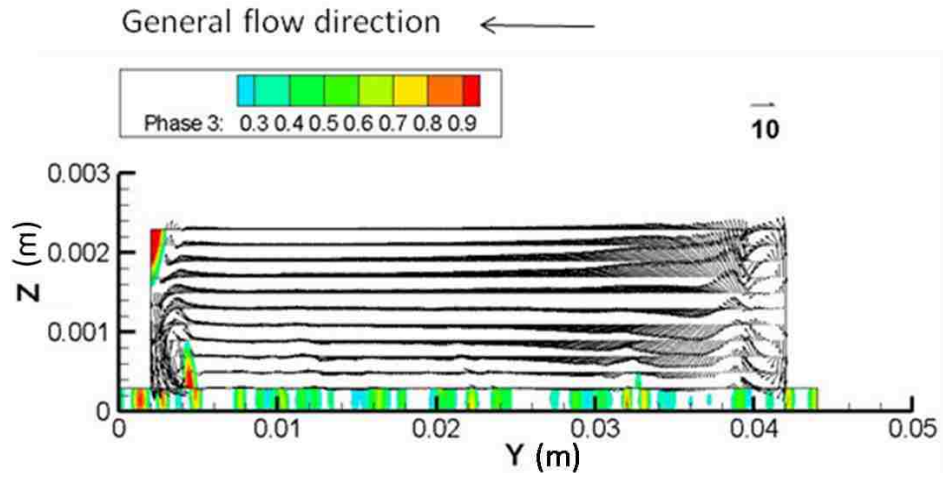

(e) t = 0.36 s

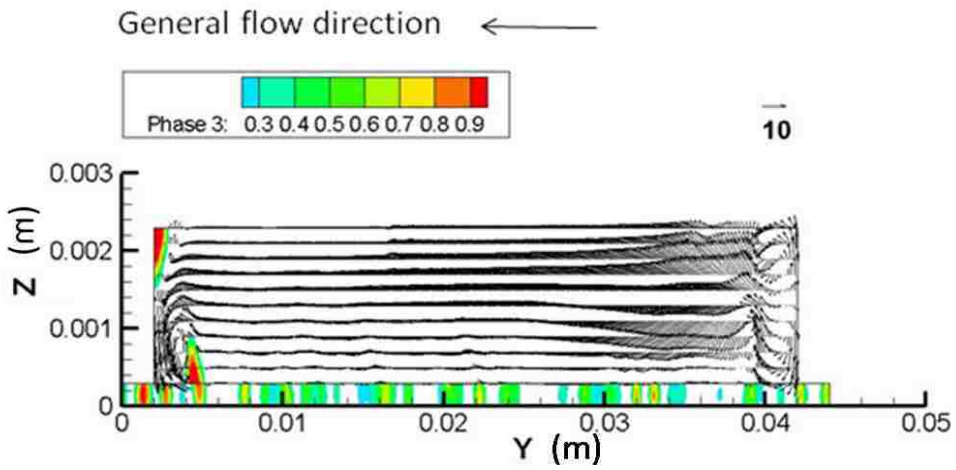

(f) t = 0.38 s

Fig. 18. The droplet held near the bending area of the channel due to the back flow

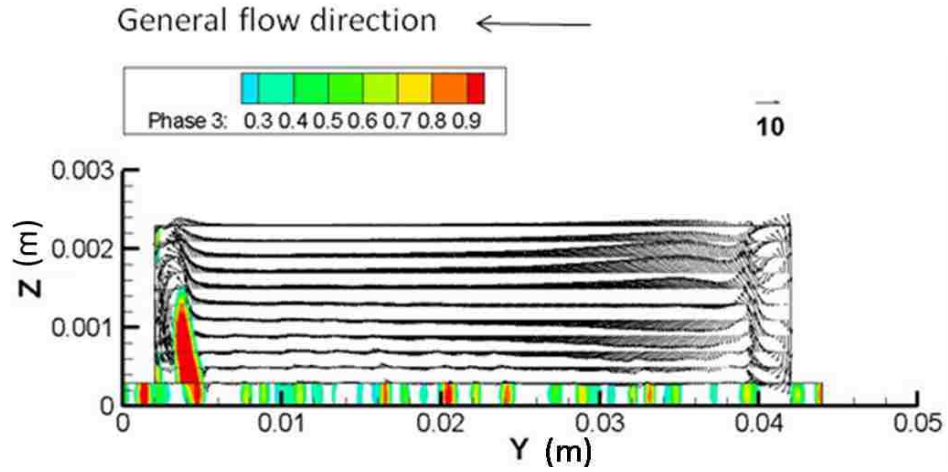

(a) t = 0.69 s

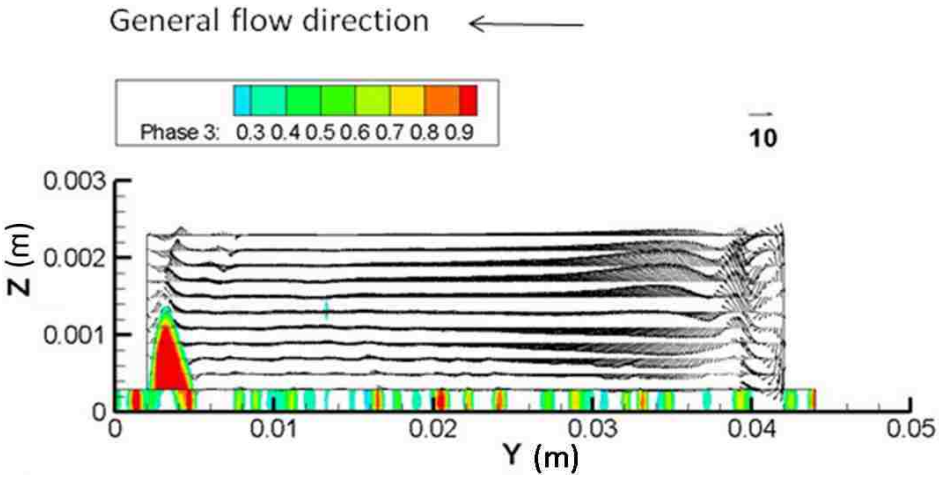

(b) t = 0.71 s

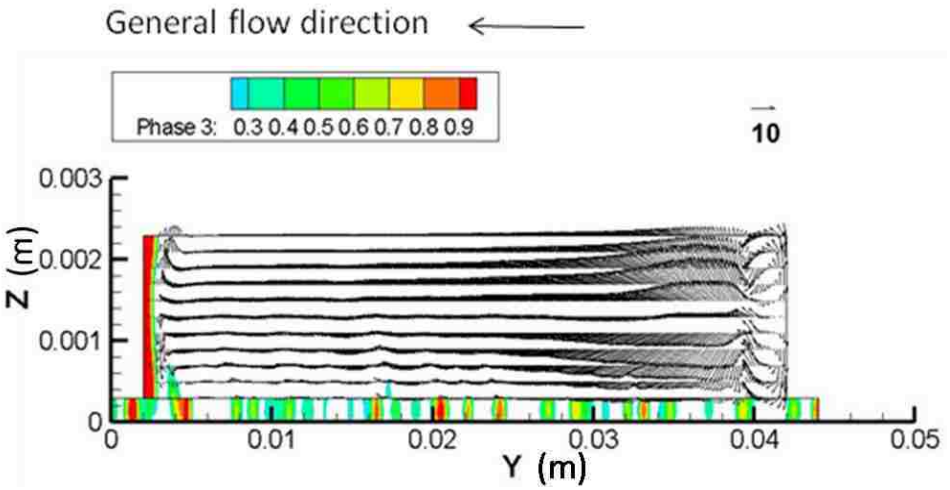

(c) t = 0.73 s

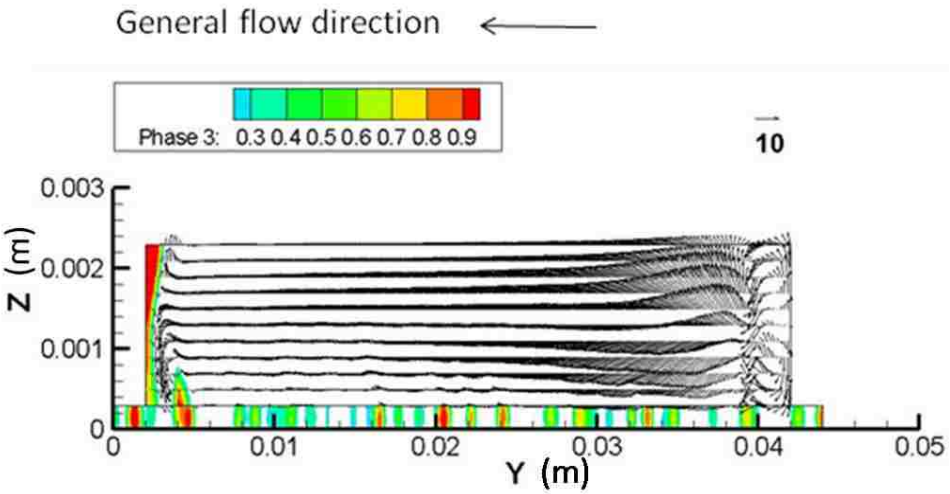

(d) t = 0.75 s

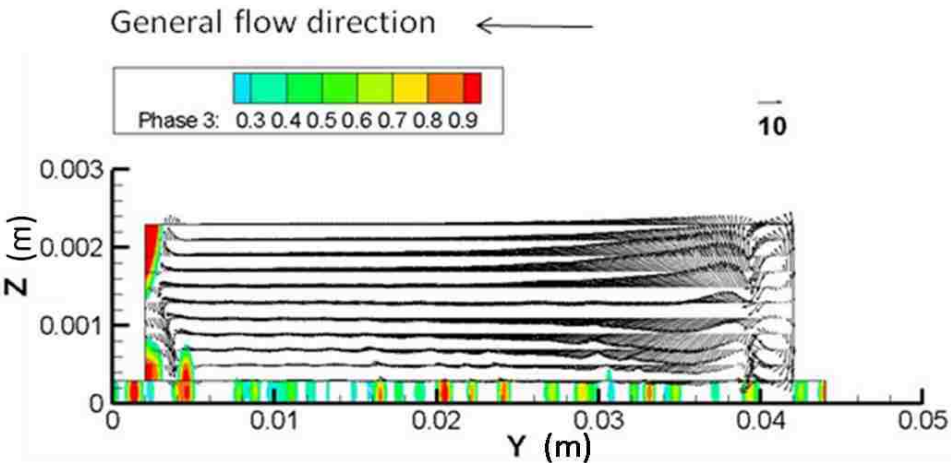

(e) t = 0.77 s

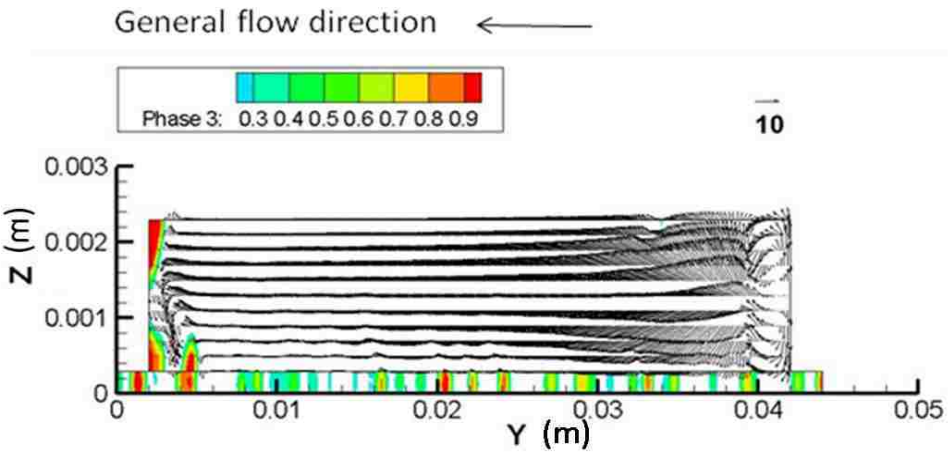

(f) t = 0.79 s

Fig. 19. The droplet collides with the wall at the bend area of the channel

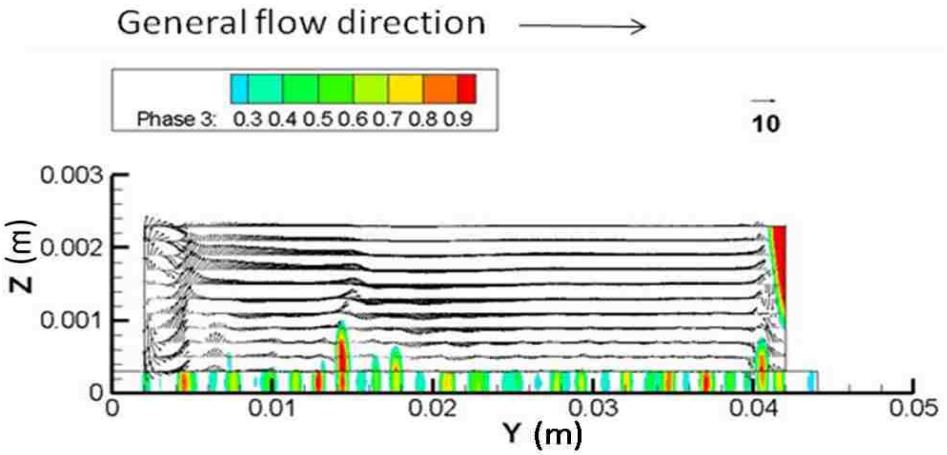

(a) t = 0.452 s

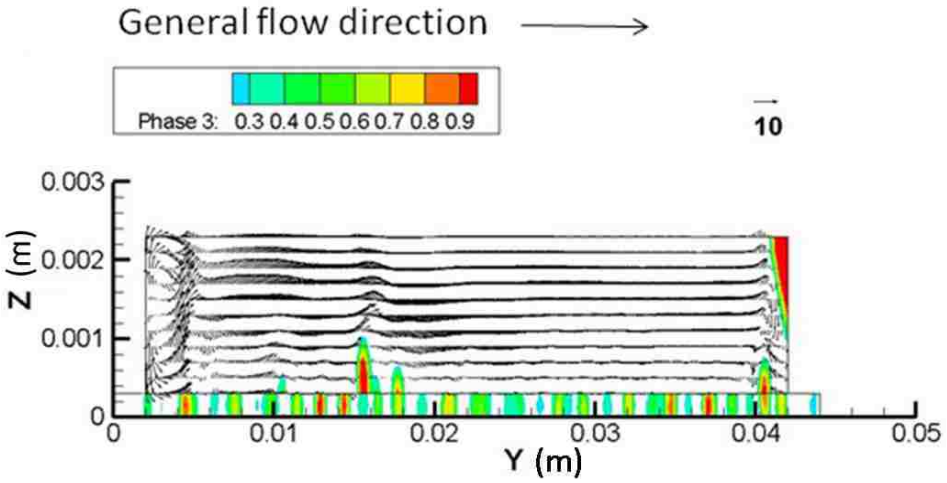

(b) t = 0.455 s

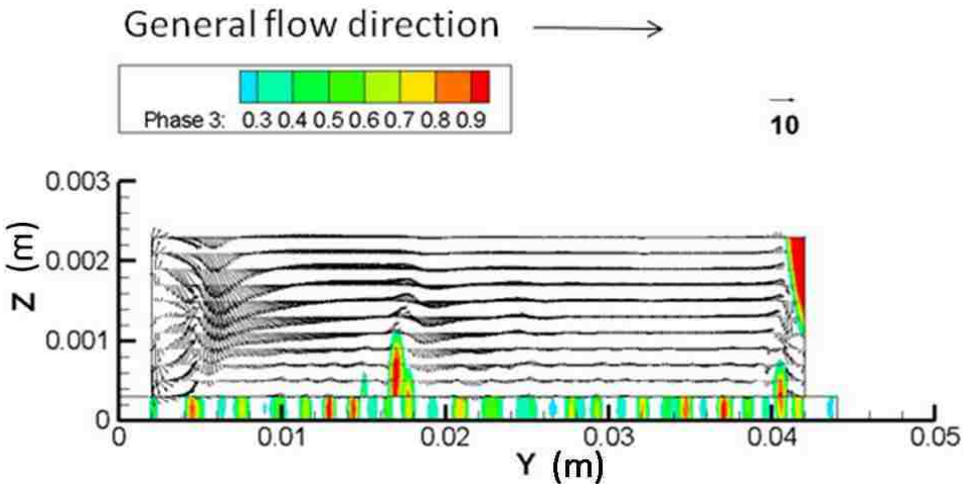

(c) t = 0.458 s

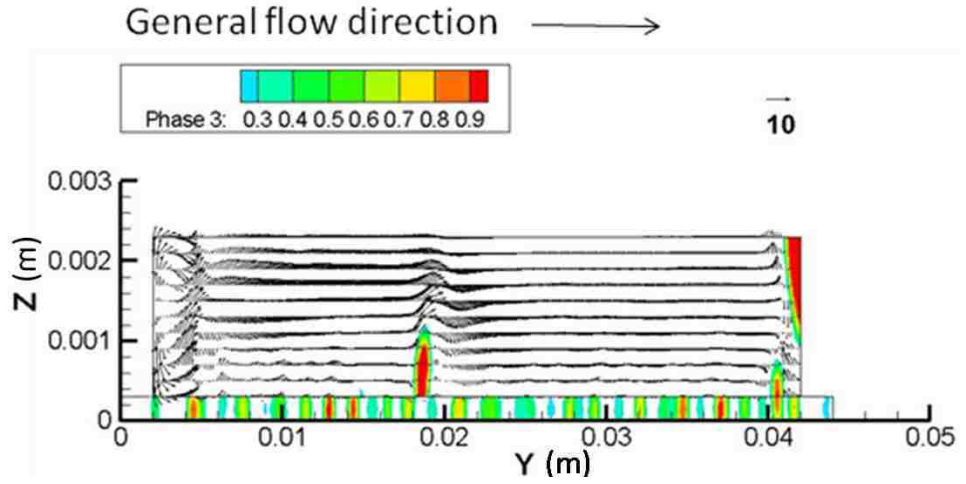

(d) t = 0.461 s

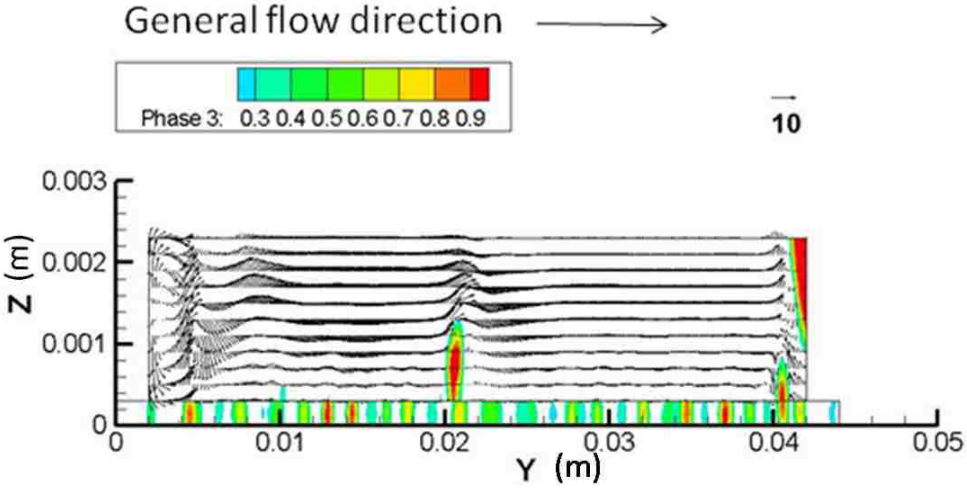

(e) t = 0.464 s

Fig. 20. One droplet catches up with another when moving along the channel

5.3 Liquid water moving inside the porous layer

While the water emerges into the channel area, the water has a certain trend of movement within the porous layer as well. Before the water appears in the porous layer of a fuel cell, there is a pressure field caused by the gas flow in both the channel and porous layer domain as shown in Figure 21. Since we set the water as a film in the middle of the porous layer, there is a gap between the water film and the channel area which allows gas and water to move through as shown in Figure 7 (b) in chapter 3. At the beginning stage, this pressure field influences the liquid water movement. It drives the gas flow to go through the porous layer under the ribs from one channel segment with higher pressure to the next with lower pressure. A part of the liquid water under the ribs is, therefore, moved by this cross flow after the simulation starts as shown in Figure 22 (a) to (c). The gas flow along the channel also helps the liquid water removal process gradually as shown in Figure 22 (d) to (f). The liquid water volume fraction under the channel area reduces faster than the edge area. Figure 22 gives the domain section at z = 0.00015 m, which is the middle slice of the porous layer. Here phase3 in these figures and all the following figures in this project represents the liquid water volume fraction. The channel is not able to be seen from this section. However to clearly observe the result, the channel boundary is included in this figure.

After about 0.2 s, the water volume fraction decreases in the entire area of the porous layer, and the original water film is gradually split into many droplets that hang in the porous layer as shown in Figure 23. Each droplet oscillates at its hanging position and can not be drained out with the gas flow due to the surface tension effect of the liquid water and the porosity of the porous media. Comparing the five pictures in Figure 23, though generally the liquid water volume fraction is decreasing along with time in this plane, there are some spots in these pictures where the liquid water volume fraction is actually increasing. This means that the portion of liquid water left inside the porous layer tends to be driven together after a period of time, and most of these high water

volume fraction areas are under the ribs of the geometry where the gas flow velocity is relatively low.

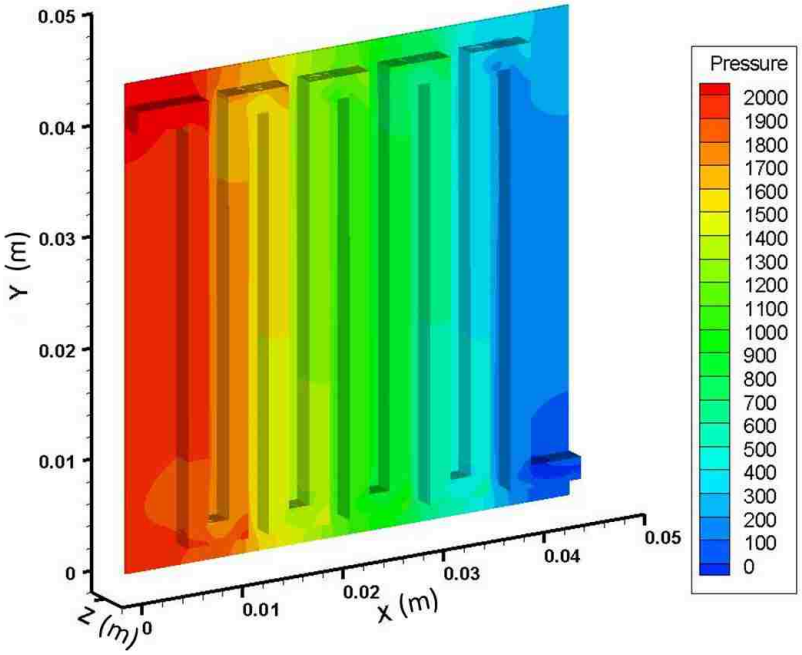

Fig. 21. Pressure field caused by gas flow before the liquid water film is set

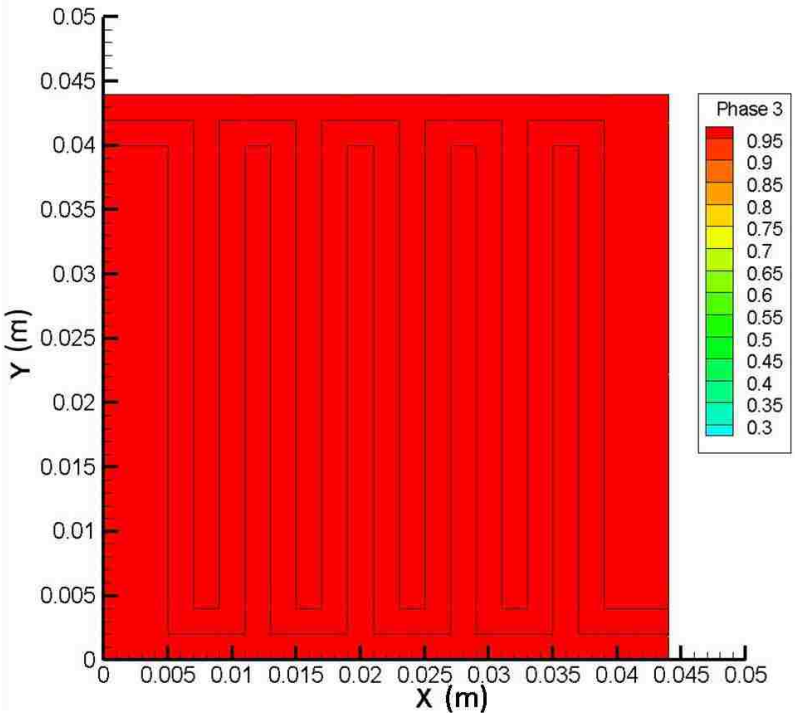

(a) t = 0 s

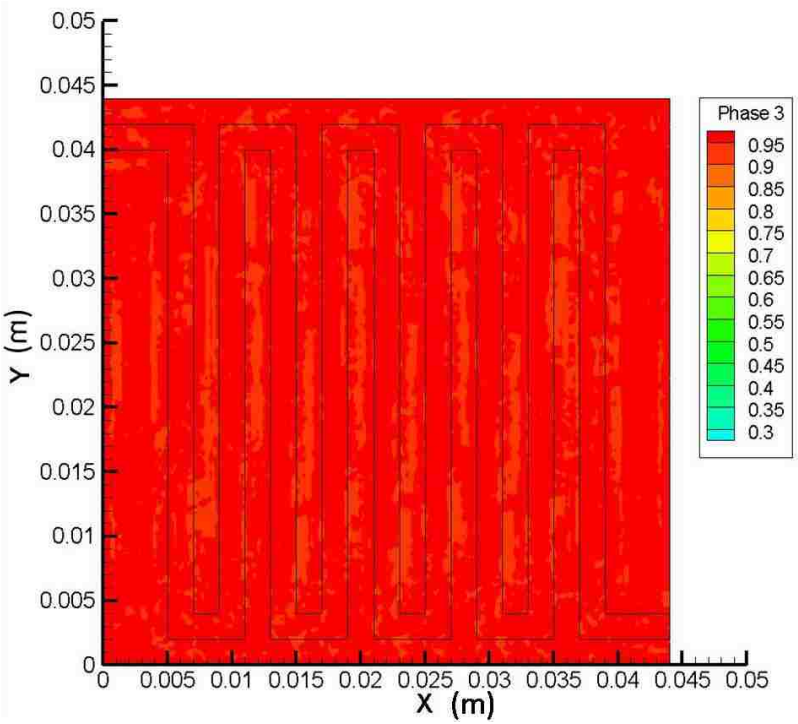

(b) t = 0.001 s

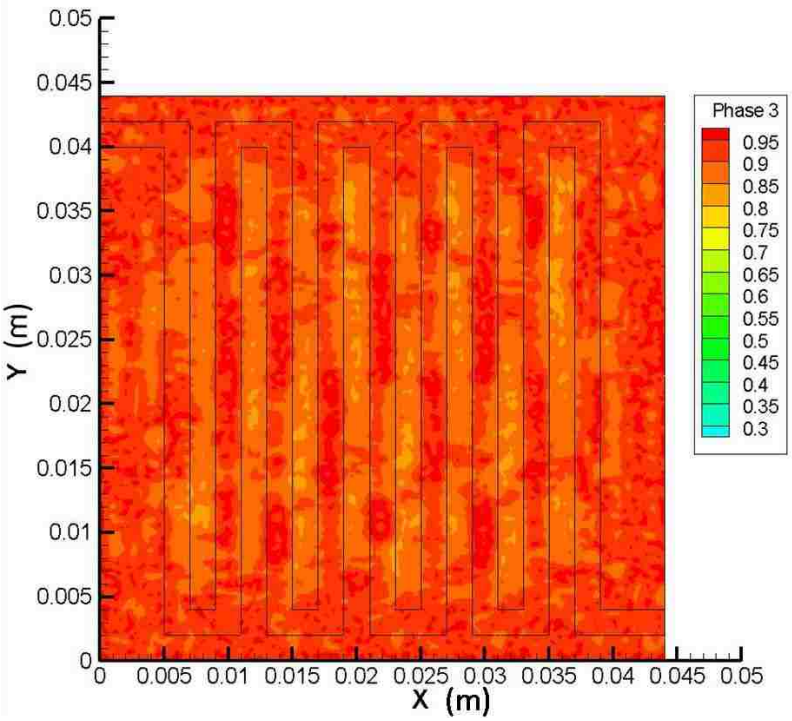

(c) t = 0.002 s

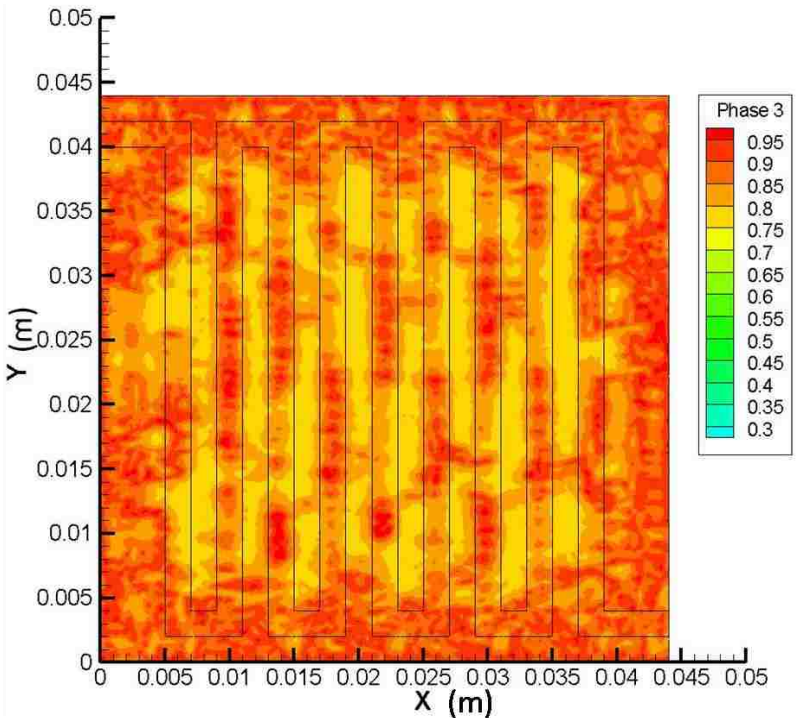

(d) t = 0.003 s

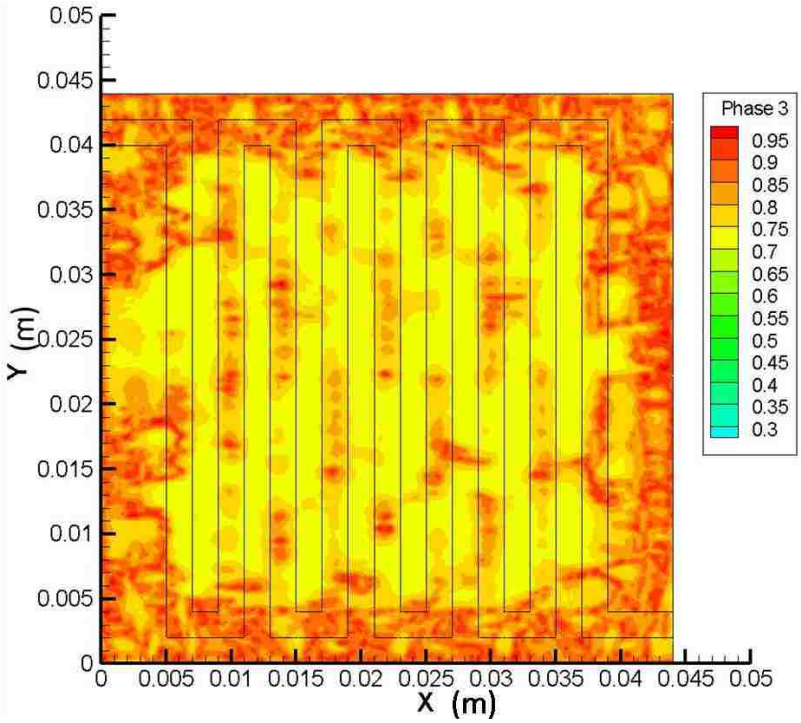

(e) t = 0.004 s

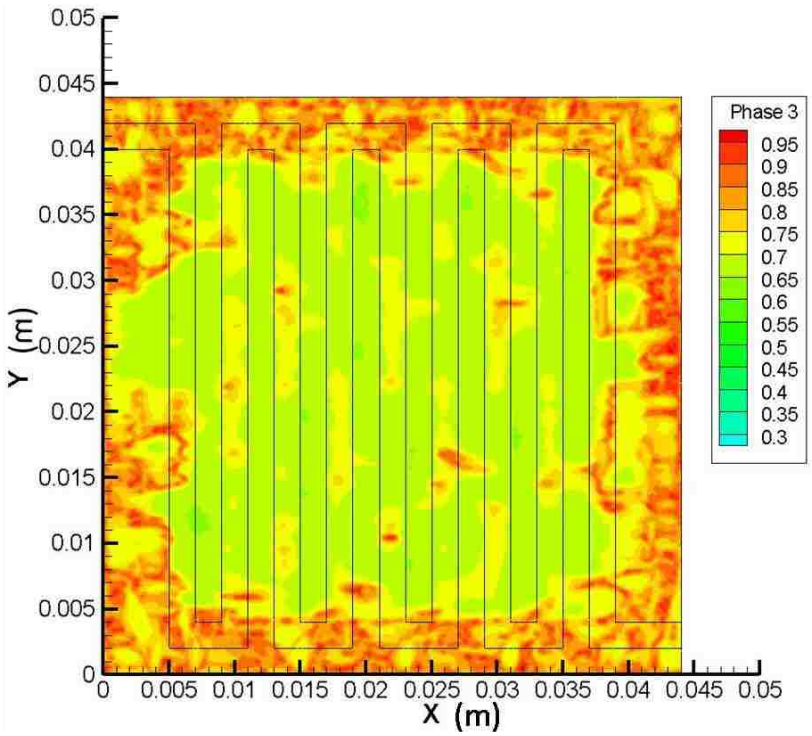

(f) *t = 0.005 s*

Fig. 22. Liquid water movement inside the porous layer at the beginning period of the simulation

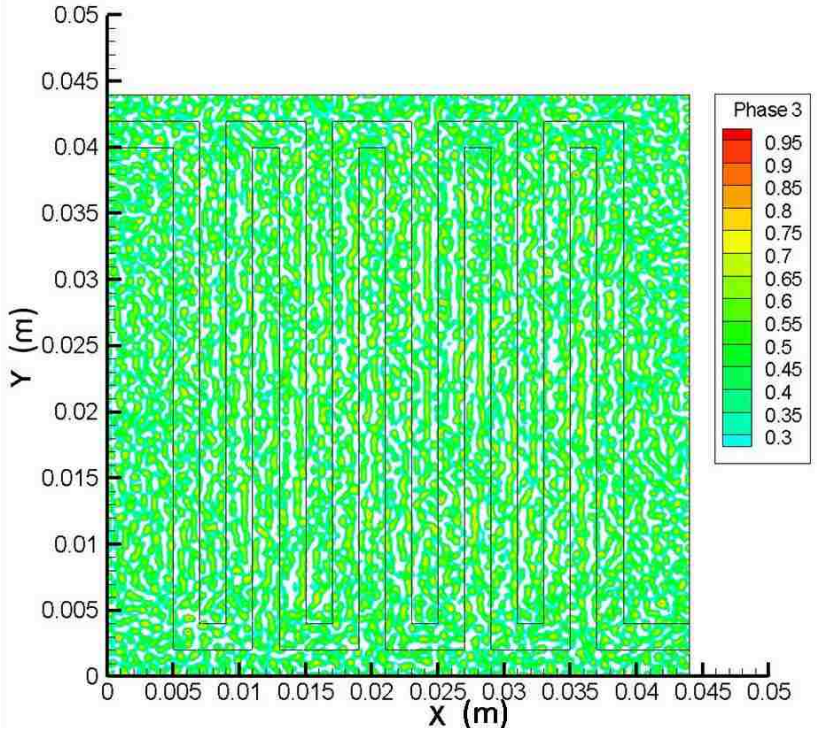

(a) t = 0.2 s

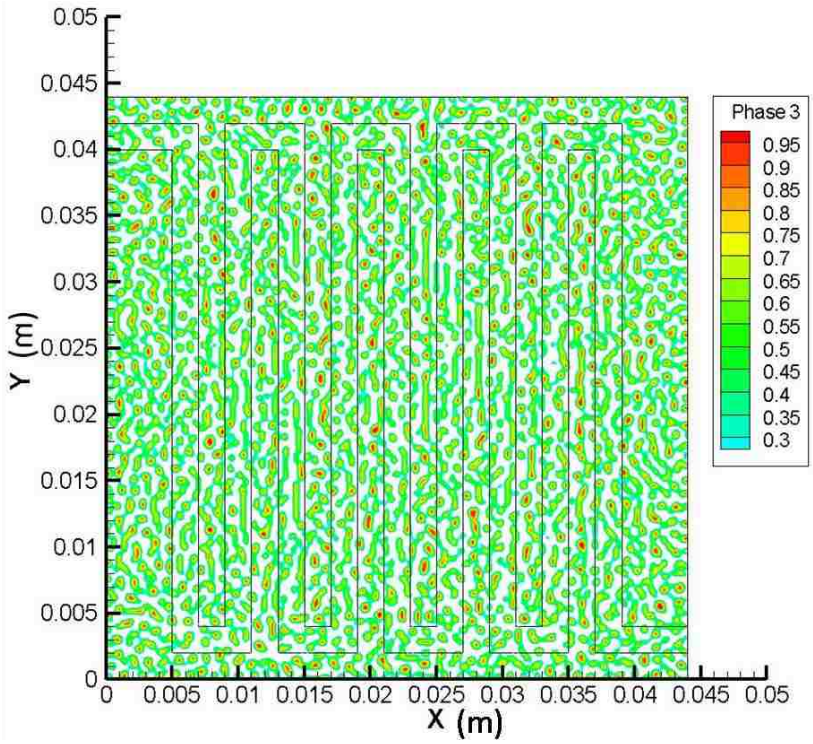
Phase 3
0.95
0.9
0.85
0.8
0.75
0.7
0.65
0.6
0.55
0.5
0.45
0.4
0.35
0.3
Y (m)
X (m)
0
0.005
0.01
0.015
0.02
0.025
0.03
0.035
0.04
0.045
0.05

(b) t = 0.4 s

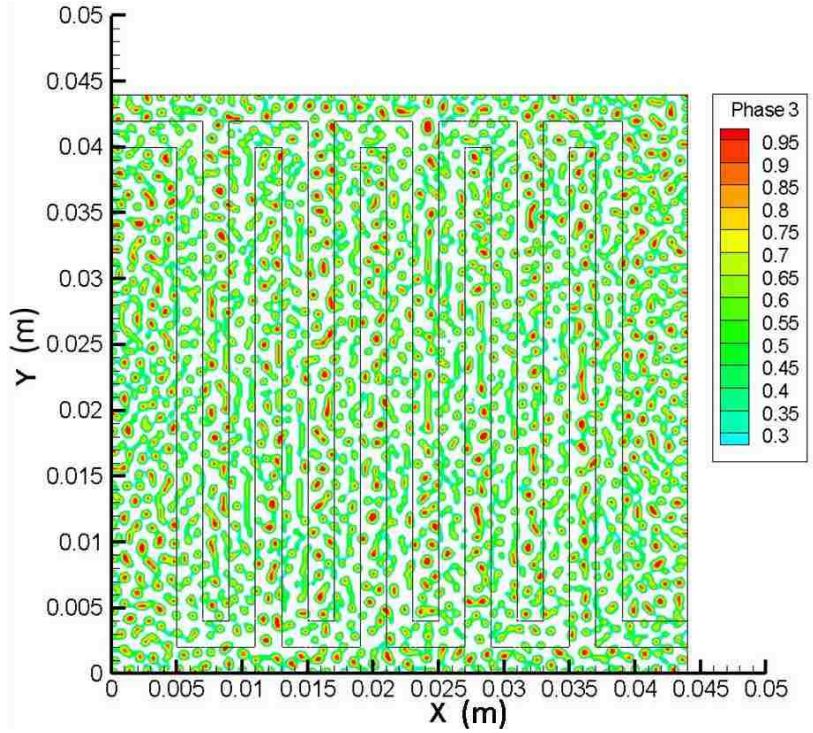
Phase 3
0.95
0.9
0.85
0.8
0.75
0.7
0.65
0.6
0.55
0.5
0.45
0.4
0.35
0.3
Y (m)
X (m)
0
0.005
0.01
0.015
0.02
0.025
0.03
0.035
0.04
0.045
0.05

(c) t = 0.6 s

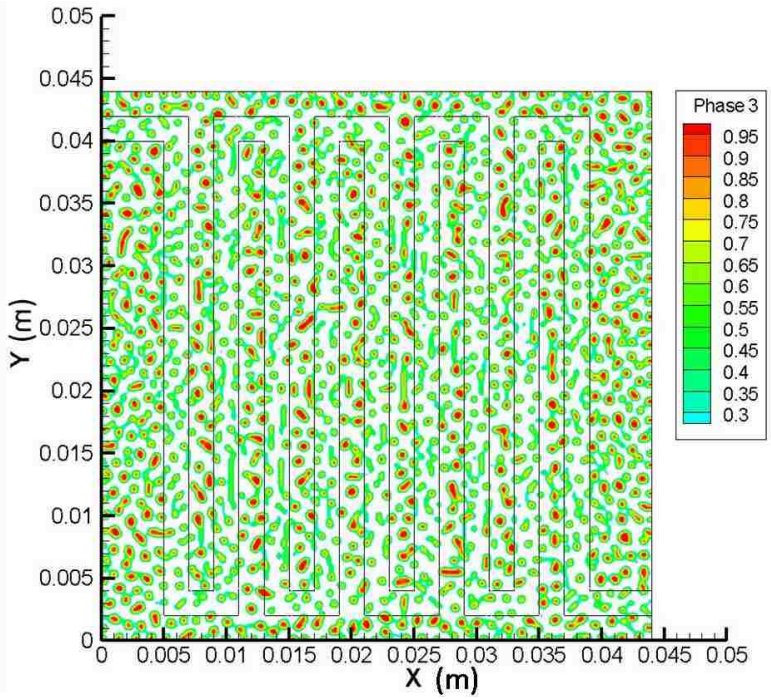

(d) t = 0.8 s

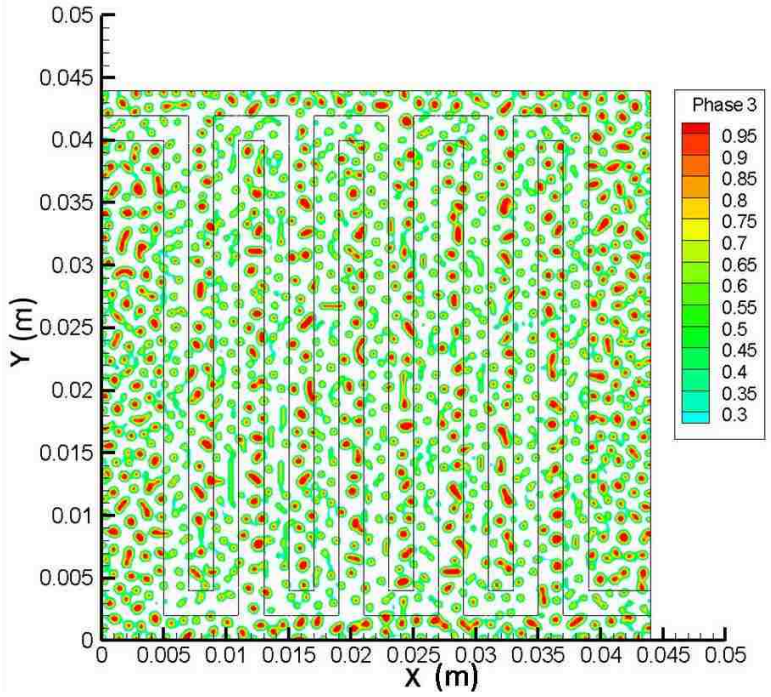

(e) t = 1 s

Fig. 23. Liquid water movement inside the porous layer along with time

5.4 Summary

1. Liquid water emerges from the porous layer to the channel area firstly from the corner area after a certain period of time.
2. Liquid water emerged into the channel area mostly attach to one of the channel walls during its movement within the channel.
3. Some liquid water droplets are trapped in the corner area of the channel.
4. Small liquid water droplets are held by the back flow at the bend area of the channel, when the liquid water held there accumulates to a certain volume, it moves forward and hits the wall in front of it.
5. Some of the small droplets catch up with each other during their movement inside the channel.
6. The volume fraction of water under the ribs in the porous layer will be first affected by the cross flow.
7. A portion of the liquid water will stay in the porous layer and gradually become droplets hang in the porous layer due to the surface tension effect of the liquid water and the porosity of the porous media.
8. The liquid water droplets in the porous layer tend to be driven together forming larger droplets after a period of time, and most of these high water volume fraction droplets appear under the ribs of the geometry where the gas flow velocity is relatively low.

CHAPTER 6

LIQUID WATER REMOVAL PROCESS IN STIRRED TANK REACTOR CHAMBER WITH POROUS LAYER

6.1 General process of liquid water removal

The general process of the liquid water removal in the STR chamber and porous layer domain is shown in Figure 24. The liquid water set in the porous layer starts to move driven by the gas flow, and the original liquid water film is split from the beginning stage. The liquid water then starts to emerge from the porous layer into the chamber. Most of it comes out of the porous layer near the edge of the pins as shown in Figure 24 (b). After a longer time, the gas flow in the porous layer brings more and more liquid water away, so the droplets hanging in the porous layer shrink with time. They still cannot be removed thoroughly due to the surface tension effect of the liquid water and the porosity of the porous media.

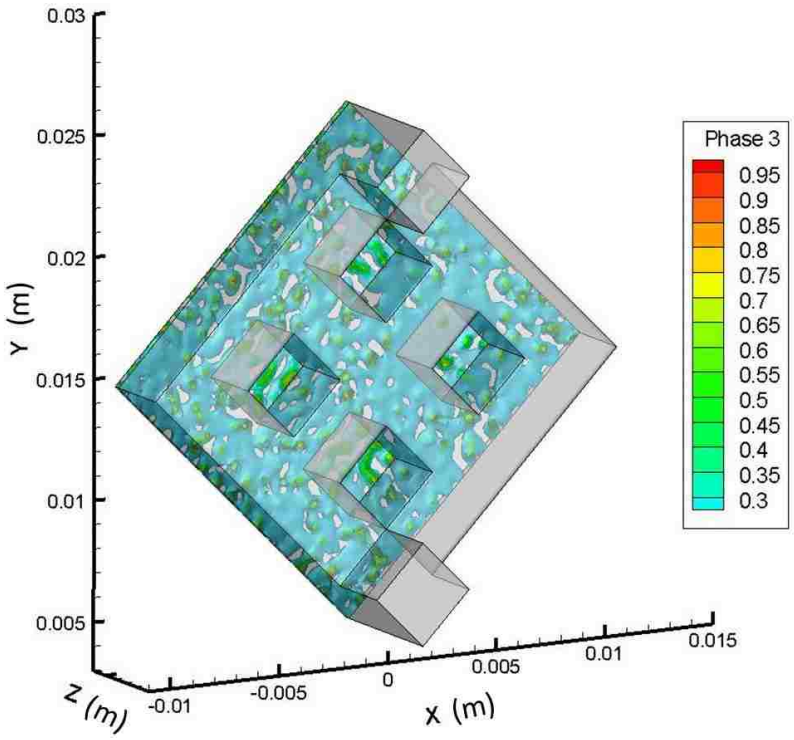

(a) t = 0.1 s

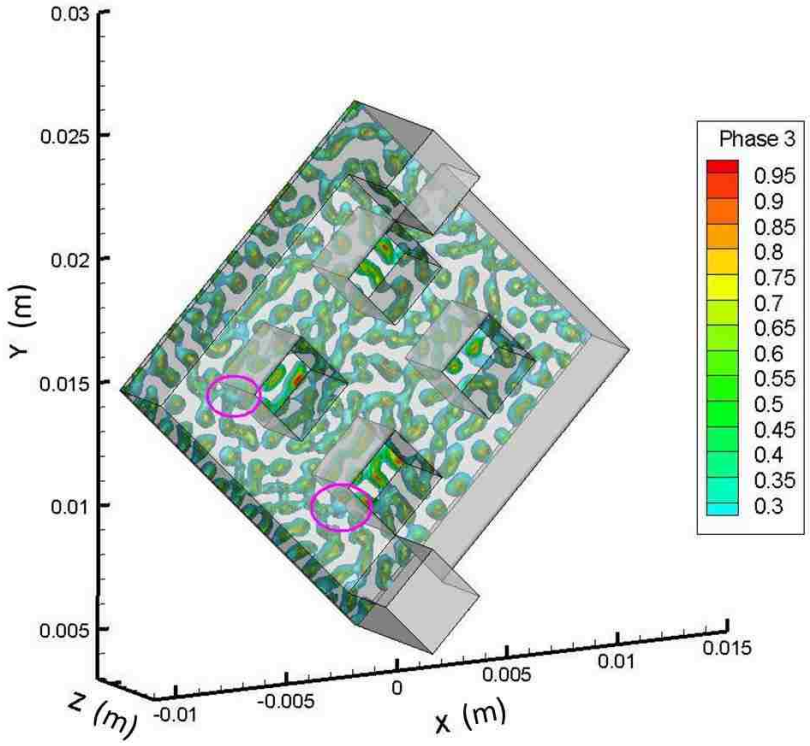

(b) t = 0.25 s

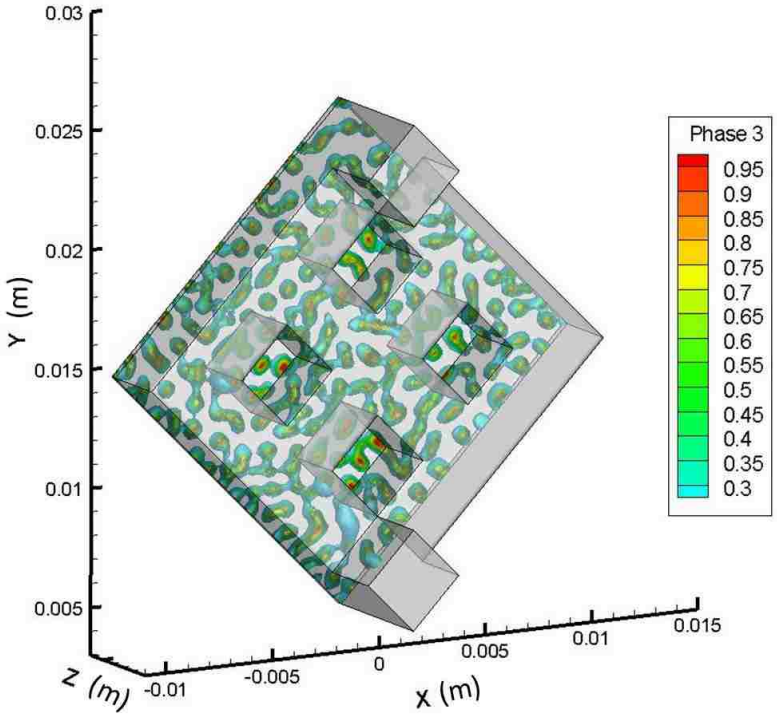

(c) t = 0.4 s

Fig. 24. General liquid water removal process in STR chamber and the porous layer domain

6.2 Liquid water moving inside the porous layer

The original liquid water film is split into droplets in the porous layer gradually after the simulation starts. Figure 25 shows the beginning period of the simulation in section z = 0.00015 m of the calculation domain. The liquid water volume fraction in the original liquid water film decreases right after the simulation started. The gas flow is forced to go through the porous layer under the pins due to the local blocking of the gas flow in the chamber. So the liquid water volume fraction under the pins decreases slightly faster. But the volume fraction of the liquid water from different positions in the liquid water film generally decreases in a similar rate at the beginning period.

After that, the liquid water film starts to be split into droplets as shown in Figure 26. The liquid water is removed firstly from several random spots. Then more liquid water is removed along with time. The original liquid water film becomes ligaments and then droplets. These droplets oscillate in the porous layer and will not be removed for a long time, however, they tend to combine with each other and form larger droplets as shown in Figure 26 (b) to (d). In these pictures, the liquid water volume fraction in each droplet in the porous layer tends to increase. This is due to the surface tension effect of the liquid water. There is a strong cohesion between water molecules.

Though these droplets cannot be thoroughly removed quickly from the porous layer, it is observed that they shrink after a longer period of time, the liquid water is gradually brought away by the gas flow goes besides the droplets. Meanwhile, the liquid water tends to accumulate in the area under the pins. The volume fraction of the liquid water droplets in those areas increases since the gas flow velocity is relatively low there.

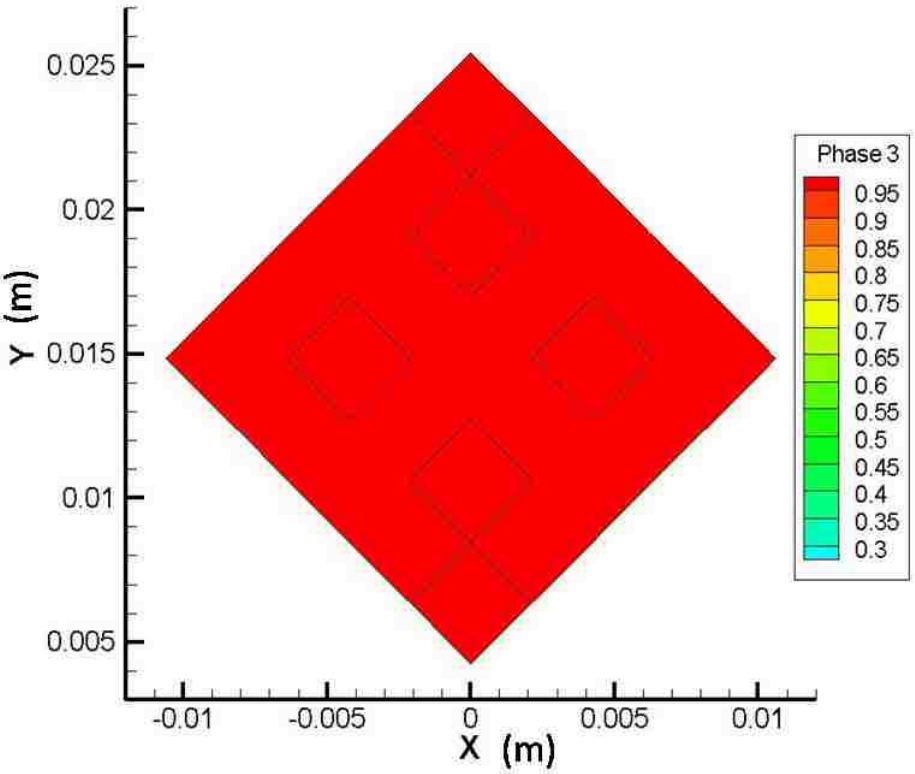

(a) t = 0 s

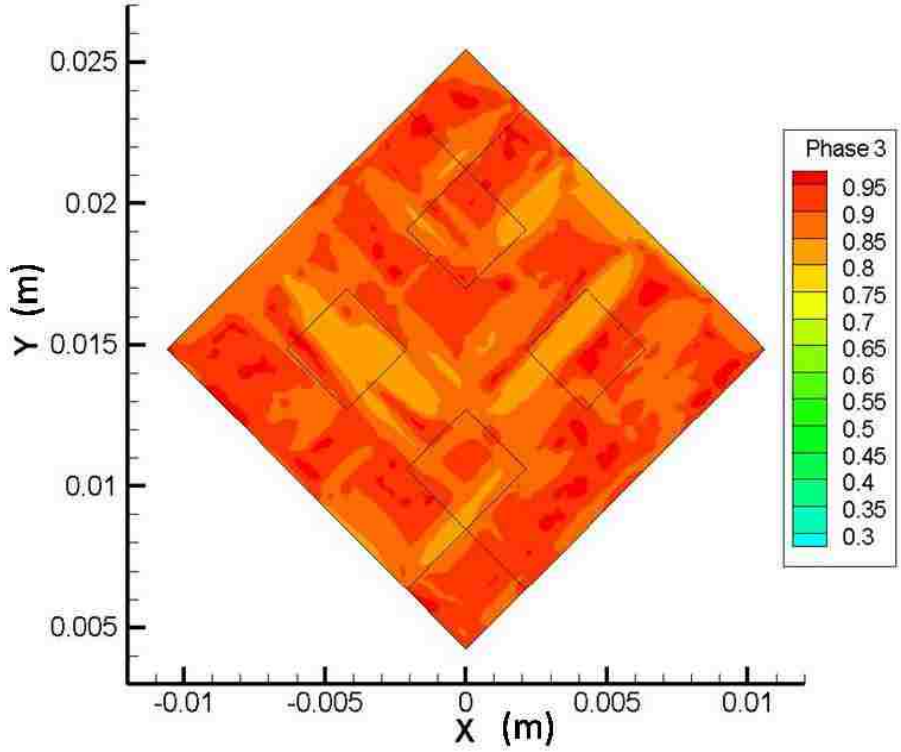

(b) t = 0.005 s

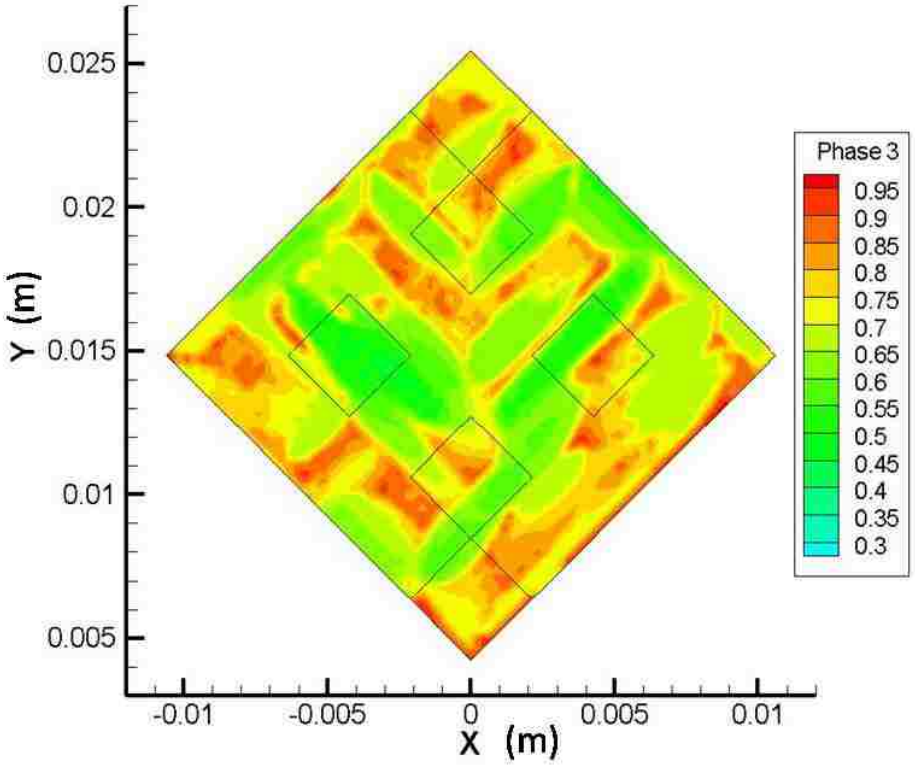

(c) t = 0.01 s

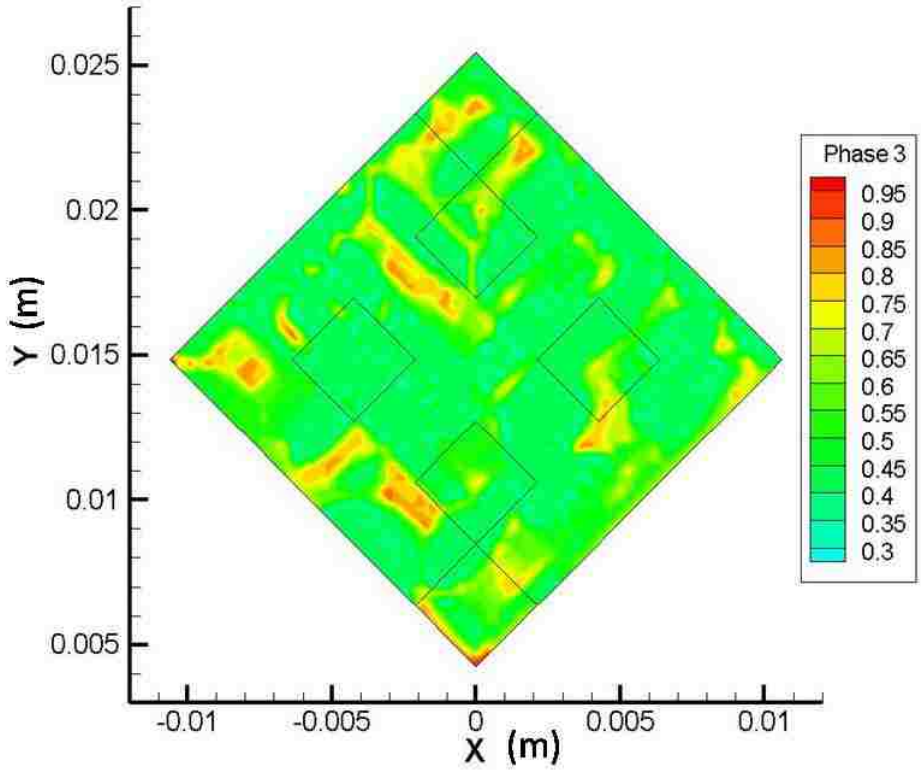

(d) t = 0.015 s

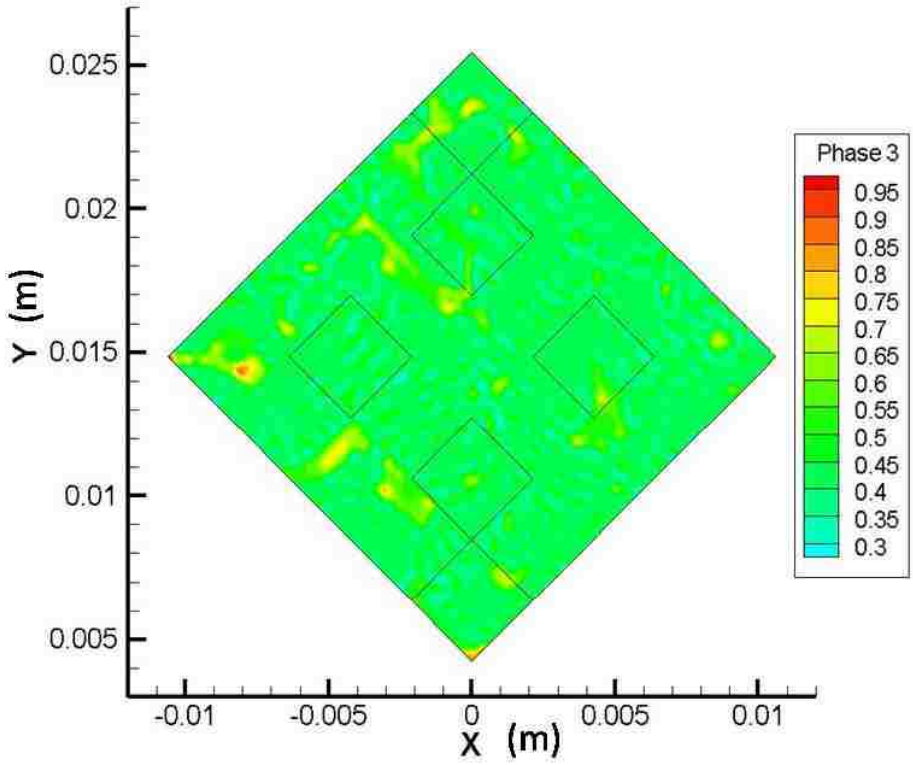

(e) t = 0.02 s

Fig. 25. Liquid water removal process in the porous layer at the beginning period

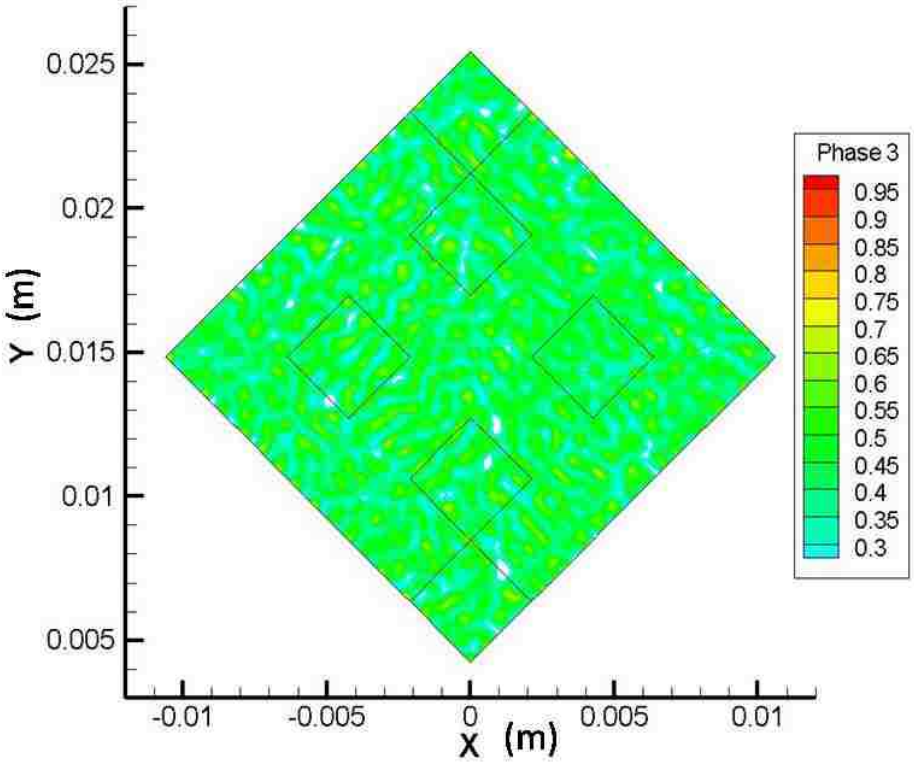

(a) t = 0.05 s

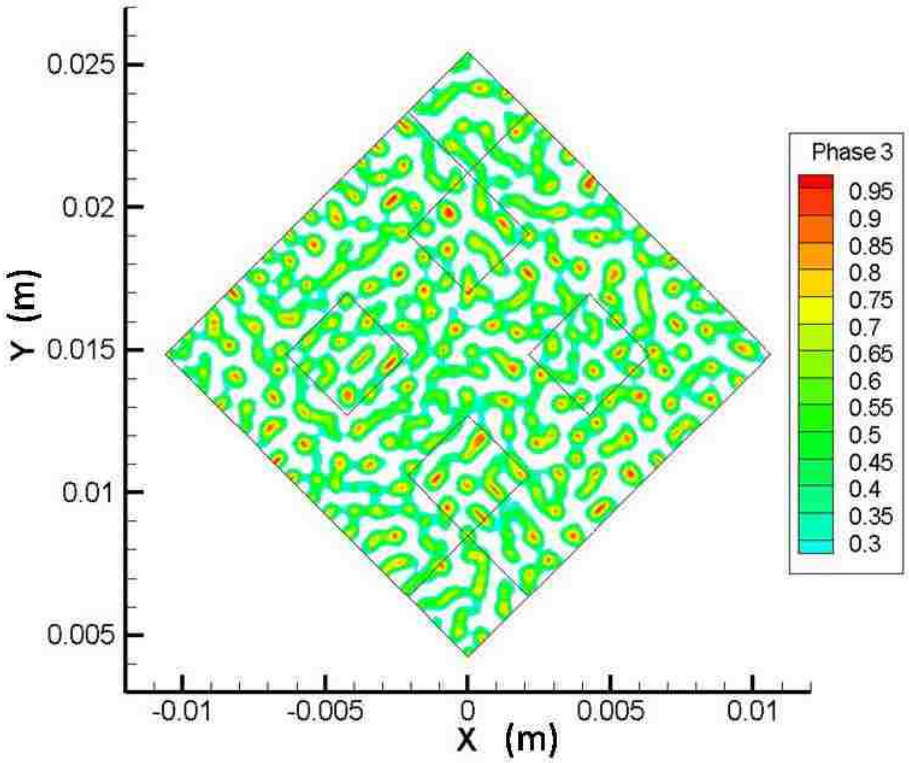

(b) t = 0.25 s

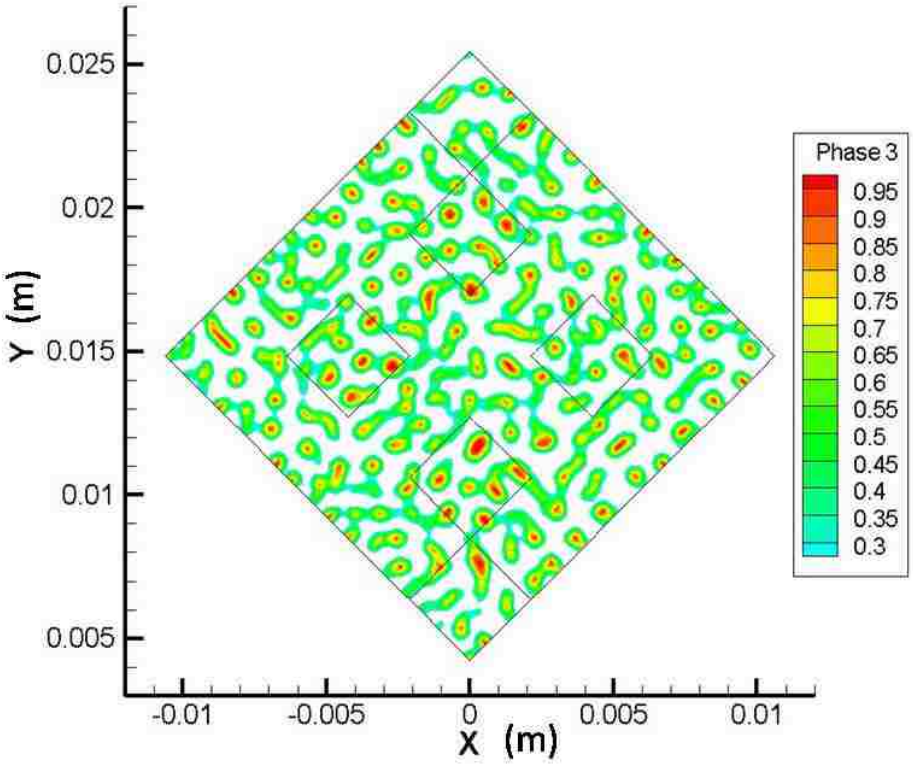

(c) t = 0.45 s

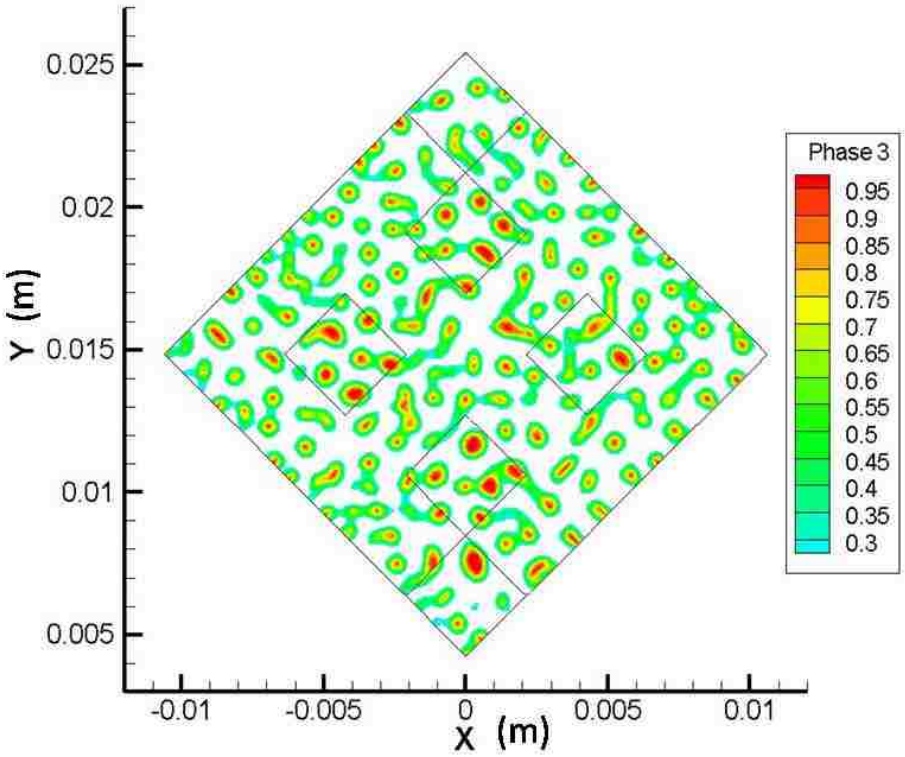

(d) t = 0.65 s

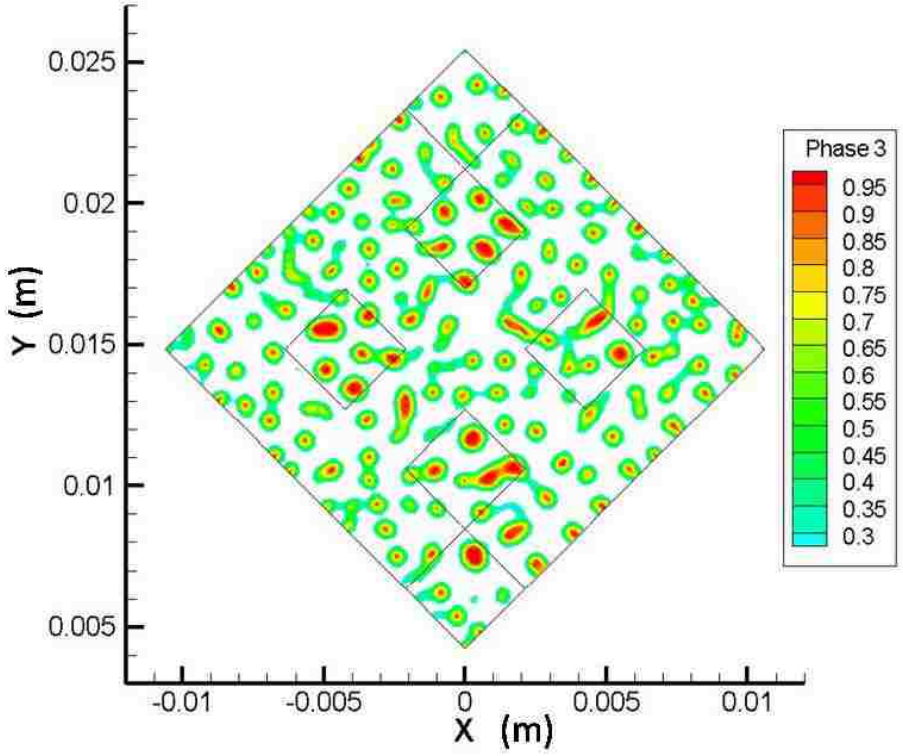

(e) t = 0.85 s

Fig. 26. Liquid water removal process in the porous layer along with time

It is also observed that the liquid water film is broken into small pieces of water ligaments by the z direction gas flow inside the porous layer. This relatively large gas flow velocity in z direction in the porous layer is induced by the air coming from the inlet of the geometry to the chamber area. It goes across the interface between the chamber and porous layer into or out of the porous layer and quickly breaks the liquid water film into pieces. Figure 27 shows the section of the STR geometry at x = 0 m. As shown in Figure 27 (a) to (c), the liquid water film deforms firstly at the area where the z direction gas flow velocity is high. Then the liquid water film tends to be split by the relatively strong gas flow and the divided portions of liquid water are squeezed together to form the ligaments in the areas where the gas flow velocity is relatively low. This film breaking process is very interesting in that the gas can break the film and flow into the porous layer in the –z direction, and within a short distance (the thickness of water ligament) the gas that already entered the porous layer between the membrane and the liquid water film will break the film in an opposite direction to let the gas out of the porous layer. This is the basic reason for the very interesting water pattern in which the water ligaments are somehow uniform in thickness.

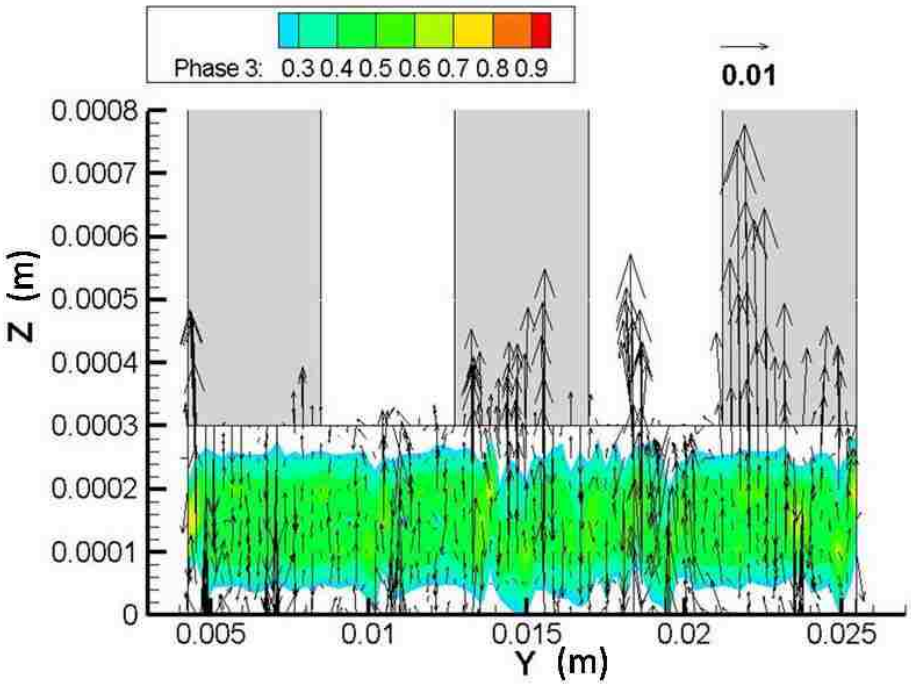

(a) t = 0.02 s

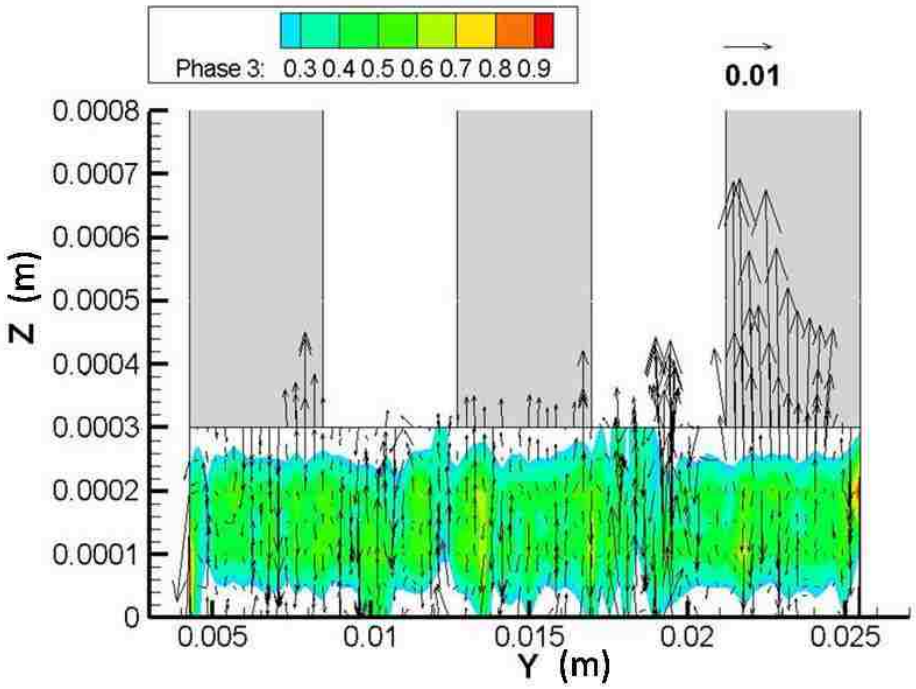

(b) t = 0.04 s

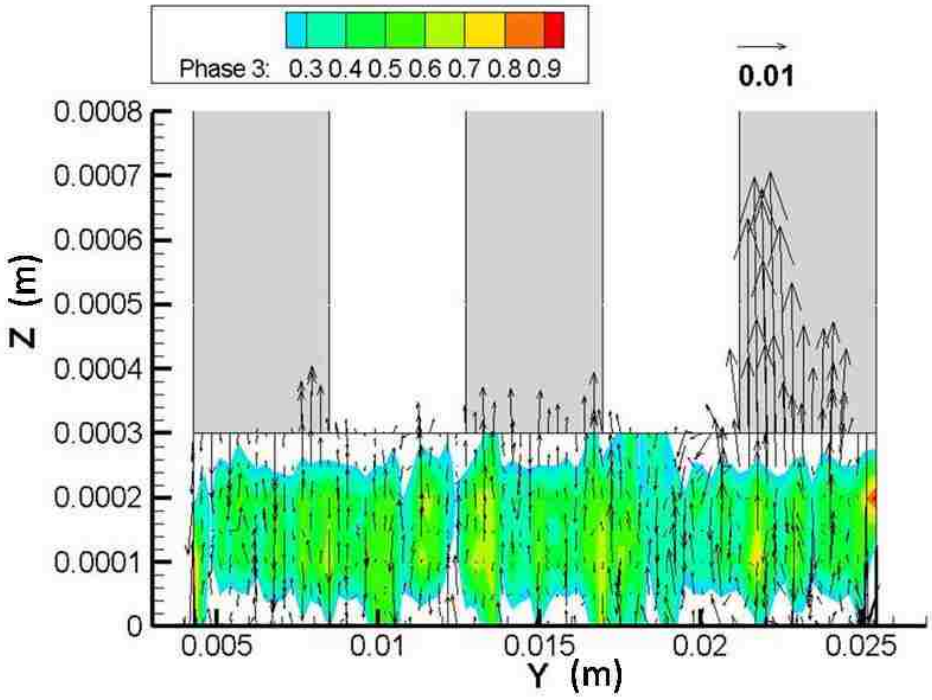

(c) t = 0.06 s

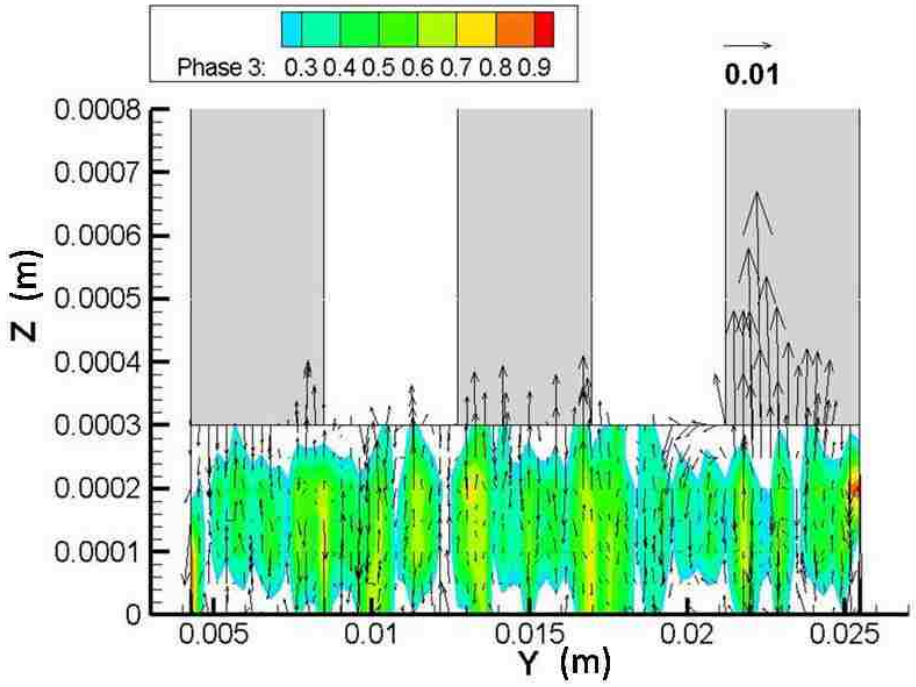

(d) t = 0.08 s

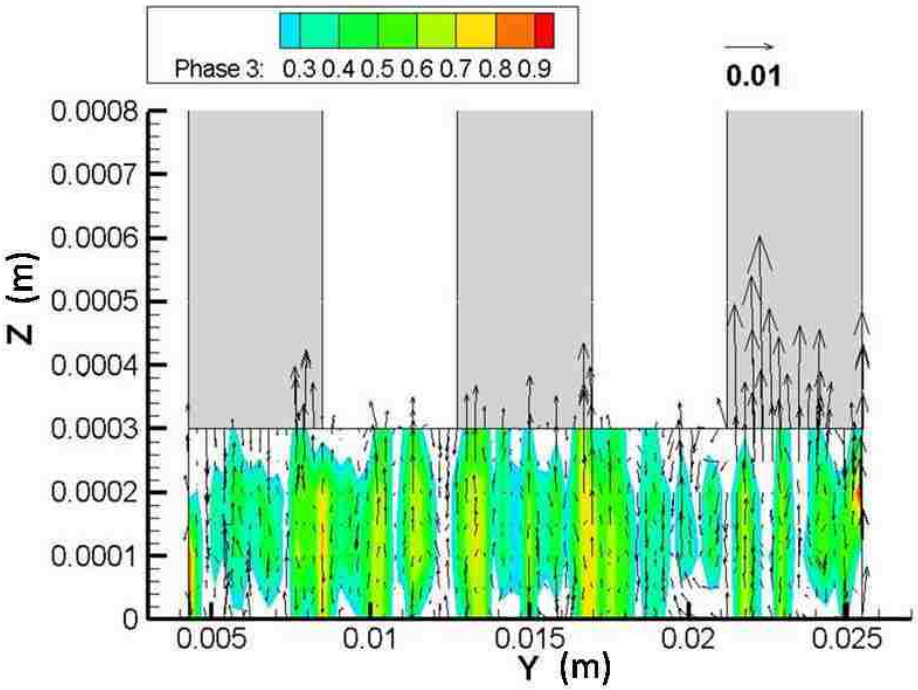

(e) t = 0.1 s

Fig. 27. Liquid water film broken into liquid water ligaments
(grey color indicates the chamber area)

6.3 Liquid water emerging into the chamber from porous layer

As shown in Figure 28, the liquid water starts to emerge into the porous layer from the edge area when the original liquid water film is split into droplets. The inlet gas flow direction perpendicular to the view in Figure 28 helps the gas flow to go into the porous layer and drive the liquid water out into the chamber area. The liquid water always tends to come into the chamber from the area where the gas flow velocity is relatively low in the chamber. The black arrows in Figure 28 indicate the gas flow velocity. Since the pins block the gas flow in the chamber area, the gas flow velocity at the downwind side of these pins is always lower than the upwind side. So the droplets coming into the chamber mostly appear from the downwind side of the pins attached to one wall and accumulate there.

It is also observed that the liquid water appears in the chamber mostly from the lower part of the geometry. This phenomenon shortens the pass way for the liquid water to be drained out through the outlet of the domain, so it is helpful for the liquid water removal process. A very important feature of the geometry which contributes to this phenomenon is the inlet gas flow direction. Unlike the serpentine channel with porous layer case discussed in previous chapter, this STR chamber has an inlet perpendicular to the porous layer. This perpendicular inlet gas flow direction greatly helps the gas to go into the porous layer and induces a relatively intense gas flow near the inlet area in the domain, so the liquid water in the porous layer can be driven downwards to the lower part of the geometry. When more and more liquid water arrives at the lower part of the geometry, it emerges into the chamber from the area where the gas flow velocity is relatively low. Also, since the gravity for the STR chamber with porous layer domain is set in the –Y direction, gravity also contributes to the phenomenon that the liquid water moves downward, and emerges into the chamber from the lower part of the geometry.

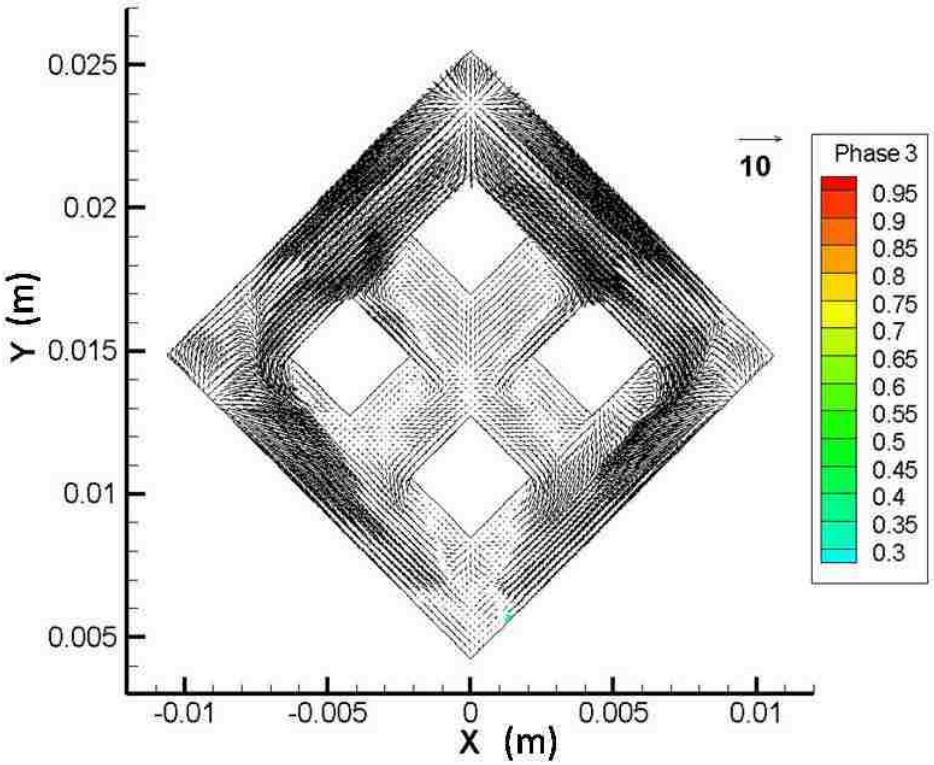
0.025
0.02
0.015
0.01
0.005
Y (m)
-0.01
-0.005
0
0.005
0.01
X (m)
10
Phase 3
0.95
0.9
0.85
0.8
0.75
0.7
0.65
0.6
0.55
0.5
0.45
0.4
0.35
0.3

(a) t = 0.1 s

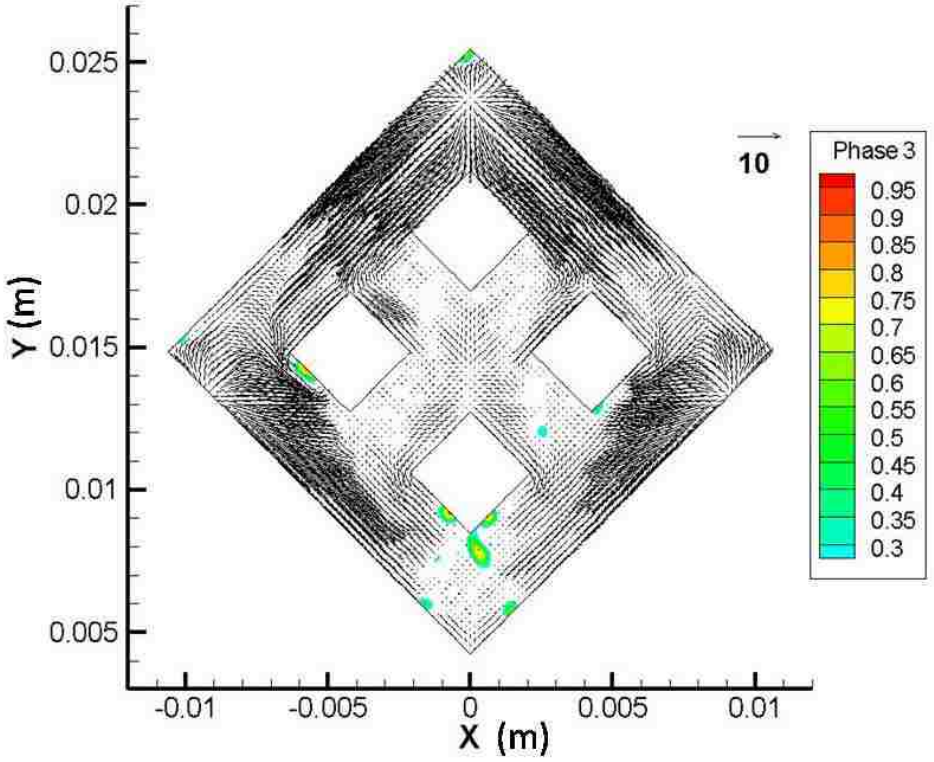
0.025
0.02
0.015
0.01
0.005
Y (m)
-0.01
-0.005
0
0.005
0.01
X (m)
10
Phase 3
0.95
0.9
0.85
0.8
0.75
0.7
0.65
0.6
0.55
0.5
0.45
0.4
0.35
0.3

(b) t = 0.3 s

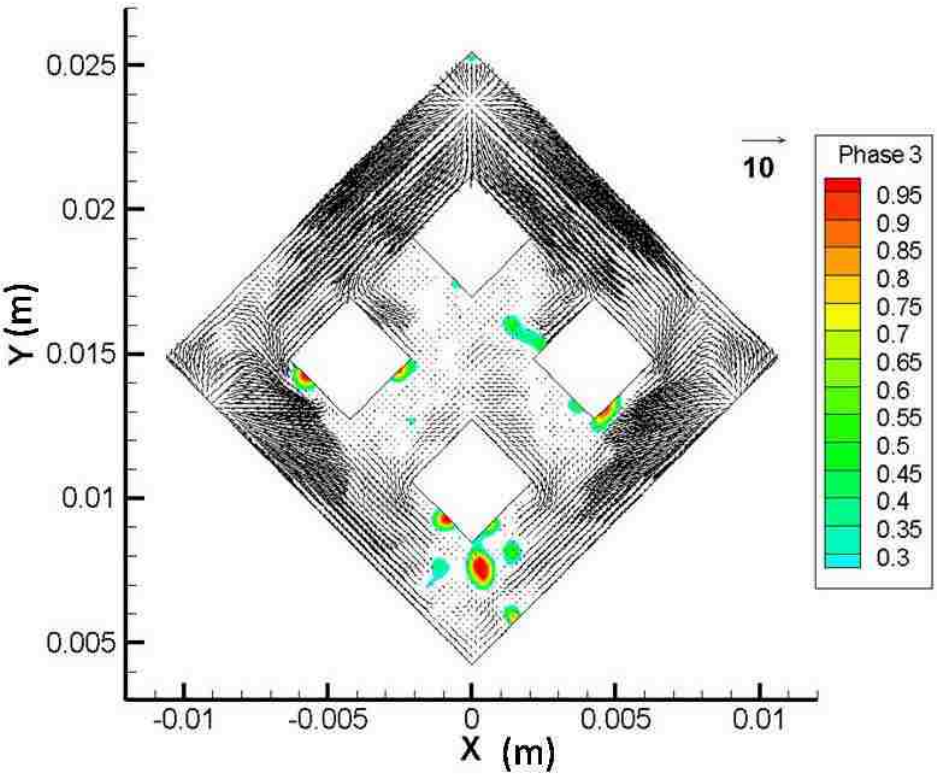
0.025
0.02
0.015
0.01
0.005
Y (m)
-0.01
-0.005
0
0.005
0.01
X (m)
10
Phase 3
0.95
0.9
0.85
0.8
0.75
0.7
0.65
0.6
0.55
0.5
0.45
0.4
0.35
0.3

(c) t = 0.5 s

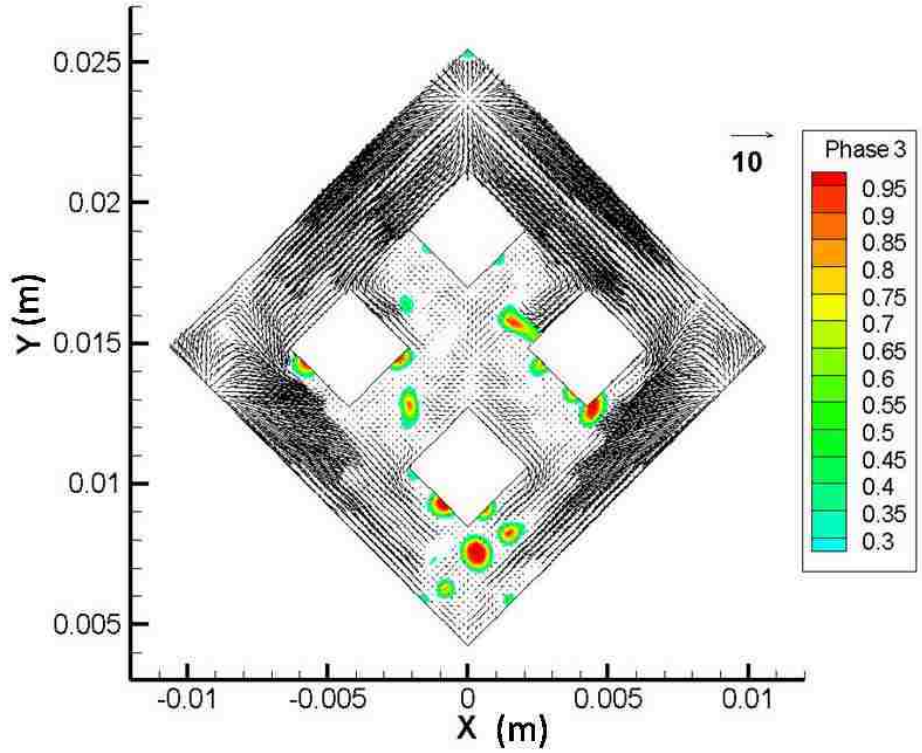
0.025
0.02
0.015
0.01
0.005
Y (m)
-0.01
-0.005
0
0.005
0.01
X (m)
10
Phase 3
0.95
0.9
0.85
0.8
0.75
0.7
0.65
0.6
0.55
0.5
0.45
0.4
0.35
0.3

(d) t = 0.7 s

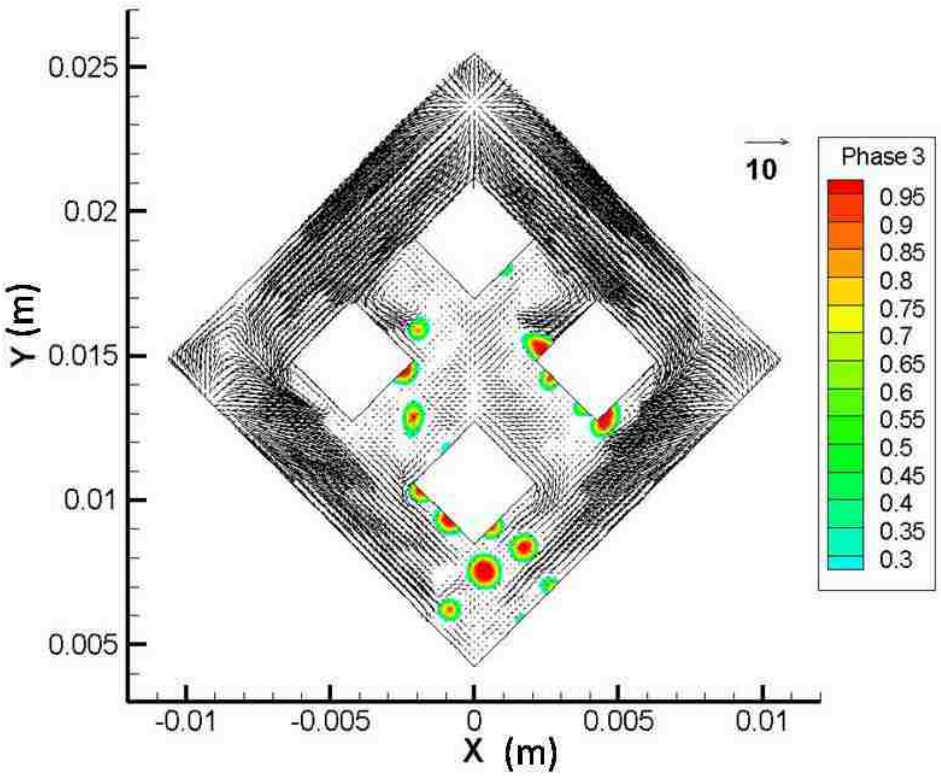

(e) t = 0.9 s

Fig. 28. Liquid water emerging into the chamber area from the porous layer

6.4 Summary

1. Though the liquid water volume fraction in the original liquid water film decreases slightly faster in the area under the pins, generally it decreases uniformly at the beginning period
2. Liquid water emerges from the porous layer to the channel area mostly from the edge of the pins after a certain period of time.
3. The original liquid water film becomes droplets oscillating in the porous layer and the droplets tend to combine each other forms larger droplets, and this part of the liquid water is drained out relatively slow.
4. The liquid water tends to accumulated in the area under the pins after the liquid water film become droplets in the porous layer.
5. The liquid water film is split by the z direction gas flow inside the porous

layer induced by the inlet gas flow perpendicular to the porous layer a short period after the simulation starts.

6. The droplets coming into the chamber mostly appear from the downwind side of the pins and accumulate there.
7. The liquid water appears in the chamber mostly from the lower part of the geometry due to the inlet gas flow direction and the gravity effect.

CHAPTER 7

LIQUID WATER REMOVAL PROCESS IN PARALLEL BAFFLE BLOCKED CHANNEL WITH POROUS LAYER

7.1 General process of liquid water removal

7.1.1 Identification of the names for different segments in the geometry

Since the PBB geometry is a newly developed geometry, different sections in this geometry have to be named before analyzing the simulation case. As shown in Figure 29, the inlet manifold, cavities, outlet manifold and baffles are identified in this figure. All these four sections together are called the channel area and the porous layer area is identified by the dark grey color. Other than these, at the facet of the porous layer which the channel area is attached to, there are some empty areas. These areas are named rib areas. This geometry contains only the channel area and porous layer in the cathode side of a PEM fuel cell, the flow field plate in which the channel area is embedded in is not shown because that part is not needed to conduct the numerical simulation.

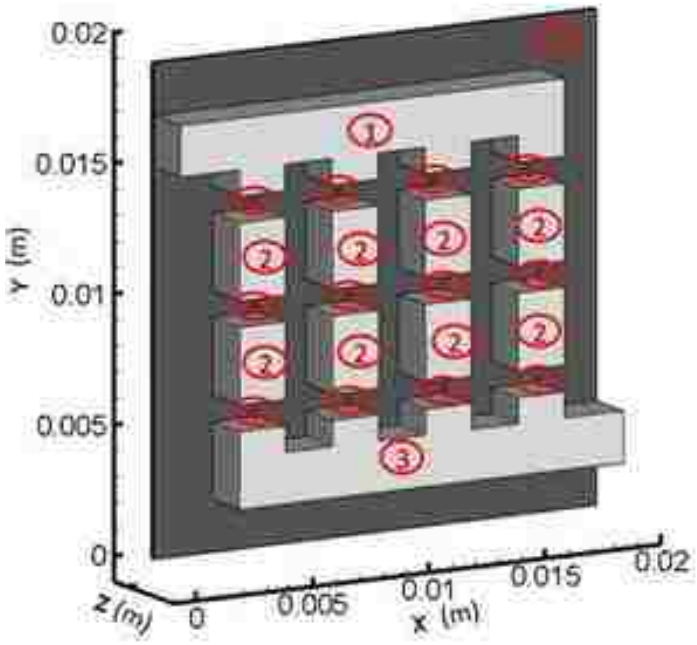

Fig. 29. PBB channel with porous layer geometry with the name of different sections (1) Inlet manifold; (2) cavity; (3)Outlet manifold; (4)Baffle; (5)Porous layer

7.1.2 General process of liquid water removal

As soon as the numerical simulation starts, the liquid water set in the porous layer begins to move driven by the gas flow. As shown in Figure 30, the baffles in this geometry block the path way of the gas flow and form dead ends in the channel area. In this case, the gas flow is forced to move through the porous layer under the baffles. When the gas flow goes through these small areas, the gas flow become more intense, and the liquid water is easily removed by the gas from these areas faster than from other areas. Along with time, the liquid water film in the porous layer between the inlet manifold and outlet manifold is split into small parts and gradually driven away by the gas flow. Some of the liquid water is brought to the channel area by the gas flow and forms droplets attached to the porous layer in the cavities, while another part of the liquid water is brought to the outlet manifold and drained out of the calculation domain with the gas flow. After a longer period of time, the liquid water trapped in the cavities is removed by the gas flow as well.

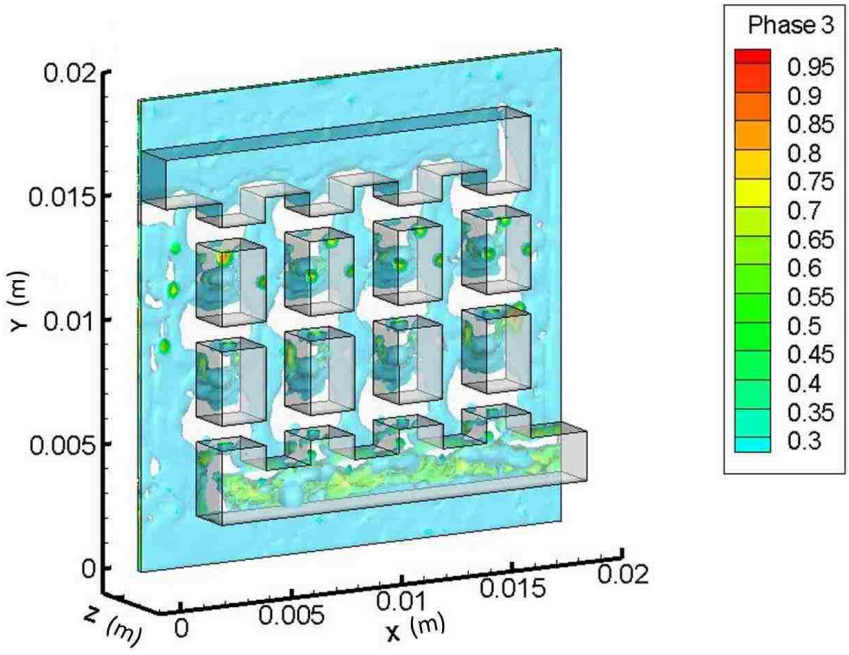

(a) t = 0.02 s

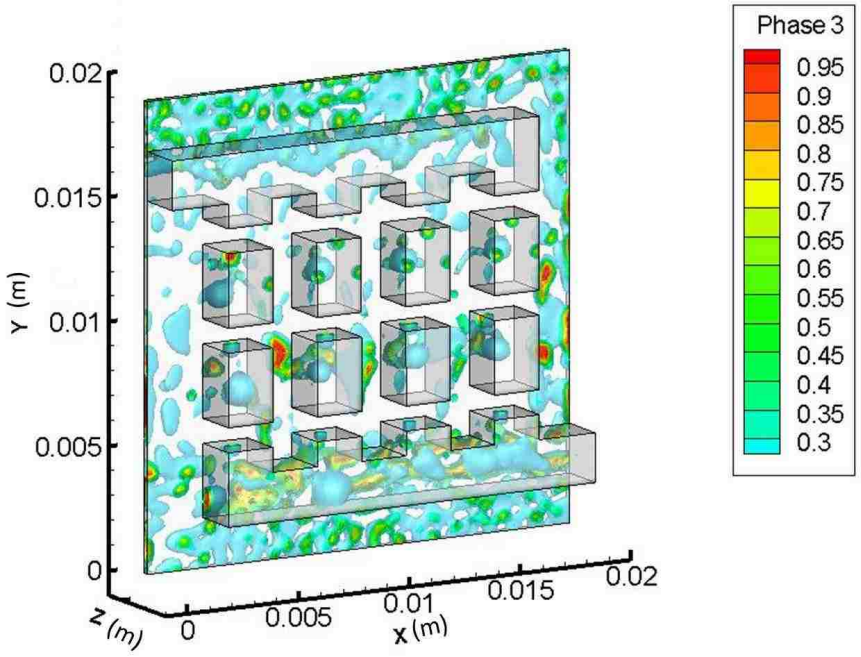

(b) t = 0.09 s

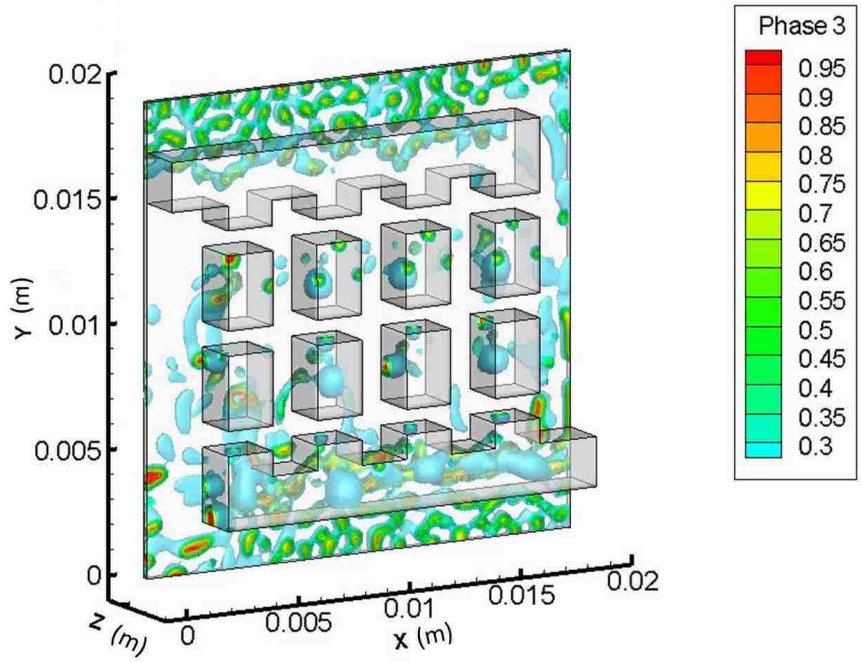

(c) t = 0.16 s

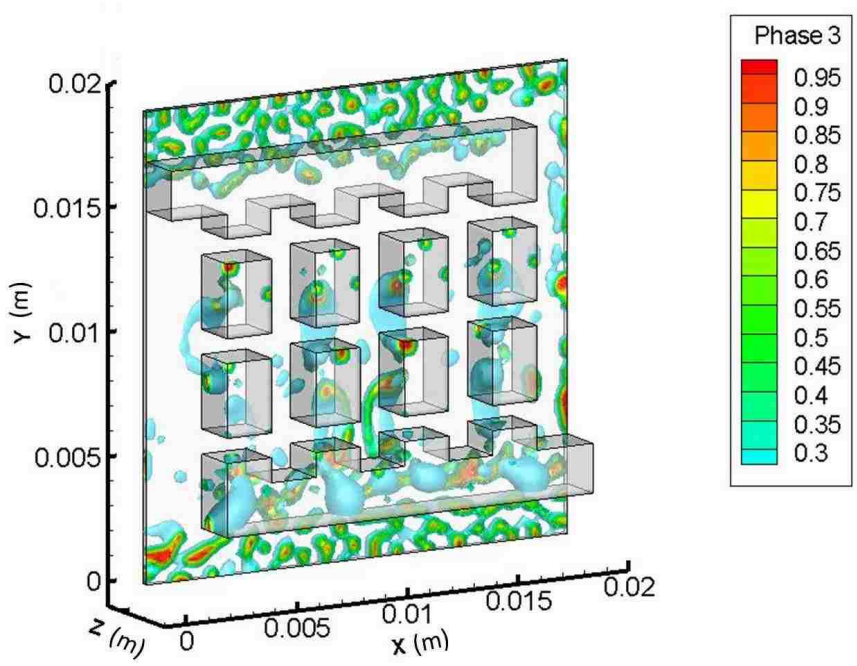

(d) t = 0.23 s

Fig. 30. General process of liquid water removal in PBB channel with porous layer domain

7.2 Liquid water behavior at the inlet manifold area

As shown in Figure 31 (a), around t = 0.05 s, some of the liquid water in the porous layer is removed by the gas flow after a period of time. However the liquid water inside the porous layer under the inlet manifold area is not removed. It is still kept in its original position. To observe and explain this phenomenon, the liquid water position as well as the gas flow velocity is shown in two sections x = 0.0075 m and z = 0.00015 m in Figure 31 (b) and (c). From Figure 31 (b), we can see that at the inlet manifold area, the gas flow velocity is very low in the porous layer, but higher in the inlet manifold. However when the gas in the inlet manifold meets the baffle in front of it, it is forced to go into the porous layer. It is observed from the figure that the gas flow under the baffle is more intense compared with the gas flow in the porous layer under the inlet manifold. In this case, the intense gas flow at these areas prevents a large amount of the liquid water in the porous layer under the inlet manifold from

moving through it even the liquid water is driven towards this area. So the liquid water under the inlet manifold is kept in its original position and is removed much slower than the liquid water in the porous layer between the inlet manifold and the outlet manifold. Viewed from Figure 31 (c), we can see that the gas flow velocity under all the baffle and rib areas around the inlet manifold is much larger compared with the gas flow velocity in the area under the inlet manifold in the porous layer. In this case, the intense gas flow forms a boundary and encloses the liquid water under the inlet manifold inside in a shape according to the shape of the inlet manifold. The liquid water can be brought away by the gas flow moving close to it and gradually the edge of this shape will retract until most of this part of liquid water is driven away. This process is much slower than the liquid water removal process in the porous layer between the inlet manifold and outlet manifold.

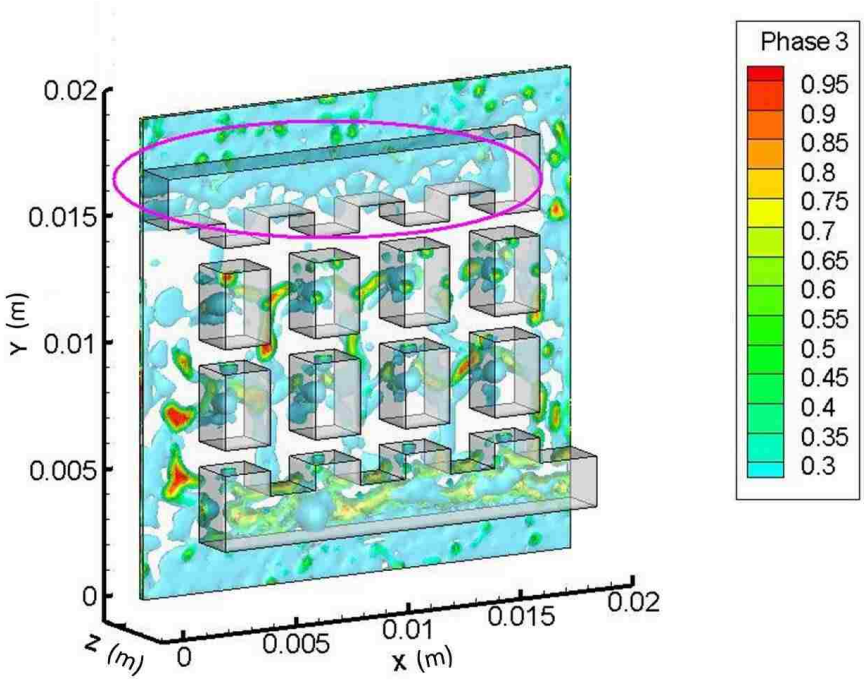

(a) t = 0.05 s; ISO view of liquid water removal process in the inlet manifold area

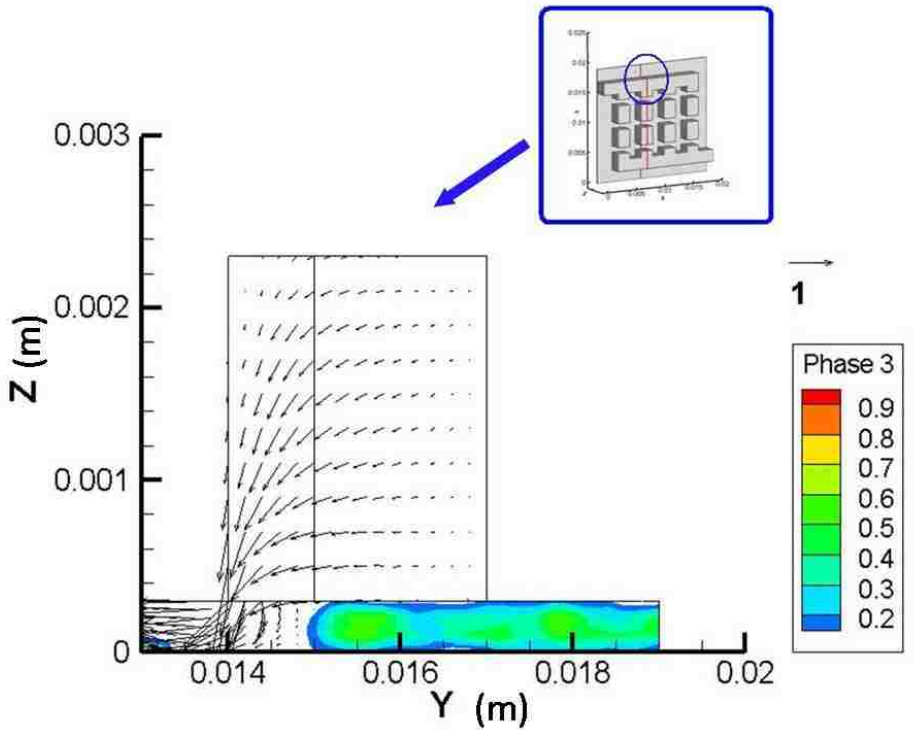

(b) t = 0.05 s; Middle section of the second branch of the geometry (x = 0.0075 m)

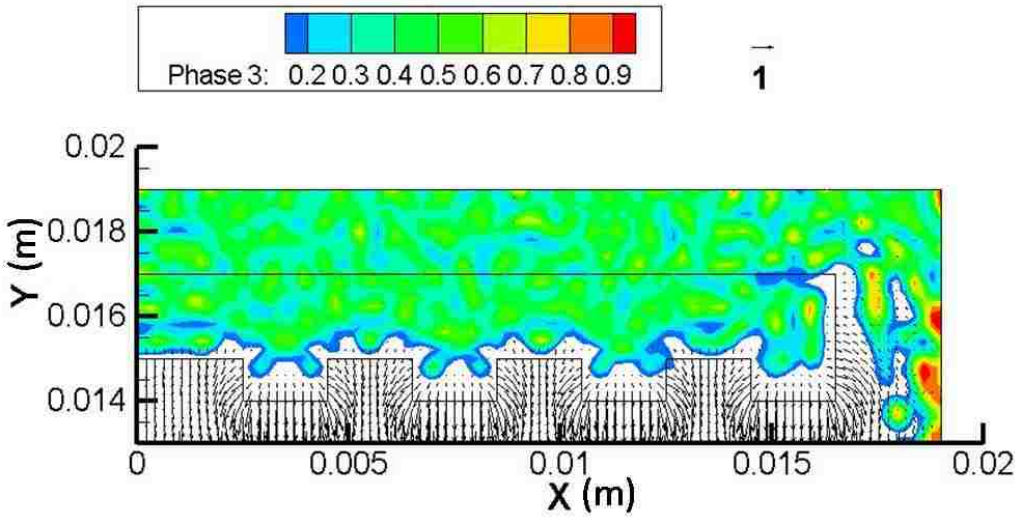

(c) t = 0.05 s; Middle section of the porous layer (z = 0.00015 m)

Fig. 31. Liquid water behavior at the inlet manifold area

7.3 Liquid water behavior at the outlet manifold area

The liquid water is brought into the outlet manifold along the edge of the outlet manifold during a period of time after the simulation starts. The gas flow coming from the porous layer under the baffle or rib area moves towards the direction away from the porous layer right after it goes into the cavities or outlet manifold, because fluid tends to go towards a lower pressure area under current condition. The liquid water is brought into the outlet manifold along with this gas flow and appears firstly at the edge area next to the baffles and the rib areas as shown in Figure 32. After a period of time, more liquid water is brought into the outlet manifold. This part of the liquid water tends to be split into several droplets by the gas flow inside the outlet manifold. A part of these liquid water droplets will be drained out of the calculation domain through the outlet, while another part of them will stay in the outlet manifold for a longer time as can be seen from Figure 33. Most of the droplets left in the outlet manifold gradually join each other to become larger droplets adversely influencing the local gas flow direction. These droplets can be removed more efficiently by increasing the inlet velocity thus increase the pressure drop inside the domain.

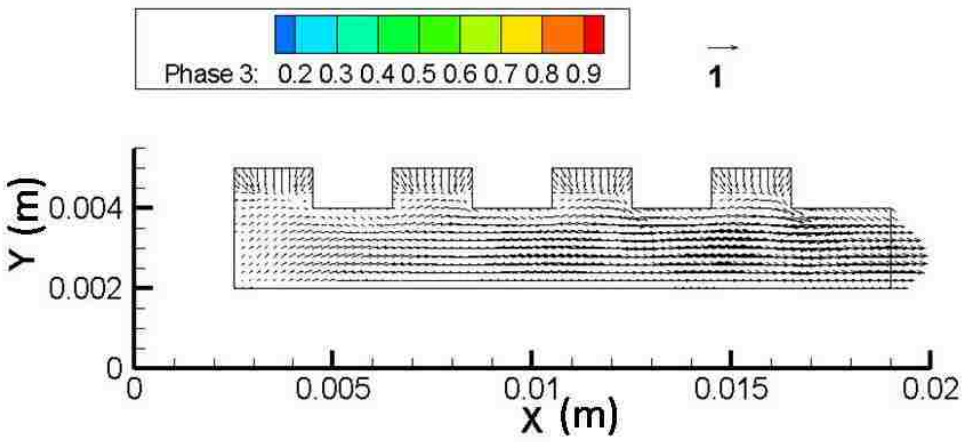

(a) t = 0 s

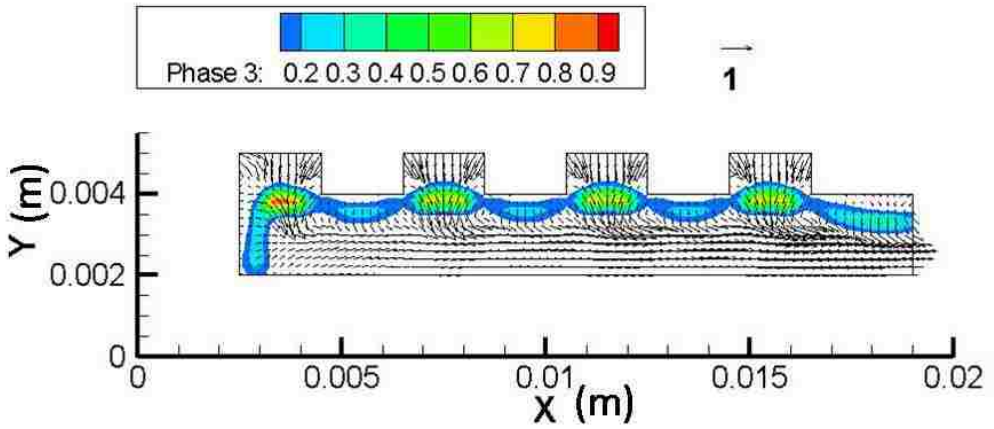

(b) t = 0.002 s

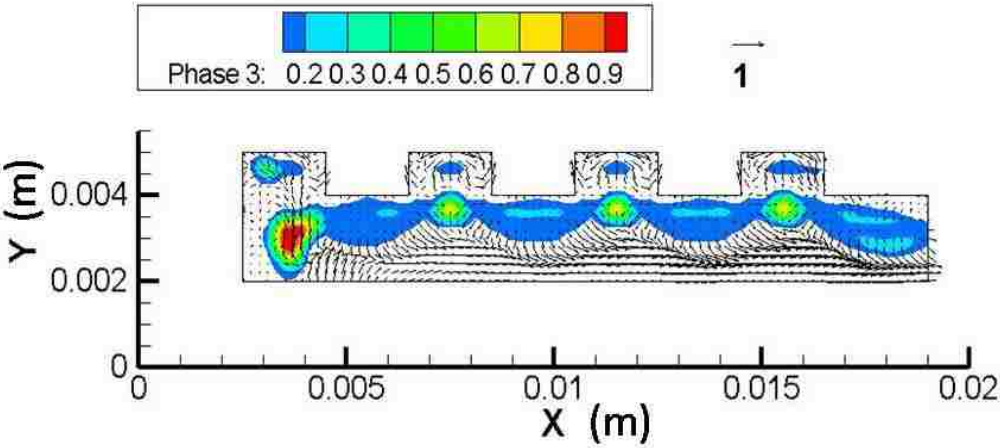

(c) t = 0.004 s

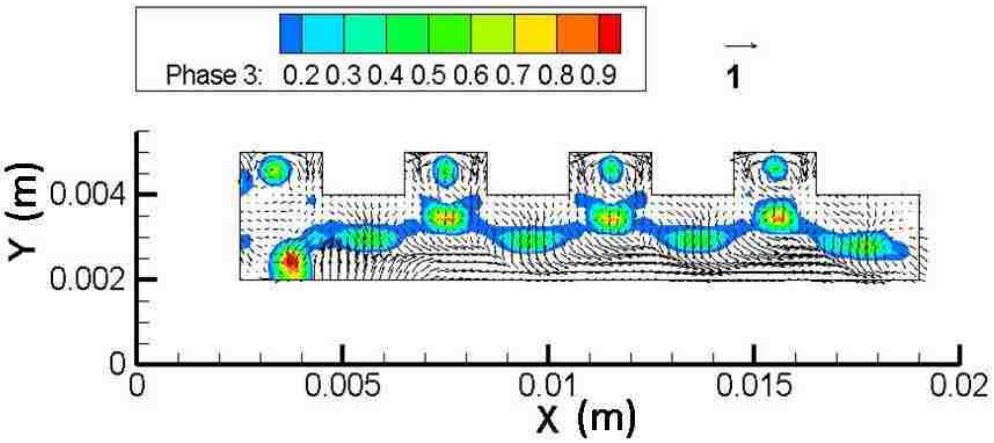

(d) t = 0.006 s

Fig. 32. Liquid water brought into the outlet manifold by the gas flow at the beginning period

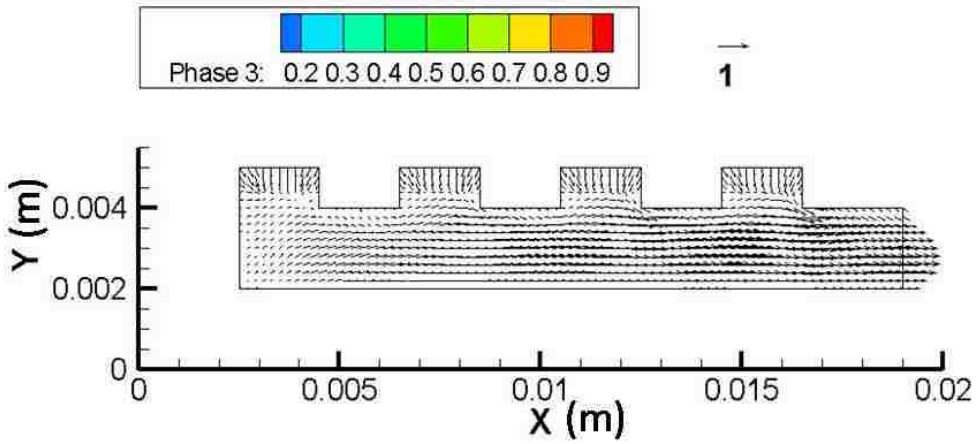

(a) t = 0 s

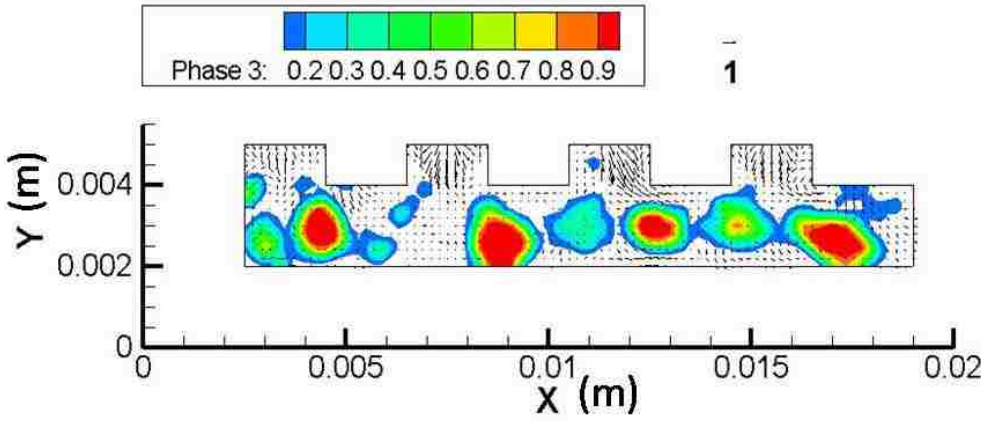

(b) t = 0.2 s

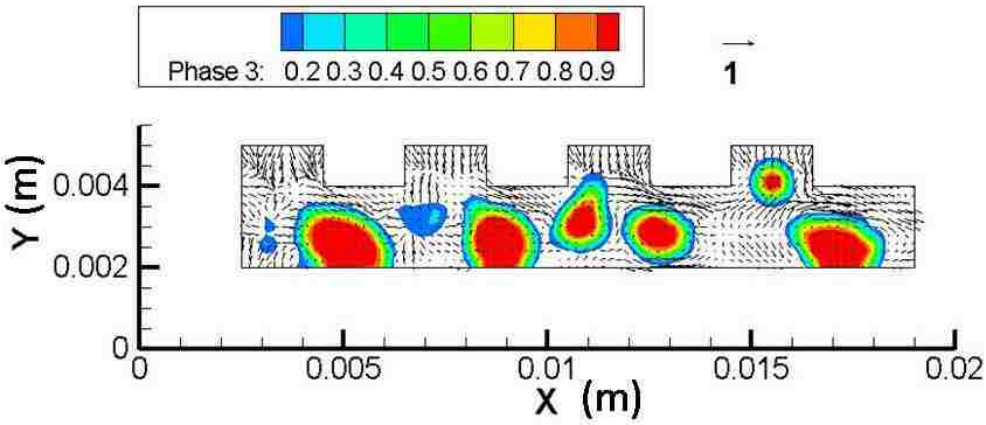

(c) t = 0.4 s

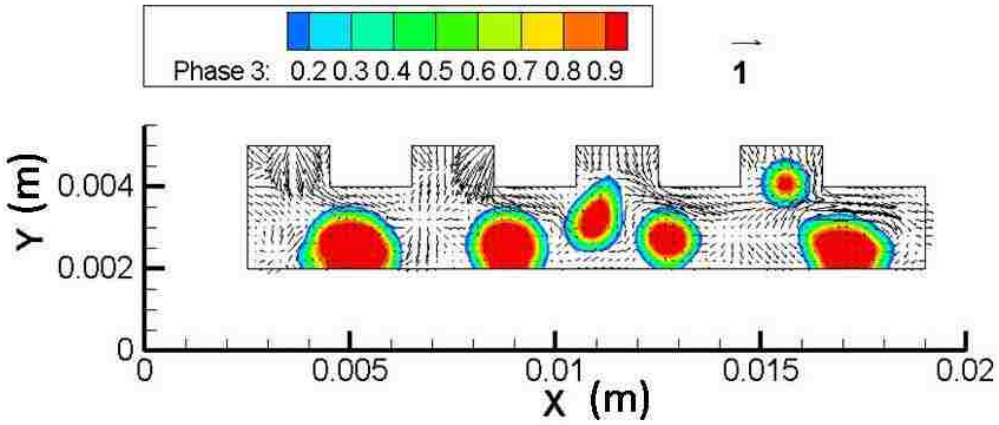

(d) t = 0.6 s

Fig. 33. Liquid water behavior in the outlet manifold along with time

7.4 Liquid water accumulation in the cavities

As can be seen from Figure 34, in the PBB geometry, a certain amount of liquid water will be trapped in the cavities with a part of it inside the porous layer. A certain amount of liquid water is necessary to enhance the ion conductivity of the membrane in a real fuel cell system, and this small amount of liquid water trapped in those positions is very helpful to keep the fuel cell membrane humidified since the porous layer directly attaches to the membrane in the real fuel cell system. This amount of liquid water is adjustable to fit the liquid water amount requirement from the membrane by changing the size of the cavities in this geometry. Other than that, it can be also observed from Figure 34 that a small amount of liquid water can be trapped at the corners away from the porous layer in the cavities during the whole liquid water removal process. This part of water does not help the fuel cell system directly, and can be removed by later improvement of this geometry, for example, adding chamfers to the corner of the cavities.

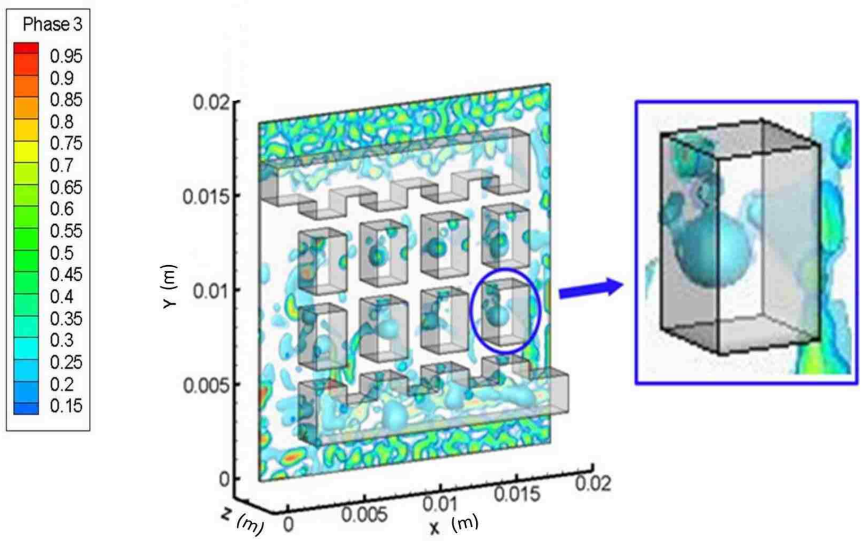

Fig. 34. Liquid water accumulated in the cavities attached with the porous layer

7.4.1 Liquid water accumulation process

The fluid flow in the Y-Z plane at x = 0.075 m is shown in detail in Figure 35. From this figure it is observed that the gas flow is forced to move through the porous layer under the baffle, and moves towards the direction away from the porous layer right after the gas reaches the next cavity after the baffle. During this process, the original liquid water film under the baffle is firstly split by the gas flow, and some liquid water is brought into the cavities or outlet manifold along with the gas flow as shown in Figure 35 (b) and (c). A part of this liquid water will go along with the gas flow into the cavity, while another part of the liquid water will stay attached to the porous layer. The gas flow in the cavity goes along the cavity walls and shows a half circle shape as indicated by the pink arrow in Figure 35 (c). When it meets the second baffle, it is forced to go through the porous layer again. During this whole process, the amount of liquid water attached to the porous layer in the cavity from the original liquid water film between these two baffles is squeezed together and stays there where the gas flow velocity is relatively low as shown in Figure 35 (d) to (g).

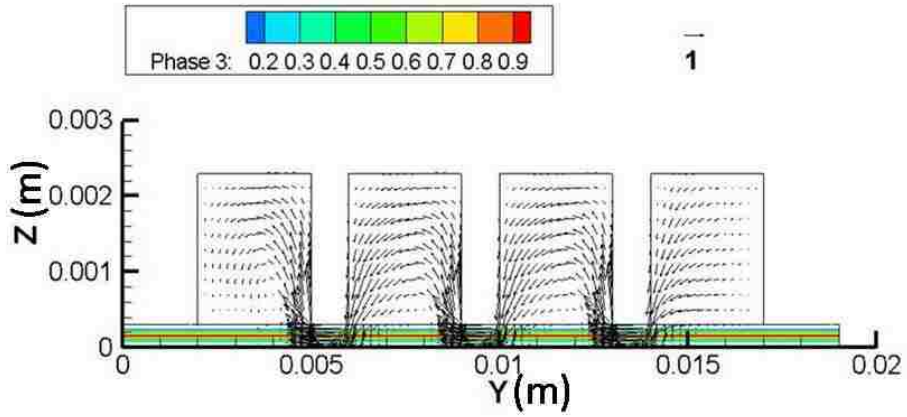

(a) t = 0 s

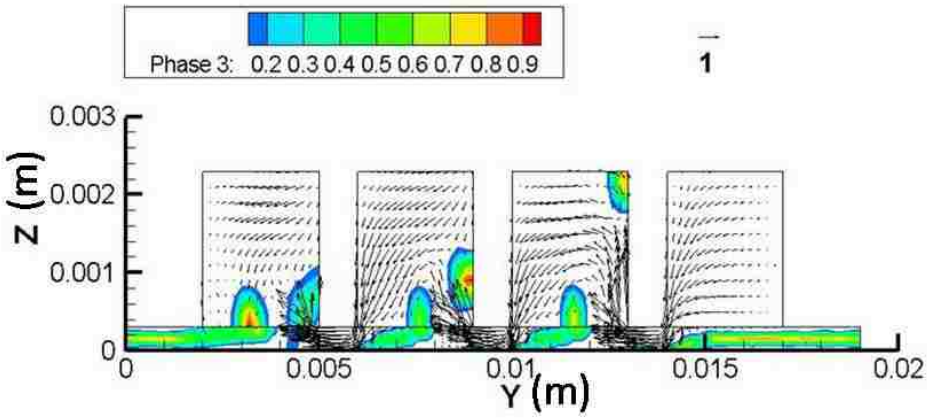

(b) t = 0.01 s

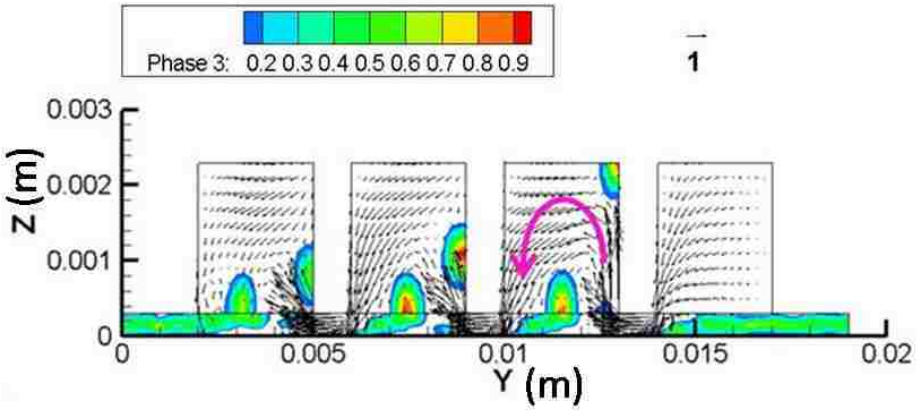

(c) t = 0.02 s

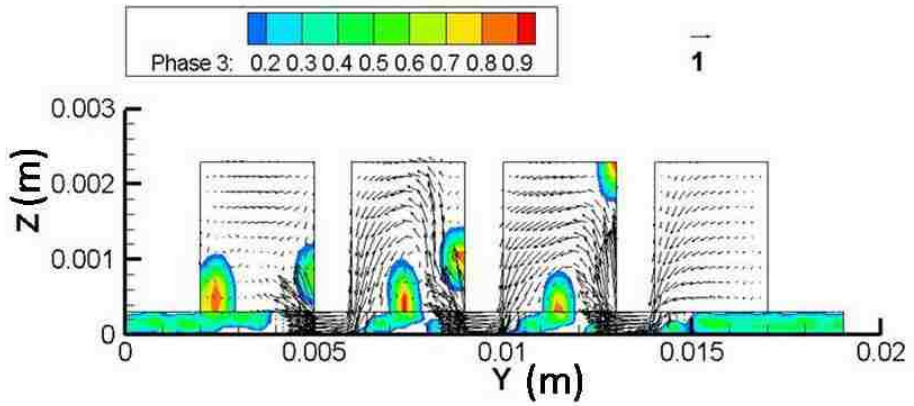

(d) t = 0.03 s

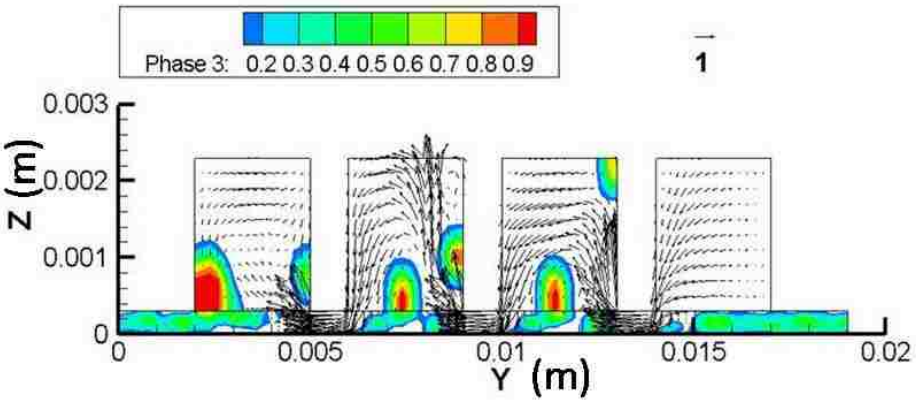

(e) t = 0.04 s

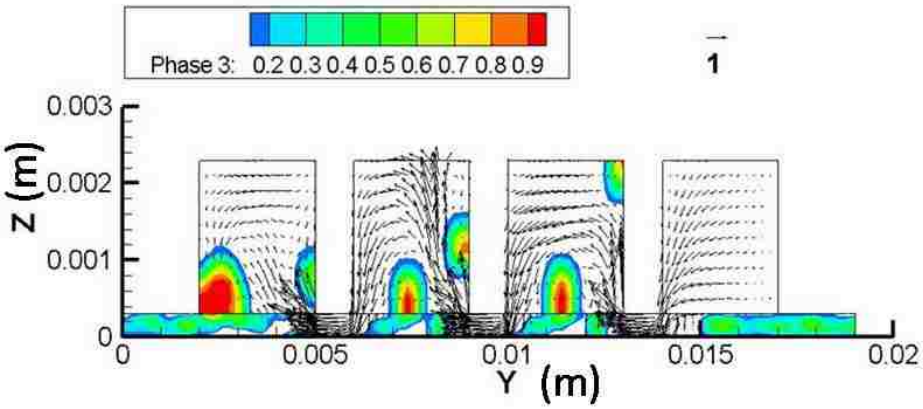

(f) t = 0.05 s

Fig. 35. Liquid water accumulation process in the cavities

7.4.2 Liquid water driven away from the cavity

After most of the liquid water in the porous layer between the inlet and outlet manifold is driven away, the liquid water inside the cavities will be driven away as well. Figure 36 shows the process when liquid water originally kept in one cavity moves to another cavity. Previously there is a relatively large amount of liquid water inside the porous layer. Due to the surface tension effect, the liquid water droplet attached to the porous layer in the cavity is hard to move. When the liquid water in the porous layer is removed gradually, less and less liquid water is left in the porous layer under the liquid water kept in the cavity. In this situation, the liquid water droplet in the cavity will driven by the gas flow as shown in Figure 36 (a) and (b). The movement of the droplet is random, but it will finally meet one of the walls of the cavity and is dragged by the gas flow through the porous layer to the next cavity or the outlet manifold. Figure 36 (c) to (f) shows the situation when the droplet meets the baffle. In this situation, the gas flow drags the droplet through the area under the baffle to the next cavity. It is observed that, due to the surface tension effect, the liquid water generally remains connected as a whole piece during the whole process, and will go through the same process again to move to the outlet manifold after it reaches the second cavity.

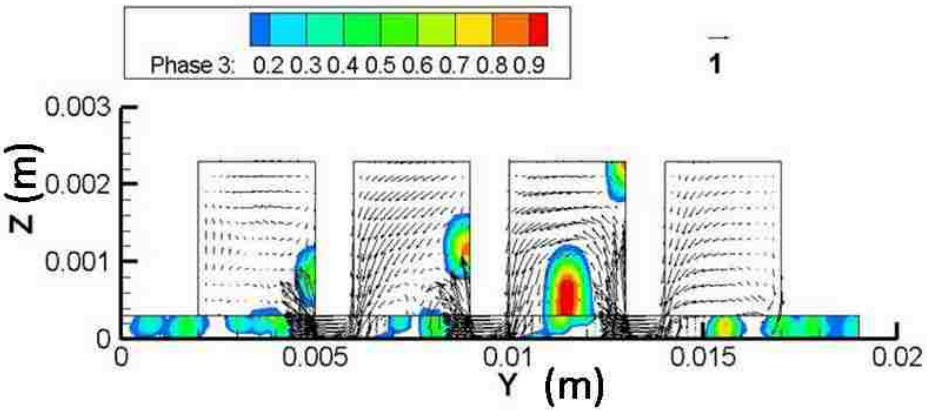

(a) t = 0.22 s

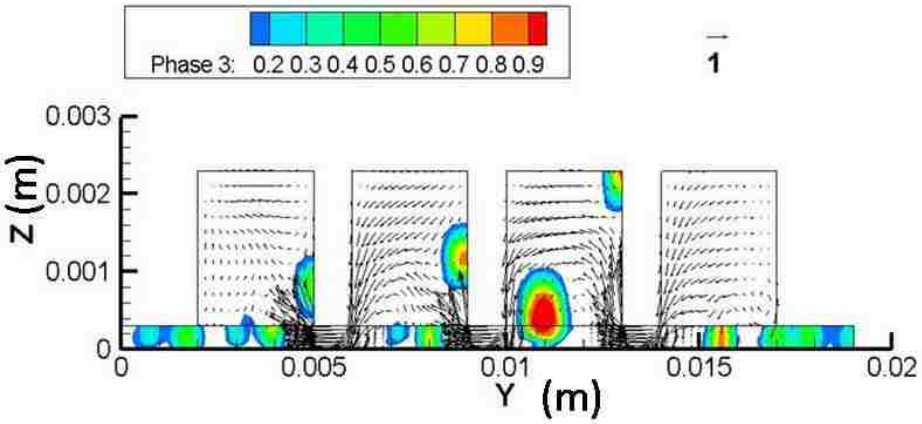

(b) t = 0.26 s

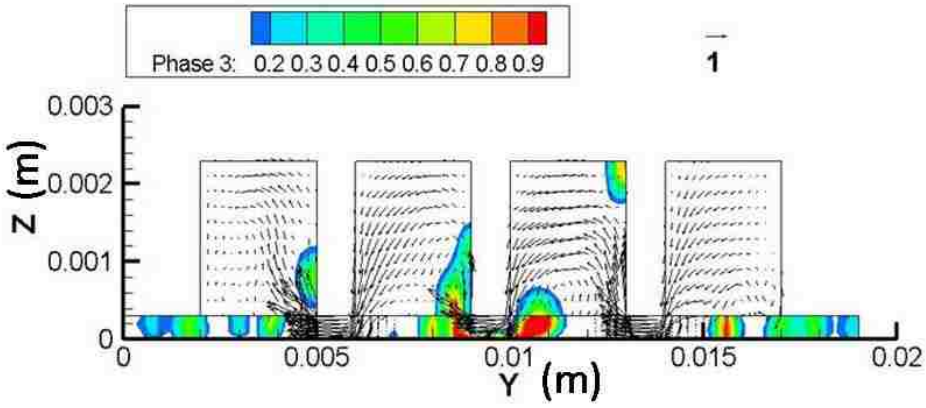

(c) t = 0.3 s

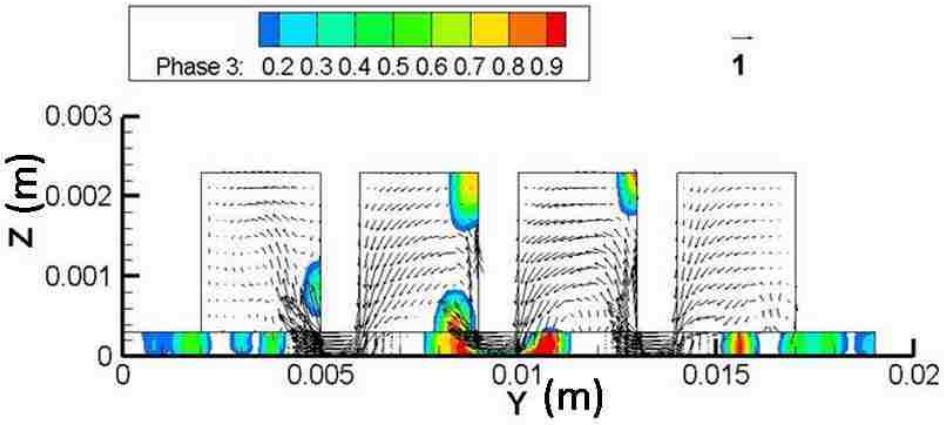

(d) t = 0.34 s

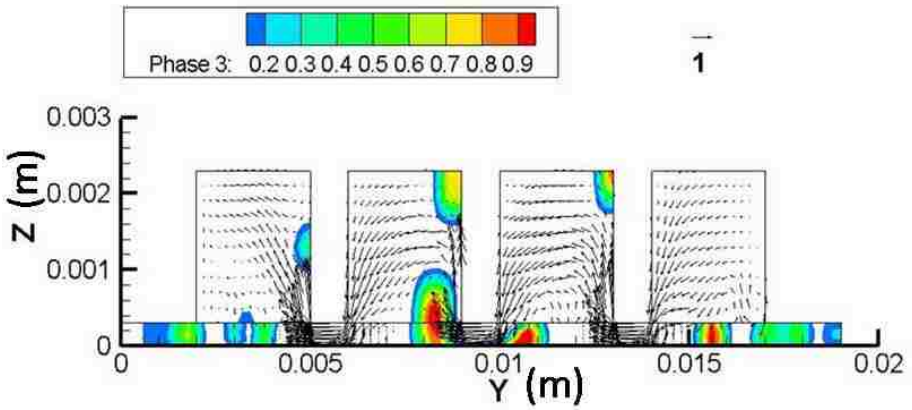

(e) t = 0.38 s

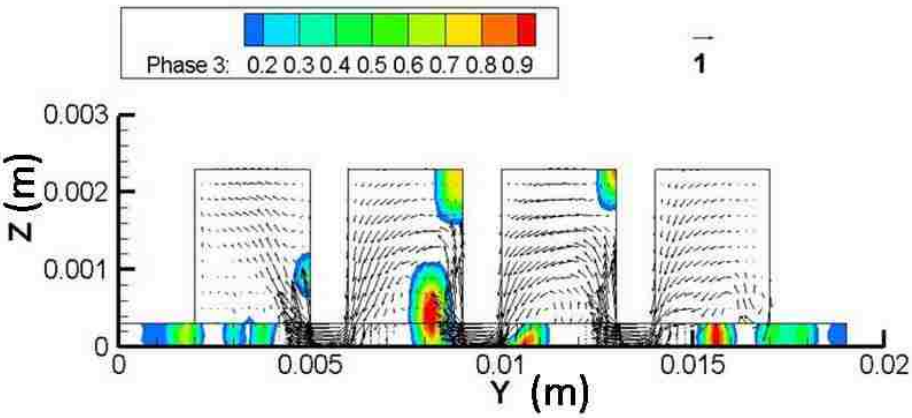

(f) t = 0.42 s

Fig. 36. Liquid water droplet driven from one cavity to the next cavity

7.5 Liquid water moving inside the porous layer

Liquid water movement has a certain trend in the porous layer in the PBB geometry as well. Firstly, a part of the liquid water is brought out of the porous layer into the cavities and outlet manifold by the relatively intense gas flow under the baffle area. Then the liquid water between the inlet manifold and outlet manifold area, say approximately between the two planes y = 0.005 m and y = 0.015 m, will be gradually removed driven by the gas flow. However some liquid water is left in the porous layer under the cavities attached to the liquid water droplets trapped in the cavities even

after a larger amount of liquid water in the porous layer is removed. This is because the gas flow moves in a direction away from the porous layer right after it goes into the cavities, and the gas flow going into a certain cavity under one baffle mostly goes out of this cavity under the next baffle. Therefore, the total force acting on the droplet is very small compared to the surface tension force connecting the part of liquid water inside the porous layer and the part of liquid water in the cavity. In this case the liquid water trapped in the cavities cannot move towards any direction at this period of time. In Figure 37, the pictures on the left show the volume fraction of liquid water in the middle section of the porous layer, z = 0.00015 m. The pictures on the right show the gas velocity vector in the same section.

Also, it can be observed from Figure 37 that after a period of time, the part of the liquid water in the porous layer between the two planes y = 0.005 m and y = 0.015 m is mostly drained out driven by the gas flow and the pressure field. However a part of the liquid water from the original water film at the edge area is split into droplets hang in the porous layer. These droplets are formed due to the surface tension of the liquid water and the porosity of the porous media. In these areas, the gas flow velocity is relatively low comparing the area between the inlet and outlet manifold in the porous layer. So the gas flow is not strong enough to overcome the surface tension effect and drive the liquid water away.

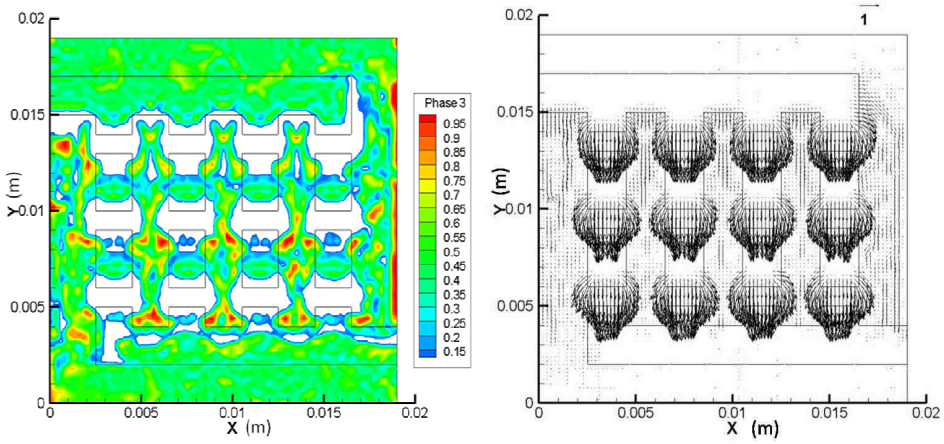

(a) t = 0.012s

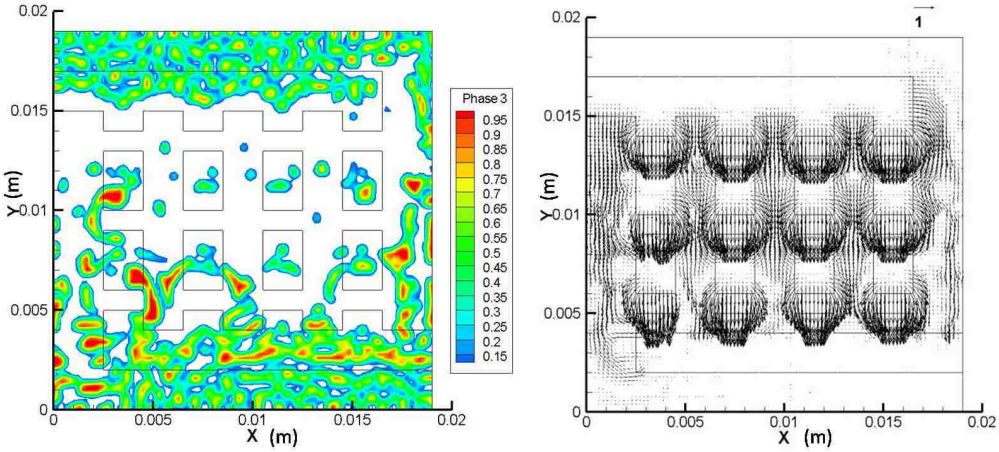

(b) t = 0.024 s

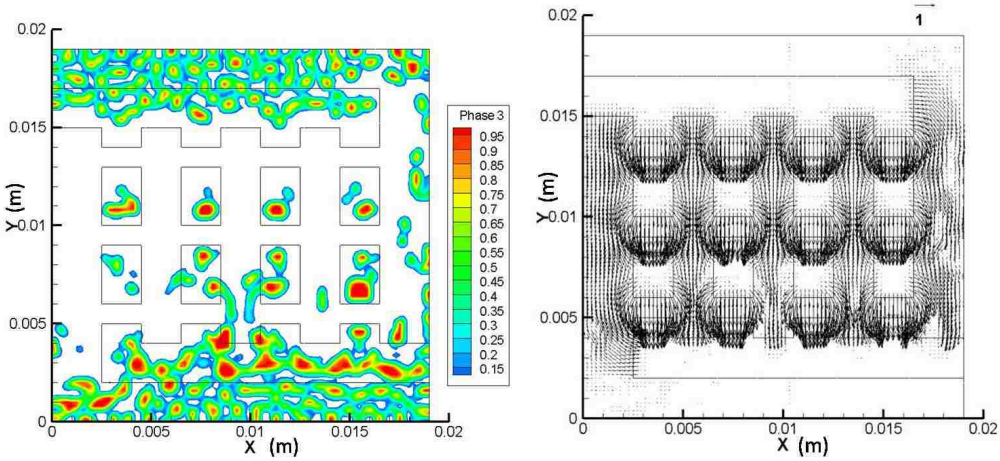

(c) t = 0.036 s

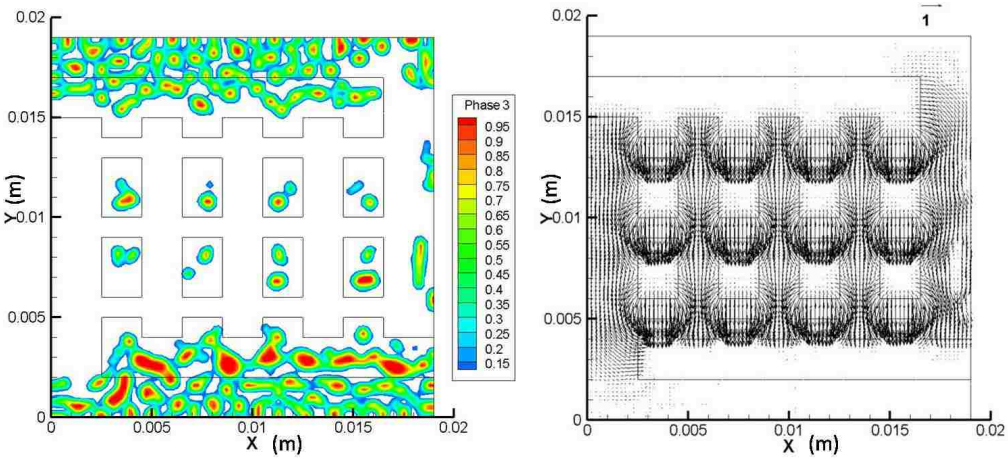

(d) t = 0.048 s

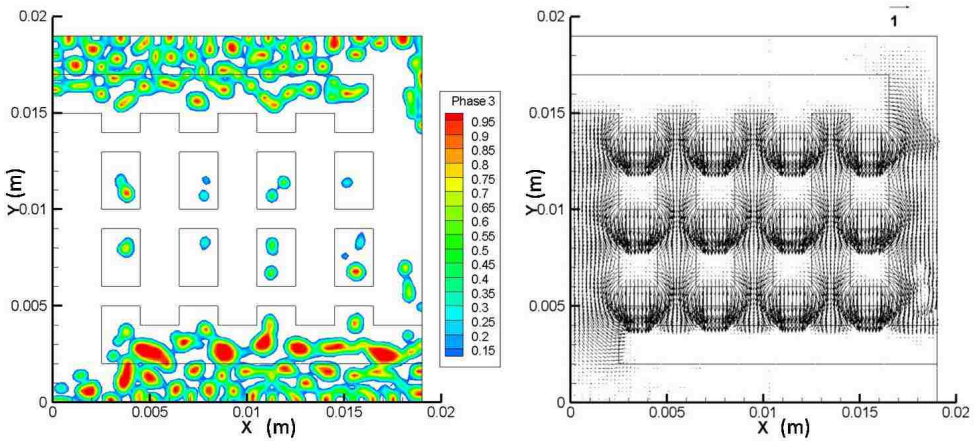

(e) t = 0.06 s

Fig. 37. Liquid water removal process inside the porous layer

7.6 Summary

1. The liquid water removal process in the inlet manifold area is much slower than the liquid water removal process in the porous layer between the inlet manifold and outlet manifold due to the relatively intense gas flow under the baffle and rib area.
2. The liquid water is brought into the outlet manifold along the edge of the outlet manifold at the beginning time period.
3. After a period of time, more liquid water is brought into the outlet manifold. This part of liquid water tends to split into several droplets by the gas flow inside the outlet manifold. Most of them gradually attach to each other become larger droplets influencing the local gas flow direction on the contrary.
4. A certain amount of liquid water is trapped in the cavities with a part inside the porous layer. This part of liquid water is helpful in enhancing the ion conductivity of the membrane, and it will be driven away relatively slowly.
5. A part of the liquid water is brought out of the porous layer into the cavities and outlet manifold by the relatively intense gas flow under the baffle area firstly.

6. The liquid water between the inlet manifold and outlet manifold area is removed efficiently by the gas flow.
7. While the part of the liquid water from the original water film between the inlet and outlet manifold is mostly drained out by the gas flow, a part of the liquid water at the edge area is split into droplets and these droplets hang in the porous layer and are removed relatively slow due to the surface tension effect of the liquid water and the porosity of the porous media.

CHAPTER 8

CONCLUSIONS

1. The methodology applied in the numerical investigation with the Volume of Fluid (VOF) model in the software package FLUENT 6.3.26 and the numerical fuel cell model constructed is validated with experiments in this study. The liquid water removal process in the channel of the fuel cell is visualized and the pressure difference in the fuel cell channel is recorded from the experiment. The results from the experiment and the validation model simulation are quite similar.
2. The liquid water removal process in the serpentine channel, stirred tank reactor (STR) chamber and parallel baffle blocked (PBB) channel with a porous layer attached on each one are studied individually using the validated model. The phenomena detected during the simulation are discussed in detail.

REFERENCE

[1] D. M. Bernardi, M. W. Verbrugge, J. Electrochem. Soc., 139 (1992) 2477

[2] T. V. Nguyen, J. S. Yi, J. Electrochem.Soc., 145 (1998) 1149

[3] H. C. Liu, W. M. Yan, C. Y. Soong, Falin Chen, J. Power Sources, 142 (2005) 125

[4] S. Dutta, S. Shimpalee, J. W. V. Zee, J. Appl. Electrochem., 30 (2000) 135

[5] P. T. Nguyen, T. Berning, N. Djilali, J. Power Sources, 130 (2005) 149

[6] S.W. Cha, R. O'Hayre, Y. Saito, F.B. Prinz, J. Power Sources, 134 (2004) 57

[7] A. Kumar, R. G. Reddy, J. Power Sources, 155 (2006) 264

[8] X. Li, I. Sabir, International J. Hydrogen Energy, 30 (2005) 359

[9] R. Boddu, U. K. Marupakula, B. Summers, P. Majumdar, J. Power Sources, 189 (2009) 1083

[10] J. P. Kloess, X. Wang, J. Liu, Z. Shi, L. Guessous, J. Power Sources, 188 (2009) 132

[11] J. Kuo, C. Chang-Jian, C. Chen, J. Applied Polymer Science, 111 (2009) 1440

[12] J. S. Yi, J. D. Yang, C. King, AIChE J., 50 (2004) 2594

[13] T. Berning, D. M. Lu, N. Djilali, J. Power Sources, 106 (2002) 284

[14] E. Hontanon, M. J. Escudero, C. Bautista, P. L. Garcia-Ybarra, L. Daza, J. Power Sources, 86 (2000) 363

[15] L. You, H. Liu, Int. J. Heat Mass Transfer, 45 (2002) 2277

[16] Z. H. Wang, C.Y. Wang, K. S. Chen, J. Power Sources, 94 (2001) 40

[17] P. Quan, B. Zhou, A. Sobiesiak, Z. Liu , J. Power Sources, 152 (2005) 131

[18] K. Jiao, B. Zhou, and P. Quan, J. Power Sources, 157 (2006) 226

[19] K. Jiao, B. Zhou, P. Quan, J. Power Sources, 154 (2006) 124

[20] K. Jiao, B. Zhou, J. Power Sources, 169 (2007) 296

[21] K. Jiao, B. Zhou, J. Power Sources, 175 (2008) 106

[22] A. D. Le, B. Zhou, J. Power Sources, 182 (2008) 197

[23] A. D. Le, B. Zhou, Electrochimica Acta, 54 (2009) 2137

[24] Z. Zhan, J. Xiao, M. Pan, R. Yuan, J. Power Sources, 160(2006) 1

[25] P. Quan, M. C. Lai, J. Power Sources, 164 (2007) 222

[26] I. S. Hussaini, C. Y. Wang, J. of Power Sources, 187 (2009) 444

[27] C. Xu, T.S. Zhao, Electrochemistry Communications, 9 (2007) 497

[28] A. M. Lopez, F. Barreras, A. Lozano, J. A. Garcia, L. Valino, R. Mustata, J. Power Sources, 192 (2009) 94

[29] W. H.J. Hogarth, J. B. Benziger, J. Power Sources, 159 (2006) 968

[30] W. M. Yan, S. C. Mei, C. Y. Soong, Z. S. Liu, D. Song, J. Power Sources, 160 (2006) 116

[31] A. Bazylak, J. Heinrich, N. Djilali, D. Sinton, J. of Power Sources, 185 (2008) 1147

[32] A. Bazylak, D. Sinton, N. Djilali, J. of Power Sources, 176 (2008) 240

[33] P. K. Sinha, P. P. Mukherjee, C. Y. Wang, J. of Materials Chemistry, 17 (2007) 3053

[34] E.C. Kumbur, K.V. Sharp, M.M. Mench, J. Power Sources, 161 (2006) 333

[35] C. Hartnig, I. Manke, R. Kuhn, S. Kleinau, J. Goebbels, J. Banhart, J. Power Sources, 188 (2009) 468

[36] B. J. U. Kothe, D. B., and Zemach, C. J. Comput. Phys, 100 (1992) 335

[37] Anh Dinh Le, Numerical and Eexperimental Studies on Transport Phenomena of Proton Exchange Membrane Fuel Cells, PhD Dissertation, University of Windsor, Ontario, Canada (2010).

[38] Jixin Chen, Experimental Study on the Performance of a 10-cell Proton Exchange Membrane (PEM) Fuel Cell stack, Master Thesis, University of Windsor, Ontario, Canada (2007).

[39] Y. A. Cengel, J. M. Cimbala, Fluid Mechanics - Fundamentals and Applications, 1st ed., McGraw-Hill, 2006.

[40] D. Spernjak, A. K. Prasad, S. G. Advani, J. of Power Sources, 170 (2007) 334

VITA AUCTORIS

NAME:	Xiaojing Liu
PLACE OF BIRTH:	Beijing, China
YEAR OF BIRTH:	1982
EDUCATION	Beijing 101 High School, Beijing 1997-2000
	Beijing Technology and Business University, Beijing, China 2000-2004 B.Sc.
	University of Windsor, Windsor, Ontario 2008-2010 MASc.